INFORMATION TO USERS

This dissertation was produced from a microfilm copy of the original document. While the most advanced technological means to photograph and reproduce this document have been used, the quality is heavily dependent upon the quality of the original submitted.

The following explanation of techniques is provided to help you understand markings or patterns which may appear on this reproduction.

1. The sign or "target" for pages apparently lacking from the document photographed is "Missing Page(s)". If it was possible to obtain the missing page(s) or section, they are spliced into the film along with adjacent pages. This may have necessitated cutting thru an image and duplicating adjacent pages to insure you complete continuity.

2. When an image on the film is obliterated with a large round black mark, it is an indication that the photographer suspected that the copy may have moved during exposure and thus cause a blurred image. You will find a good image of the page in the adjacent frame.

3. When a map, drawing or chart, etc., was part of the material being photographed the photographer followed a definite method in "sectioning" the material. It is customary to begin photoing at the upper left hand corner of a large sheet and to continue photoing from left to right in equal sections with a small overlap. If necessary, sectioning is continued again — beginning below the first row and continuing on until complete.

4. The majority of users indicate that the textual content is of greatest value, however, a somewhat higher quality reproduction could be made from "photographs" if essential to the understanding of the dissertation. Silver prints of "photographs" may be ordered at additional charge by writing the Order Department, giving the catalog number, title, author and specific pages you wish reproduced.

University Microfilms

300 North Zeeb Road
Ann Arbor, Michigan 48106

A Xerox Education Company

INFORMATION TO USERS

This dissertation was produced from a microfilm copy of the original document. While the most advanced technological means to photograph and reproduce this document have been used, the quality is heavily dependent upon the quality of the original submitted.

The following explanation of techniques is provided to help you understand markings or patterns which may appear on this reproduction.

1. The sign or "target" for pages apparently lacking from the document photographed is "Missing Page(s)". If it was possible to obtain the missing page(s) or section, they are spliced into the film along with adjacent pages. This may have necessitated cutting thru an image and duplicating adjacent pages to insure you complete continuity.

2. When an image on the film is obliterated with a large round black mark, it is an indication that the photographer suspected that the copy may have moved during exposure and thus cause a blurred image. You will find a good image of the page in the adjacent frame.

3. When a map, drawing or chart, etc., was part of the material being photographed the photographer followed a definite method in "sectioning" the material. It is customary to begin photoing at the upper left hand corner of a large sheet and to continue photoing from left to right in equal sections with a small overlap. If necessary, sectioning is continued again – beginning below the first row and continuing on until complete.

4. The majority of users indicate that the textual content is of greatest value, however, a somewhat higher quality reproduction could be made from "photographs" if essential to the understanding of the dissertation. Silver prints of "photographs" may be ordered at additional charge by writing the Order Department, giving the catalog number, title, author and specific pages you wish reproduced.

University Microfilms

300 North Zeeb Road
Ann Arbor, Michigan 48106

A Xerox Education Company

THE CHEMICAL AND MORPHOLOGICAL VARIATIONS OF ZIRCONS FROM THE BOULDER BATHOLITH, MONTANA

A dissertation submitted to the

Division of Graduate Studies
of the University of Cincinnati

in partial fulfillment of the
requirements for the degree of

DOCTOR OF PHILOSOPHY

1972

BY

Igol Effimoff

B.S., St. Lawrence University, 1968

UNIVERSITY OF CINCINNATI

May 9 19 72

I hereby recommend that the thesis prepared under my supervision by Igol Effimoff

entitled The Chemical and Morphological Variations of Zircons from the Boulder Batholith, Montana

be accepted as fulfilling this part of the requirements for the degree of Doctor of Philosophy

Approved by:

Leonard H. Larsen

Frank L. Koucky

J. Attila Vilcsin

Form 668—Grad. School—1M—3-69

ABSTRACT

Electron microprobe analyses of zircons from rocks of the epizonal composite Boulder batholith, Montana, suggest that zircons begin to crystallize early and continuously from these granitic melts. The crystal habits of zircons vary systematically with (Y+Hf)/Th ratio and may be in large part controlled by the Y/Th ratio wich normally increases with differentiation of granitic melts.

A comparison of zircon populations, separated from hand speciments, based on their reduced major axes (RMA) and mean elongation ratio (MER), shows that each such zircon sample from the batholith behaves as a distinct population. This is due to the continuous crystallization of zircon from the melts and the variation of zircon crystal habit in response to differing physiochemical changes in the melt. This interpretation of the behavior of zircons in granitic melts is contrary to that proposed by Larsen and Poldervaart (1957) and Alper and Poldervaart (1957), who considered that zircons crystallized early but ceased crystallizing early as well.

Hf/Zr ratios of zircon populations from plutons of the Boulder batholith support the interpretation of the batholith's origin, which considers it to be a composite body with a series of plutons closely related in time and space and differentiated from two different magma sources.

TABLE OF CONTENTS

CONTENTS - CONTINUED

ILLUSTRATIONS

Figures - Continued

Tables

ACKNOWLEDGEMENTS

I am grateful to Dr. L. H. Larsen who suggested the problem on the variation of zircons from the Boulder batholith and provided much helpful advice, discussion, and encouragement throughout the duration of this investigation. I am also indebted to Drs. F. L. Koucky, I. A. Kilinc, and L. H. Lattman who provided much criticism and advice.

Dr. R. I. Tilling of the U. S. Geological Survey generously provided much information and discussion on the nature of the Boulder batholith. Drs. E. White and H. Görz provided much advice on and access to the electron microprobe at the Materials Research Laboratories of The Pennsylvania State University. Drafting of maps and figures was skillfully done by Mr. T. Deaton and typing of the dissertation was done by Mrs. W. Osborne.

This project was generously funded by the Penrose Bequest Research Grant of the Geological Society of America, the Ohio Academy of Science, the Alpha Delta chapter of Sigma Gamma Epsilon and the Department of Geology at the University of Cincinnati.

I. INTRODUCTION

A. Statement of Problem

The purpose of this investigation is to determine the extent to which the chemistry and morphology of zircons reflect the intrusive and crystallization history of a composite epizonal batholith and to develop a model for zircon crystallization in such a body. As a well studied composite epizonal pluton, the northern two-thirds of the Boulder batholith, Montana provides an excellent base for such a study.

The study is necessitated by two factors. One is that zircons have been used to draw conclusions on the petrogenesis of granitic rocks on the assumption that zircons crystallize early and, for a short duration, from a granitic melt. It is necessary to test this idea of zircon crystallization. The other factor is that zircons concentrate a large amount of the rare earth elements and most of the zirconium and hafnium in granitic melts. An understanding of zircon chemistry will help elucidate the behavior of these elements in granitic melts.

In order to understand the chemical and morphological behavior of zircons from the Porphyritic granodiorite stock and the Biotite granite of the Boulder batholith, the magmatic affiliation of the Porphyritic granodiorite stock and the intrusive position of the Biotite granite must be understood. The other plutons comprising the Boulder batholith are well understood in terms of their magmatic affiliation and sequence of intrusion.

B. Objectives and Limitations

The objectives of this study are six fold: 1) the separation of zircon crystals from samples of rock from the Boulder batholith, using heavy liquids and the Frantz isodynamic separator; 2) the description of zircon crystals from each sample in terms of their crystal habit, zoning, and inclusions; 3) the analyses of zircon crystals for Zr, Hf, Y, Th, U, and Si using electron microproble techniques; 4) the whole rock chemical analysis of samples from the Porphyritic granodiorite stock and the petrographic analysis of the Biotite granite; 5) the measurement of the length and width of zircon crystals from each sample, and the calculation of a reduced major axis and a mean elongation ratio for that zircon population; and 6) the discussion of the data generated by the study in conjunction with a critical synthesis of zircon literature.

The foremost limitation of this study is the lack of zircon standards for the electron microprobe which necessitated the use of single pure element standards for the analysis of each element. Since pure element standards do not approximate the composition of zircons, extensive corrections had to be made, which resulted in a loss of accuracy in the analyses.

The other limitation which affected the scope of this study was the fact that the electron microprobe was not readily accessible and quite costly to operate on a rental basis. These factors resulted in the analyses of fewer samples for fewer elements.

II. GEOLOGY OF THE BOULDER BATHOLITH

A. Regional Setting

Western Montana is divisible into three major tectonic blocks which are separated by east-west lineaments related to the Precambrian basement (Fig. 1). The northern block is a thick sheet of Precambrian Belt series rocks, faulted and folded along a northwest axis parallel to the regional Rock Mountain Trend and displaced northeastward at the Lewis thrust plate. The southern block is a large stable mass of Archean gneiss, schist, and granite southeast of Butte which has maintained its relative position in the regional framework and resisted deformation since Precambrian time. Between the northern and southern block is a central wedge shaped mass extending from the Lewis and Clark lineament to the east-west lineament south of Butte which marks the northern edge of the Archean block. This central mass has been a zone of recurrent subsidence since the Precambrian, and it coincides areally with a major eastward embayment in Belt sedimentation, It is also characterized internally by extensive deformation, with infolding of Belt and younger formations. The central block has migrated eastward relative to both the southern and northern blocks, with major dislocation along its northern margin on the Lewis and Clark lineament. This eastward movement was obstructed on the south by the stable Archean mass, inducing clockwise rotation within the central block and causing bulging and thrusting of formations southeastward onto the flanks of the crystalline buttress. The rotational movement accounts for the reversed S-shaped deflection of the structural trend from northwest in the northern block, through the northeast in the central block, and then

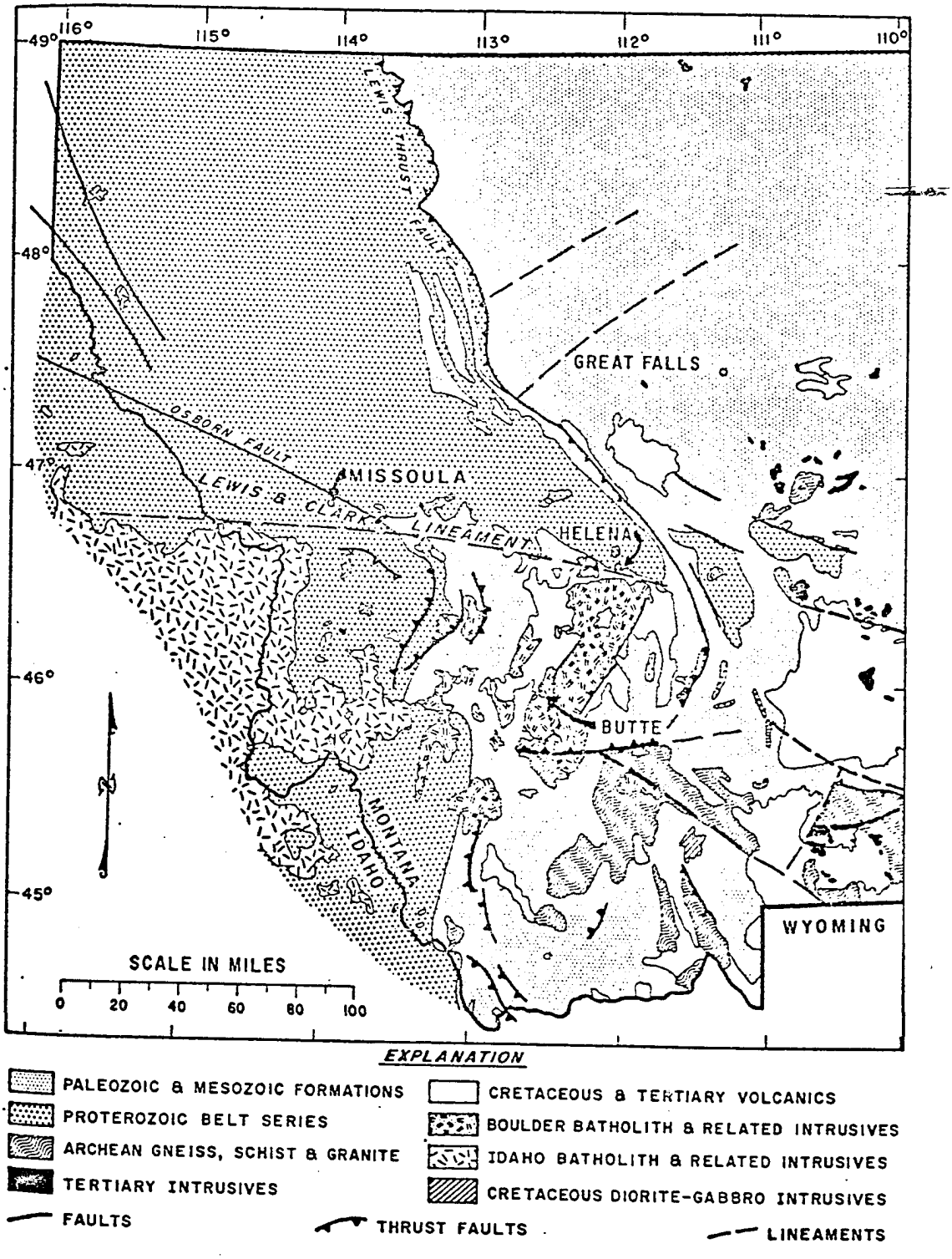

Fig. 1. Tectonic elements of western Montana. The Boulder batholith is shown relative to major tectonic elements (Meyer, et al., 1968).

back to the northwest in the southern block (Meyer, et al., 1968). The Boulder batholith is located in the central block and lies east of a salient of the Idaho batholith.

B. Local Setting

The Boulder batholith is a north-northeast trending calc-alkaline composite body about 70 miles long and 35 miles wide, extending from Helena to south of Butte (see geologic map in pocket). It is composed of at least fifteen separate plutons ranging from gabbro to granite. The bulk of the batholith is quartz monzonite and granodiorite. Satellite stocks and dikes are numerous and are of rocks similar to those that make up the batholith. The intrusives are overlain by rocks as young as the Lowland Creek volcanics of Eocene age, isotopically dated at about 50 m.y. old (Smedes and Thomas, 1965). Isotopic dates indicate that the oldest pluton crystallized about 78 m.y. ago and the youngest pluton about 68 m.y. ago; the bulk of the batholith crystallized about 72 m.y. ago, during late Cretaceous time (Tilling, et al., 1968) (Fig. 2a,b).

The batholith and its satellites are epizonal plutons which intruded upper Precambrian to Cretaceous sedimentary strata of miogeosynclinal and shelf facies and the upper Cretaceous Elkhorn Mountain volcanics. The volcanics formed the roof and walls of much of the exposed part of the batholith.

The Butte quartz monzonite, the largest single pluton, makes up the bulk of the batholith. The straight, near vertical eastern margin of this pluton is a result of intrusion along a north-northeast trending fault. Remnant of this fault north of the batholith and in a metamorphosed screen

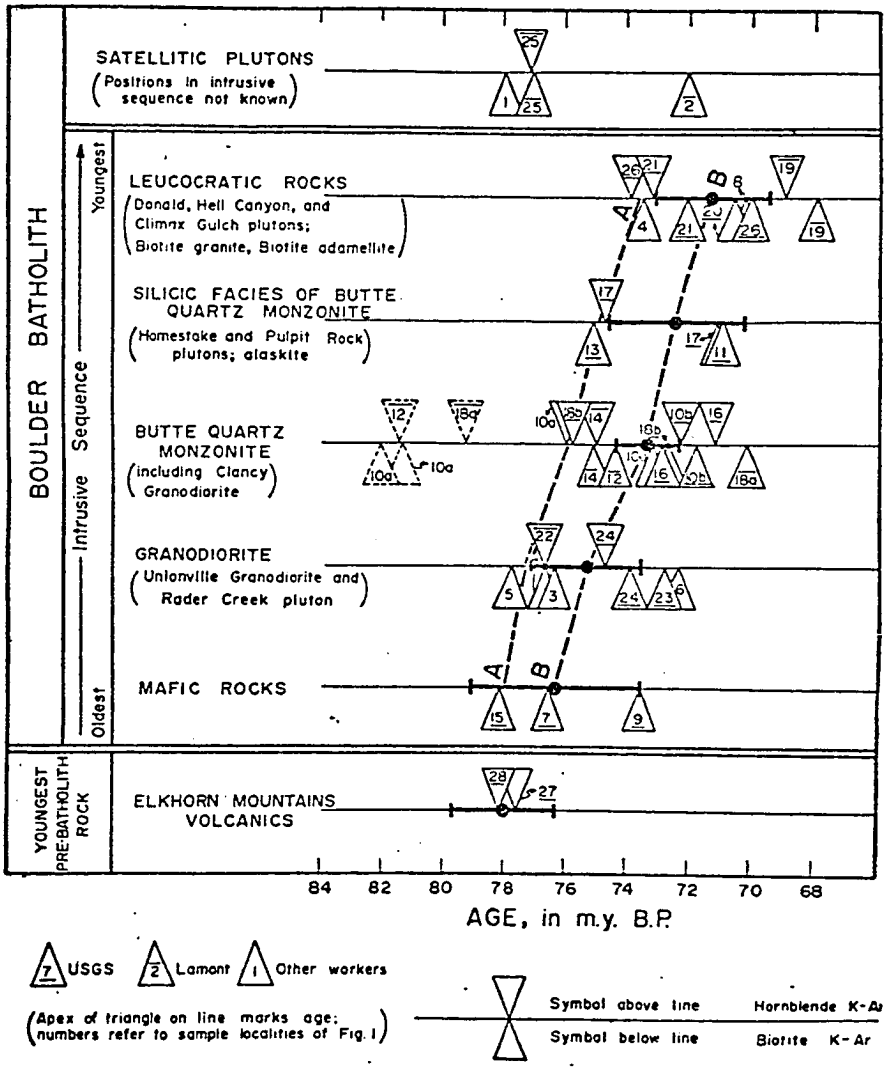

Fig. 2a. K-Ar ages of the Boulder batholith and of the Elkhorn Mountain volcanics. Ages of batholith rocks are grouped according to position in the intrusive sequence as determined by field relations. Ages indicated by dashed triangles are considered anomalous. The curve AA may approximate the beginning times of emplacement of the groups of the date plutons. Curve BB links the mean ages of the various groups of rocks; bars give error of the mean at the 95% confidence level (Tilling, et al., 1968).

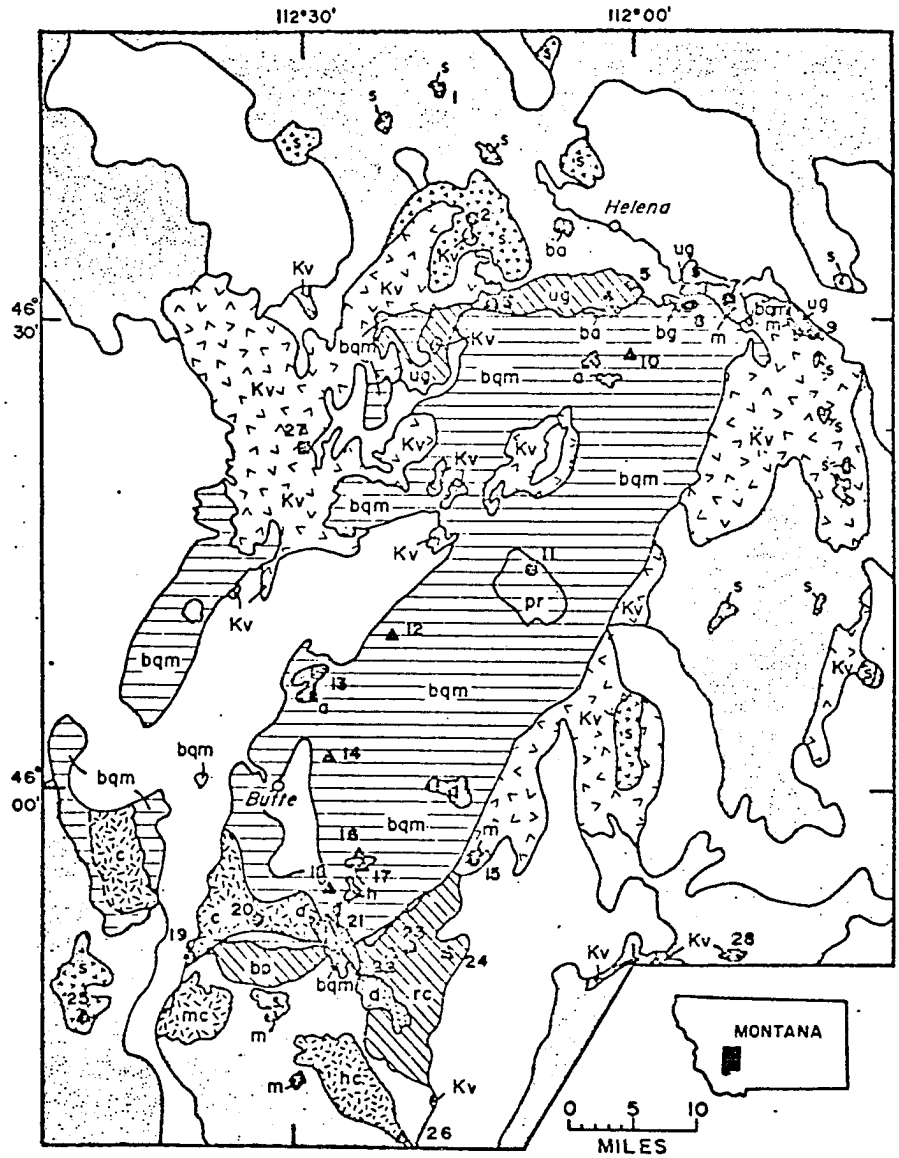

Fig. 2b. Location map of the Boulder batholith showing sample locations for the K-Ar age dates (Tilling,et al., 1968).

between the Butte quartz monzonite and granodiorite of the Rader Creek pluton in the south indicate emplacement of the Butte quartz monzonite pluton was in part accommodated by raising the eastern part of its roof more than 1000 meters (Smedes, 1966). The western contact of the batholith is grossly concordant with roof rocks and dips gently westward (Becraft, et al., 1963). The structurally complex north and south margins of the batholith indicate great deformation and shouldering aside of the wall rock (Knopf, 1957). The north-northeast trending faults west of and subparallel to the fault that controlled the eastern margin of the Butte quartz monzonite pluton were active repeatedly during and after emplacement of the batholith (Klepper, et al., 1957).

The mode of emplacement of this epizonal batholith and its configuration at depth has been the source of much discussion. Hamilton and Meyers (1967) suggested that the emplacement of the batholith was "in effect a gigantic mantled lava flow....only a few kilometers (5-6km) thick", that flowed east to west under a crust of its own ejecta, across a broad structural basin. Klepper, et al. (1971) disagrees with this interpretation on the basis of additional geologic and predominantly geophysical data. Rather than a thin, laterally emplaced flow capped by volcanics, they suggest that the volcanic cover is a stable roof and part of a volcanic plateau twice the size of the batholith beneath which the batholith intruded at a relatively steep angle. Geophysical and some geologic evidence demonstrates that the batholith is steep sided and at least 15 km thick. It appears that Hamilton and Meyers' interpretation of the emplacement of the entire Boulder batholith were based on observations from the northern portion of the batholith which is not a represen-

tative sample of the rest of the body.

Chemical, spatial, temporal, and structural relations of the pre- and post-batholithic volcanics and most of the batholithic rocks suggest that they were probably derived from genetically related magmatic sources (Smedes, 1966; Becraft, et al., 1963; Protska, 1966; and Ruppel, 1963). Lead and strontium isotope data on the plutonic rocks, however, cannot be interpreted in terms of any model having a single, isotopically uniform source of magma (Doe, et al., 1968). On the basis of additional strontium and lead isotope and major element chemical data, R. I. Tilling (personal communication, 1971) supports Doe, et al. (1968) interpretation and further suggests the presence of two separate magmatic series operating in the Boulder batholith. One is a sodic series best represented in the southern plutons and the other is the main or potassic series which comprises the bulk of the batholith.

C. Description of Major Plutons

The plutons that make up the Boulder batholith were intruded generally in order of increasing SiO_2 content. Most of the plutons can be assigned to one of the following groups:

1. Early mafic rocks -

    a. The Knapp stock (Knopf, 1963), renamed the Kokoruda Ranch complex (Smedes, 1966), is located 15 miles southeast of Helena. It is a very heterogenous body composed of norite, syenogabbro, syenodiorite, monzonite, calcic monzonite, augite bearing quartz monzonite, and rare bands of peridotite in gabbro. Zones of shonkonite,

orthoclase rock, and scapolite- and garnet-rich rocks form locally.

b. The Scratchgravel Hills, located 5 miles north-northwest of Helena is a stock composed of syenodiorite, consisting of plagioclase (An_{35}), microperthite, augite, and hornblende. Along the northern border of the stock is a Bytownite gabbro which predates the stock (Knopf, 1963). This stock is considered a satellitic pluton and a member of the main magma series (R. I. Tilling, personal communication, 1971).

2. Granodiorites -

a. The Unionville granodiorite is the earliest of the major intrusives in the northern part of the batholith. South of Helena is an augite-biotite-hornblende granodiorite. In some localities the Unionville has basic facies of hypersthene granogabbro which contain plagioclase of laboradorite (An_{55}) composition (see chemical analyses on Table 1). From the high mountainous portion of the Unionville granodiorite, southeast of Helena, is described another possible facies of the Unionville called "graphophyre" by Knopf (1963). It contains phenocrysts of labradorite and clinopyroxene in a well developed micropegmatitic groundmass. The Unionville granodiorite is a member of the main series (R. I. Tilling, personal communication, 1971).

b. The Rader Creek pluton, located in the southwest portion

TABLE 1

ANALYSES OF SOME PLUTONIC ROCKS FROM THE NORTHERN PART OF THE BOULDER BATHOLITH, MONTANA (Knopf, 1957).

	I	II	III	IV	V	VI	VII	VIII	IX	X
SiO_2	61.14	61.40	54.63	65.49	66.14	71.28	68.48	56.01	64.13	51.95
Al_2O_3	15.28	15.41	16.60	14.49	15.69	14.50	14.93	17.84	16.77	12.58
Fe_2O_3	1.90	2.26	3.32	2.11	1.93	1.04	1.32	3.56	1.96	3.12
FeO	4.52	3.76	5.62	2.90	2.05	1.19	2.07	3.05	1.69	3.91
MgO	3.41	2.99	4.65	2.45	1.60	.98	1.37	2.57	1.29	5.62
CaO	5.51	4.86	7.93	4.29	3.71	2.45	2.61	7.39	2.72	13.00
Na_2O	2.78	2.69	2.48	2.80	3.50	3.16	3.01	4.01	3.92	2.85
K_2O	3.34	4.12	2.10	3.66	3.54	4.29	4.59	3.33	5.77	4.61
H_2O+	.65	.55	.85	.56	.47	.43	.60	.61	.39	.76
H_2O-	.09	.18	.14	.05	.05	.13	.12	.24	.19	.03
TiO_2	.82	.80	.89	.65	.43	.26	.39	.65	.52	.55
P_2O_5	.26	.25	.42	.21	.24	.09	.17	.42	.23	.46
CO_2	.08	.07	.02	.05	.08	.10	.31		.02	
MnO	.12	.09	.16	.10	.10	.06	.07	.19	.05	.14
SrO	.04	.07	.04	.04	.08	.02	.02	.10	.02	.06
BaO	.08	.12	.05	.05	.13	.11	.11	.12	.10	.05
S	.01	.02	.04	.01	.03	.01			.01	.01
		99.65	99.94		99.74					
Less O = S		.02	.02		.01					
Total	100.03	99.64	99.94	99.91	99.73	100.10	100.17	100.09	99.78	99.88
d	2.78	2.76	2.84	2.71	2.70	2.65	2.67	2.76	2.66	2.93

I Unionville granodiorite; type locality, old quarry 0.9 mi. NW of BM4589, Clark Gulch. Analyst, J. J. Engel.

II Unionville granodiorite; near Benson xenolith. Analyst, Doris Thaemlitz.

III Granogabbro; at contact NW of Park City. Analyst, Doris Thaemlitz.

IV Clancy granodiorite; Kain quarry, Clancy Creek. Analyst, J. J. Engel.

V Porphyritic granodiorite; Schimpf quarry, 7 mi. W of Helena. Analyst, Doris Thaemlitz.

VI Biotite adamellite; ridge between Jackson Creek and Lump Gulch. Analyst, J. J. Engel.

VII Biotite adamellite; Broadwater stock, Helena. Analysts, B. Smith and R. B. Ellestad.

VIII Syenodiorite: old quarry near Great Northern Railway, Scratchgravel Hills. Analyst, L. C. Peck. SrO determined by S. S. Goldich.

IX Priests Pass leucomonzonite; road cut just west of Priests Pass. Analyst, H. Baadsgaard.

X Nepheline shonkinite; 3/4 mi. southeast of Montana City. Analyst, H. Baadsgaard.

of the batholith, is a homogenous appearing pluton. It is characteristically equigranular diorite which grades imperceptibly into porphyritic varieites at the eastern margin. A detailed study, however, shows that there are significant variations in the modal and normal composition, which indicate that this "homogeneous" pluton is actually compositionally zoned (Tilling, 1964). The Rader Creek pluton is a member of the sodic magma series.

c. The Burton Park pluton, located in the southernmost part of the batholith, is a granodiorite mass which has not been mapped or studied in any detail. It may have intruded contemporaneously with the Rader Creek pluton and the Unionville granodiorite (Doe, et al., 1968). Preliminary strontium isotope and major element chemical data suggests that the Burton Park pluton belongs to the main magma series.

3. The Butte quartz monzonite and relative silicic facies -

a. The Butte quartz monzonite, synonymous with the Clancy granodiorite of Knopf (1963), is a quartz monzonite and granodiorite of many textural and compositional varieties which makes up the bulk of the batholith. Quartz monzonites are the main rock type with granodiorites being subordinate. The boundary between the two rock types is artificial and based on the proportion of plagioclase and K-feldspar with many of the rocks lying on or near the boundary (Fig. 3). The rocks range in

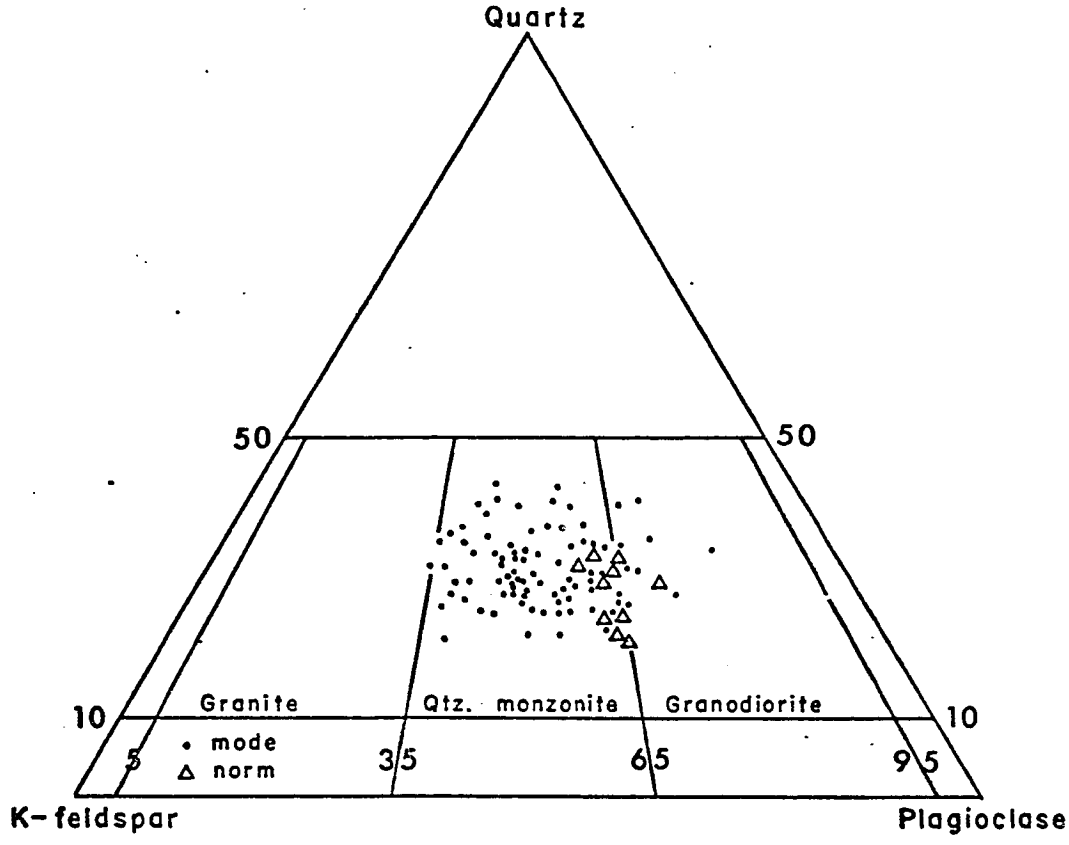

Fig. 3. Triangular diagram showing the proportions of modal and normative quartz, K-feldspar and plagioclase in the Butte quartz monzonite (Becraft, et al., 1963).

composition from 20 to 48 percent plagioclase, 15 to 45 percent K-feldspar, 15 to 40 percent quartz, less than 1 to 12 percent biotite, less than 1 to 8 percent hornblende, and less than 1 to 3 percent magnetite, sphene, zircon, apatite, allanite (?) and rutile (?) combined. Pyroxene is scarce, but some rocks contain as much as 5 percent augite. Tourmaline is a common accessory mineral in certain restricted areas. The average grain size of the minerals ranges from less than 1 mm to 3 mm. Textures are commonly allotriomorphic or hypautomorphic, equigranular, or seriate; but many of the rocks are porphyritic and some contain large potassium feldspar crystals as much as 3 cm long (Becraft, et al., 1963).

The Unionville granodiorite and the Rader Creek pluton are both cut by dikes of the Butte quartz monzonite. There are no perceptible chill selvages against the Unionville granodiorite suggesting that not much time elapsed between intrusion of the two phases. The Butte quartz monzonite is the major member of the main magma series.

b. The silicic facies of the Butte quartz monzonite consists of many small to moderate sized dikes, sheets, and irregular bodies of silicic rock which in places grade into, and in places crosscut, the Butte quartz monzonite and are genetrically related to it. These silicic facies include the Pulpit Rock mass, the Homestake mass,

and a large number of pegmatites, alaskites, and aplite dikes. Field and petrographic evidence suggests that these rocks crystallized from local concentrations of residual Butte quartz monzonite magma rather than from separate batches of younger magma.

Mineralogically the silicic phases consist mainly of quartz (33%), K-feldspar (33-50%) and plagioclase of oligoclase to albite composition (Fig. 4). Tourmaline is often present. Trace amounts of zircon, apatite, hematite, magnetite, and pyrite are common. The secondary minerals are dickite or kaolinite, chlorite, limonite, hematite, leucoxene, and epidote (Becraft, et al., 1963). The chemistry of two silicic phase alaskites is presented in Table 2.

4. Late leucocratic quartz monzonite, granodiorite, and granite -

a. The Biotite adamellite forms the Broadwater stock west of Helena and some small bodies that intrude into the Unionville granodiorite and the Butte quartz monzonite. The plagioclase (An_{40}) content is approximately equal to the K-feldspar content and the rock contains 71 percent silica. The only ferromagnesian mineral present is biotite. The Biotite adamellite is a member of the main magma series.

b. The Biotite granite or Muscovite-biotite-adamellite (Knopf, 1963) is located 6 miles southeast of Helena. It is a medium grained biotite granite low in plagioclase

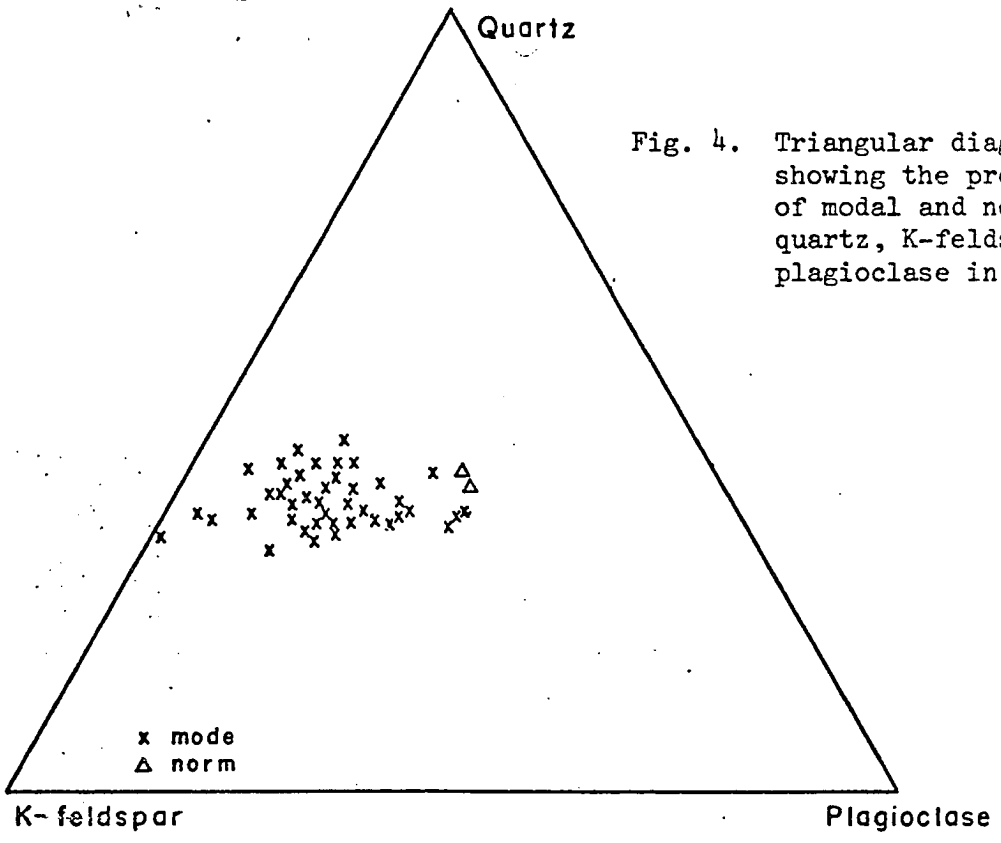

Fig. 4. Triangular diagram showing the proportions of modal and normative quartz, K-feldspar and plagioclase in alaskite.

Chemical analyses		
SiO_2	77.8	77.9
Al_2O_3	12.9	12.7
Fe_2O_3	.35	.34
FeO	.17	.15
MgO	.14	.18
CaO	.68	.37
Na_2O	3.1	3.5
K_2O	4.8	4.8
TiO_2	.06	.05
P_2O_5	.01	.01
MnO	.01	.01
H_2O	.20	.14
Norms		
Quartz	40.0	38.4
Orthoclase	28.4	28.4
Albite	26.2	29.3
Anorthite	3.6	1.7
Corundum	.9	1.2
Hypersthene	.3	.4
Magnetite	.5	.5

TABLE 2. Chemical analyses and norms for two alaskites (Becraft, et al., 1963).

(An_{30}) content. Muscovite of deuteric origin is often present. Although Knopf (1957, 1963) has described it as a separate pluton intruding the Butte quartz monzonite, it may very well be merely a facies of the Butte quartz monzonite based on evidence presented later in this study. Its relation to the Biotite adamellite is not known. It is generally tourmaliniferous and in places it is crowded with tourmaline nodules and with tourmaline developed along fractures. Analyses of rocks from the Biotite granite ascribe it to the main magma series (R. I. Tilling, personal communication), which is understandable since it may represent a variety of the Butte quartz monzonite.

c. The Hell Canyon, Moose Creek, Climax Gulch, and Donald plutons, all located at the southern end of the batholith have not been mapped or studied in any detail. They have been placed in this group on the basis of preliminary reconnaissance (Smedes, et al., 1968). R. I. Tilling (personal communication, 1971) includes all these plutons in the sodic magma series.

D. Discussion of Intrusive Sequence

There are twenty or more stocks which occur near the Boulder batholith. Because of their isolated occurrence in country rocks of diverse ages, it is impossible to rank the satellitic plutons into an intrusive sequence. Due to the large overlap of radiometric age dates for the

various major intrusive phases, the age date determinations on these satellites have not been useful in determining their position in the intrusive sequence.

The Porphyritic granodiorite stock, located 10 miles west of Helena, is one of these satellitic plutons of unknown intrusive position (see map in pocket). It is composed of two units separated on the basis of texture and composition. One unit is the Kpg or porphyritic phase of the stock. It is characterized by large orthoclase phenocrysts and has a plagioclase composition of An_{20} to An_{35}. The other unit designated as Kgd is the more basic unporphyritic granodiorite possible equivalent of Kpg. It has an average plagioclase composition of An_{45} in the basic portions found at lower altitudes and grades into a white granodiorite at higher altitudes.

Knopf (1963, 1964) proposed that the Porphyritic granodiorite is the third intrusive in the sequence of progressively silica rich intrusives which were probably generated from a single differentiating magmatic source. The intrusive sequence he proposed, based on field evidence and chemical and isotopic data, starting at the oldest is the Unionville granodiorite, the Clancy granodiorite, the Porphyritic granodiorite, the Biotite adamellite, and the Biotite granite. Intrusive contacts exist between some of these phases but not between the Porphyritic granodiorite stock and the northwest boundary of the batholith. Contacts between the stock and the batholith may be concealed under a thick volcanic cover. There is a septum of sedimentary strata which separates the stock from the batholith, but it disappears under the volcanic cover as well. Knopf's conclusion was thus inferential, based primarily on the level of SiO_2

content of the rocks in the stock and the radiometric age date which placed it temporally between the Clancy granodiorite and the Biotite adamellite. Most U.S.G.S. maps show the Porphyritic granodiorite as a stock until further evidence is available to the contrary.

Another facet of the problem with the Porphyritic granodiorite is that it is a member of the sodic magma series and therefore could not be part of the intrusive sequence suggested by Knopf although it is temporally related. Evidence for the establishing of the Porphyritic granodiorite as a pluton representing the sodic magma series is presented later in this paper and is based on major element chemical data.

The position of the Biotite granite in the intrusive sequence is also dubious. Knopf (1963) considered it to be the final intrusive phase based on the amount of SiO_2 present in these rocks and the anorthite content of the plagioclase. Intrusive relations for the Biotite granite are not obvious except that it intrudes the Clancy granodiorite in certain locations. Biotite granite does not, however, show any intrusive relations with the preceding Biotite adamellite.

Becraft, et al. (1963) describes a variety of the Butte quartz monzonite called the "mla" unit which petrographically resembles the Biotite granite. This unit shows sharp as well as gradational contacts with adjacent Butte quartz monzonite units. Becraft attributes the presence of these textural and composition variations to "intermittent movement and mixing between fractions of a single magma that had reached different degrees of crystallinity". The greatest amount of variation in the unit types occurs near contacts which is also the position of the Biotite granite in the batholith. On the basis of structural criteria and petro-

graphic data, presented later, it can be stated that the Biotite granite is probably a facies of the Butte quartz monzonite.

Considering the two modifications on the intrusive position of the Porphyritic granodiorite and the Biotite granite, it can be said that the Boulder batholith is composed of plutons derived from two magmatic sources, as suggested by R. I. Tilling (personal communication, 1971), which operated simultaneously over a relatively short period of time. The products of the main magma series on sequence of intrusion are the Unionville granodiorite and its time equivalent Burton Park pluton, the Butte quartz monzonite and its related facies, and, finally, the Biotite adamellite. The products of sodic magma series intruded contemporaneously with the main series are the Rader Creek, the Donald, the Hell Canyon, the Climax Gulch, and the Porphyritic granodiorite plutons.

III. X-RAY EMISSION MICROANALYSIS

The following is a brief discussion of some of the fundamentals of X-ray emission microanalysis, colloquially known as electron microprobe analysis. The subjects discussed are 1) an outline of the general principles of operation of the electron microprobe, 2) some aspects of sample preparation, and 3) a discussion of quantitative analyses with electron microprobe. In preparing the discussions on these three topics, review articles by the following authors were heavily drawn upon: J. V. Smith (1965), Sweatman and Long (1969), Keil (1967), Beaman and Isasi (1970), and White (1970).

A. General Operational Principles

The electron microprobe is presently the principal non-destructive technique for micron scale elemental chemical analysis of solids. It can be used routinely in analysis of all elements heavier than beryllium (Z=4).

The electron microprobe works by producing a finely focused beam (probe) of high energy electrons which, upon striking the surface of the sample, produce an X-ray spectrum containing the characteristic lines for each element present in the volume of the sample penetrated by the beam. X-ray spectrometers are used to disperse the X-ray spectrum and to measure the characteristic X-ray intensities, which are related to elemental concentration. As in other instrumental techniques, intensities from unknown samples are compared with intensities from the same element in a standard of know composition.

Not all electrons that strike the surface of the sample become

absorbed. A significant fraction of the incident beam may be elastically scattered back from the sample. At a given accelerating potential, the backscatter coefficient is a function of the average atomic number of the target material.

The beam is generally focused to a spot as small as 0.2 microns, although it is usually 1 to 2 microns in diameter. Upon penetrating the surface, the electrons begin a sort of "random walk" and diffuse into a volume that is generally considered a sphere buried beneath the surface (Fig. 5). The range of the electron beam (size of sphere) is a function of accelerating voltage of the beam and the density of the specimen. It is the volume of this sphere that limits the spatial resolution in probe analysis, and not the minimum spot size.

X-rays generated in the specimen as a result of the electron bombardment emerge from the specimen surface in a hemisphere. Because of the minute size of the X-ray source, it is essential to use curved crystal X-ray spectrometer to disperse the emerging spectrum. Use of flat crystal spectrometers would result in prohibitively low count rates (White, 1970).

Most electron microprobes accommodate two to four spectrometers simultaneously thus allowing analysis for more than one element at a time.

B. Some Aspects of Sample Preparation

Sample preparation has a considerable effect on the quality of the results obtained in electron microprobe analysis, since the analyses are made in the outermost part of the specimen, generally less than 2 microns in depth. Surface preparation is therefore critical. Care must

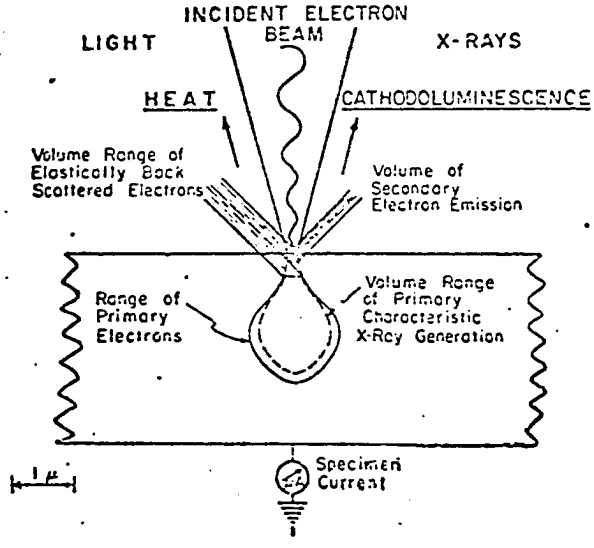

Fig. 5. Schematic summary of phenomena occurring in a target bombarded by a finely focussed electron beam. Shown in cross-section (White, 1970).

be taken to have a flat, smooth surface which has not been disturbed chemically. Surface roughness affects the electron backscatter, the generation of X-rays, and the absorption of the emitted X-rays (Sweatman and Long, 1969).

Many preparations are complicated by the polishing agent used. It is necessary to avoid using grinding or polishing media that contain elements to be analyzed in the specimen. Some specimens, such as glasses, can be prepared by breaking the sample and thus exposing a smooth fracture surface.

Certain materials are electrical insulators. It is therefore necessary to provide a conductive path to ground the electron beam. This is done by vacuum evaporation of a conductive material, such as carbon, aluminum or chromium, onto the prepared surface of the specimen. It is important to coat standards and unknowns with identical thickness because electron energy losses occur in the coating that affect intensities of emerging X-rays.

Although some materials are conductive, they have high resistivities. In analyses of these materials it is necessary to provide additional conductive paths in the form of silver paint strips from the specimen holder to a close proximity of the area under analysis. Poor conductivity to ground lowers the accelerating potential of the beam, thus reducing X-ray generation efficiency.

C. Analysis with Electron Microprobe

Quantitative analysis with electron microprobe requires the use

of a correction equation which converts apparent concentration of an element in a compound to the true concentration. This correction equation takes into consideration matrix effects which are due to differences in absorption, fluorescence, and atomic numbers of the elements in the unknown and the standard. The accuracy of calculated corrections is affected by the accuracy of the values substituted in the correction equation, namely the accuracy in the composition of the standard and the accuracy of the constants used in the formula, such as mass absorption coefficients of various elements. The accuracy of measurements with electron microprobe can therefore range from ± 3 percent or less, if great care is used in selection of standards and all matrix corrections are applied, to ± 20 percent if there are no matrix corrections and a discussion of factors necessitating the corrections are reviewed by Keil (1967) and Smith (1965).

Factors limiting the accuracy of measurements in this study are predominantly related to the standards used. Since zircon standards are not available for electron microprobe analysis, pure element standards were used for the analysis of zirconium, hafnium, yttrium, thorium, and uranium. Quartz (SiO_2) was used as a standard in the analysis for silicon. Only one standard was used in the analysis of each element. The composition of the standards did not approach the composition of the zircon, since zircons are silicates and the standards are pure metals. Also, the quantity of each element in zircon and standard differed greatly. Because of these differences between zircon and the standards used in their analysis, the measurements in this study, after the necessary matrix corrections, are accurate to ± 10 percent or better of the amount present.

The analyses for zirconium and silica are more reliable than those for hafnium, yttrium, thorium, and uranium since zirconium and silica are the most abundant elements in zircon whereas hafnium, yttrium, thorium, and uranium are present in amounts around 1 percent or less and are less homogeneously distributed, thus also affecting the precision of their analysis. Since oxygen is usually determined by difference, its value will be the weight percent oxygen, plus any elements that were not analyzed.

In order to improve accuracy in zircon analysis with electron microprobe, it would be advisable to resort to a series of synthetic zircon standards whose compositions would approach that of natural zircons. These synthetic zircons would have to be accurately analyzed and tested for homogeneous distribution of elements. Keil (1957) states that homogeneity in synthetic standards is very difficult to achieve and is therefore a serious problem in microprobe analysis, since it affects the precision of analysis.

The precision of readings in microprobe analysis, as in other methods of analysis, depends on the stability of the instrument used and the condition of the sample. The precision expected from a stable instrument is $\pm$ 1 percent or better of amount present (Keil, 1967). The mean relative error in this study is 0.8 percent.

IV. ZIRCON CRYSTAL CHEMISTRY AND PARAGENESIS

A. Introduction

Zircon ($ZrSiO_4$) is the chief mineral of zirconium and hafnium in the earth's crust. Interest in zircon is derived from its widespread distribution in igneous, sedimentary, and metamorphic rocks, its high melting point, its resistance to recrystallization and alteration, and its application in radiogenic age determinations.

Historically, zircon has received much attention in igneous petrology. Inquiry into the "granite" problem during the 1930's and again in the 1950's gave momentum to quantitative zircon studies as zircons were thought to provide information on the petrogenesis of granitic rocks (Poldervaart, 1956).

The following is a review of the crystal structure, the chemistry, and the paragenesis of zircons. Although zircons do occur in sedimentary and metamorphic rocks, their presence in these rocks is often relict. This review, therefore, is limited to their presence in igneous rocks only.

B. Optical and Physical Properties

Zircon is an uniaxial positive mineral, with strong dispersion and extreme birefringence. Optical properties vary with zircon composition and the various states of crystallinity. The original crystal may occasionally alter to an amorphous state and thus become metamict due to radioactive effects of uranium and thorium. With increasing degrees of metamictness, dispersion, birefringence, hardness and density of

zircon decreases (Deer, et al., 1962). Table 3 illustrates this variation.

TABLE 3

OPTICAL AND PHYSICAL PROPERTIES OF ZIRCONS
IN VARIOUS STATES OF CRYSTALLINITY (WINCHELL, 1951)

	Normal Zircon	Intermediate Zircon	Metamict Zircon
No	1.92 - 1.96	1.90 - 1.92	1.76 - 1.90
Ne	1.96 - 2.02	1.92 - 1.96	1.76 - 1.92
Ne-No	0.04 - 0.06	0.02 - 0.04	0.00 - 0.02
Sp. gr.	4.6 - 4.7	4.2 - 4.6	3.9 - 4.2
H	7.5	7	6

Zircons are colored yellow, brown, gray or colorless. In thin section they are colorless to pale brown or gray. Pleochroism is not seen in thin section.

Large zircons commonly form square prisms, are moderately elongate, and are terminated by pyramid faces. Small crystals of microscopic size have numerous habits with differing degrees of prism and pyramid faces. The most common forms are {111}, {100}, {110}, {221}, and {131}. (See Fig. 6). Twinning, although uncommon, occurs on {111}. Zircon has poor prismatic {110} cleavage.

Internal structures of zircons include inclusion, zoning, and zenocryst cores. Inclusions consist of gas, gas-fluid, or mineral phases. Mineral phase inclusions concist of minute uraninite or thorite cubes or, most commonly, needles of zircon, apatite, xenotime and rutile. Zoning is common, particularly in cored crystals.

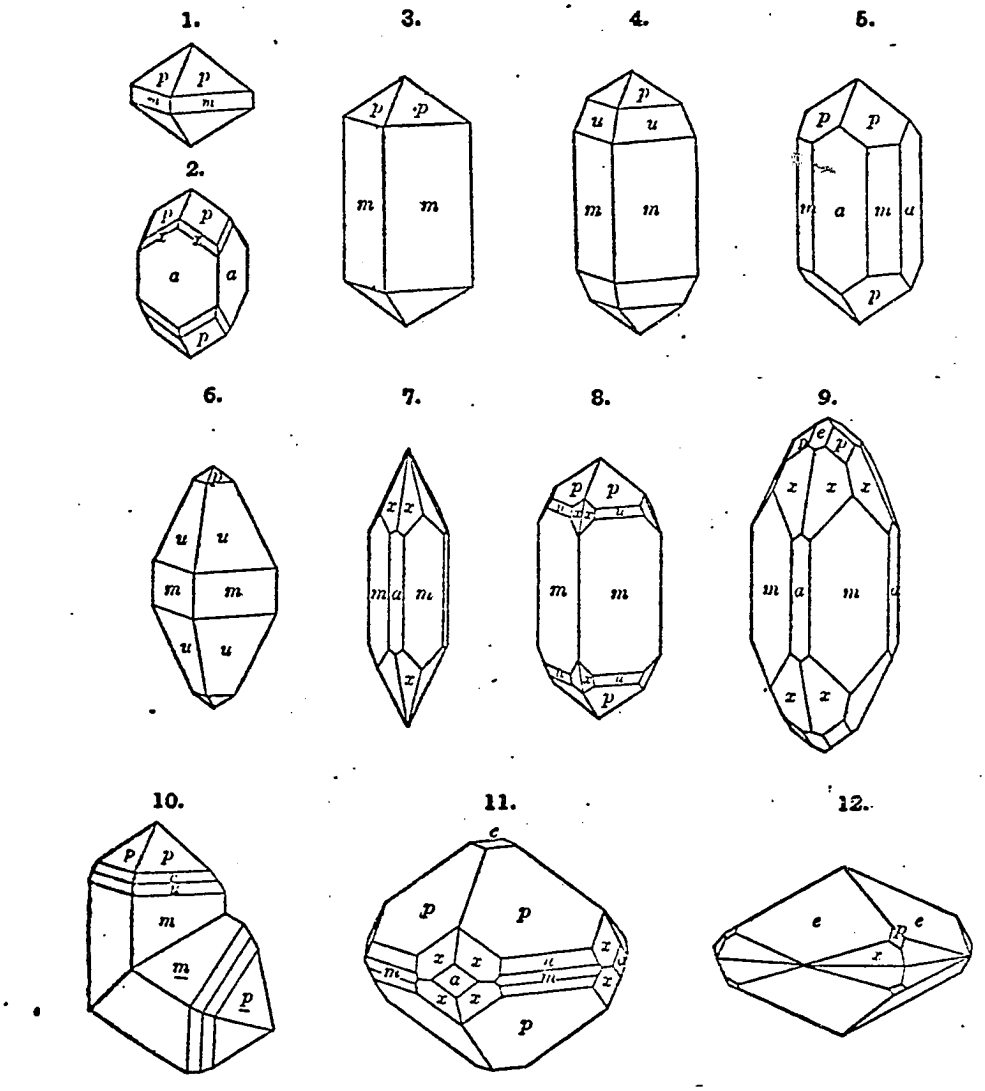

Fig. 6. Some crystal habits of zircon.
1-5, Common forms; 6, Pitcairn, N. Y.; 7, Ural, U.S.S.R.; 8, N. Carolina; 9, McDowell Co., N. C.; 10, Renfrew Co., Canada; 11, Cheyenne Mt., Colorado; 12, Tomsk, U.S.S.R.
(After Dana, 1893)

Common forms illustrated: m{110}, a{100}, c{001}, p{111}, x{311}, u{331}, e{101}, v{221}.

C. Crystal Structure

Zircon belongs to the tetragonal crystal system and has an orthosilicate structure. It belongs to space group I 4/a md.

The principal structural unit in zircon is a chain of alternating, edge-sharing SiO_4 tetrahedra and ZrO_8 triangular dodecahedra extending parallel to the c-axis. The chains are joined laterally by edge-sharing dodecahedra and are thus responsible for zircon's prismatic habit, its {110} cleavage, its birefringence and optically positive character (Robinson, et al., 1971) (Figs. 7 and 8).

Recent investigation shows that oxygen in zircon by Robinson, Gibbs, and Ribbe (1971) have refined the cell dimensions, the O-O distances in the SiO_4 tetrahedron, the Zr-O distance and the Zr-Zr distance in this mineral. This study shows that oxygen in zircon is coordinated in a planar array by one silicon at 1.622 Å and two zirconiums at 2.131 and 2.268 Å (Fig. 9). The two O-O edges shared by the ZrO_8 dodecahedron are short, 2.430 Å, and opposite the O-Si-O angle of 97.0°. The unshared edges are 0.32 Å longer opposite the O-Si-O angle of 116.1°.

The ZrO_8 polyhedron can be best described as a triangular dodecahedron (Fig. 10). The two edges are shared by SiO_4 groups and four others with other dodecahedra (2.494 Å). There are two sets of unshared edges, eight at 2.842 Å and four at 3.071 Å. There are two non-equivalent Zr-O distances. The Zr-O bonds to the edges shared between tetrahedra and dodecahedra are both 2.268 Å; those to edges shared by dodecahedra are 2.131 and 2.268 Å, as are those to the eight short unshared edges. The bands to the four long unshared edges are 2.131 Å (Robinson, et al., 1971). Table 4 summarizes the interatomic distances and angles in zircon.

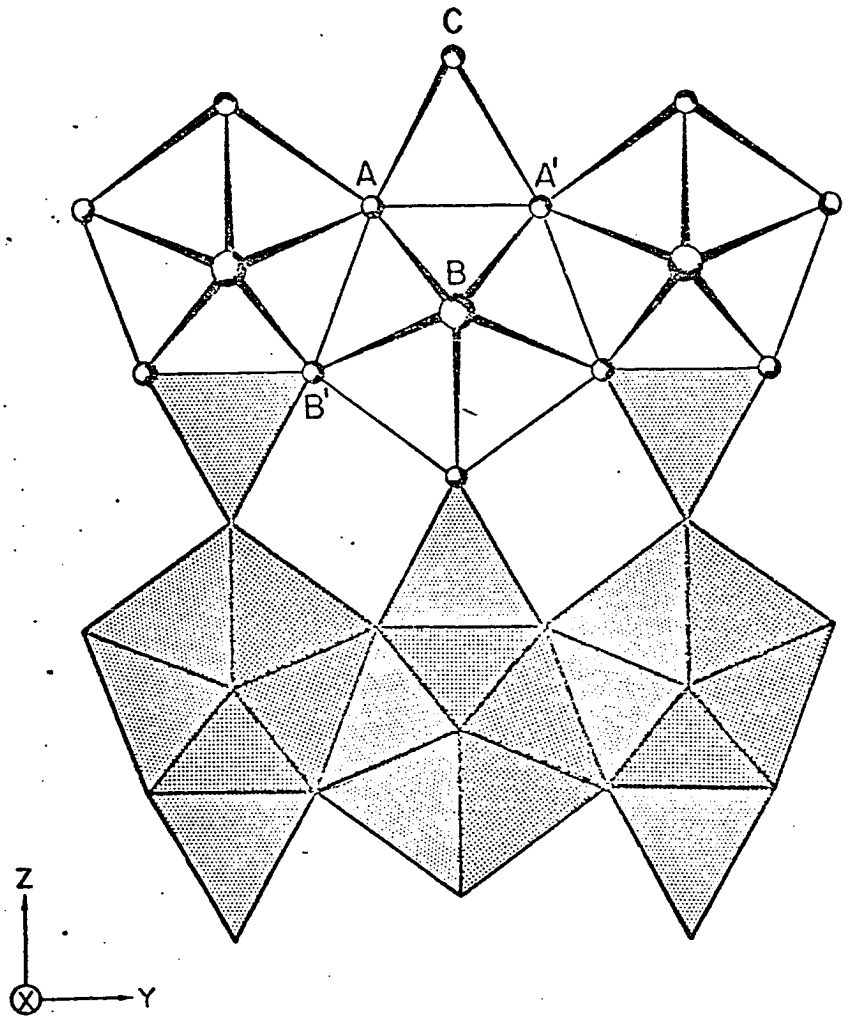

Fig. 7. Chains of alternating edge-sharing SiO_4 tetrahedra and ZrO_8 triangular dodecahedra extending parallel to c and joined laterally by edge sharing dodecahedra (Robinson, et al., 1971).

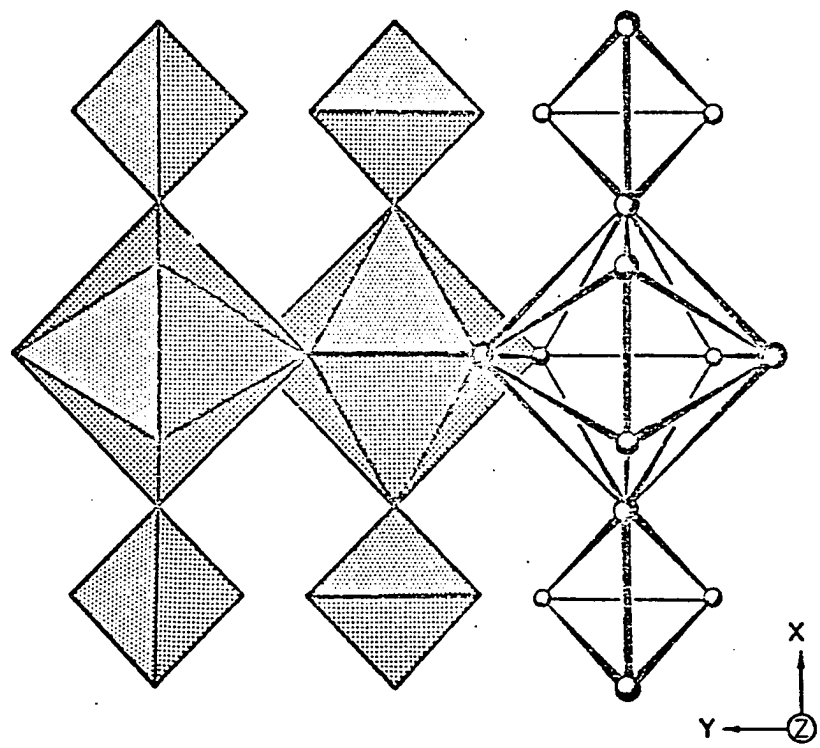

Fig. 8. The chains of alternating edge-sharing SiO_4 and ZrO_8 dodecahedra projected on {001} and showing the sharing of the edges between dodecahedra (Robinson, et al., 1971).

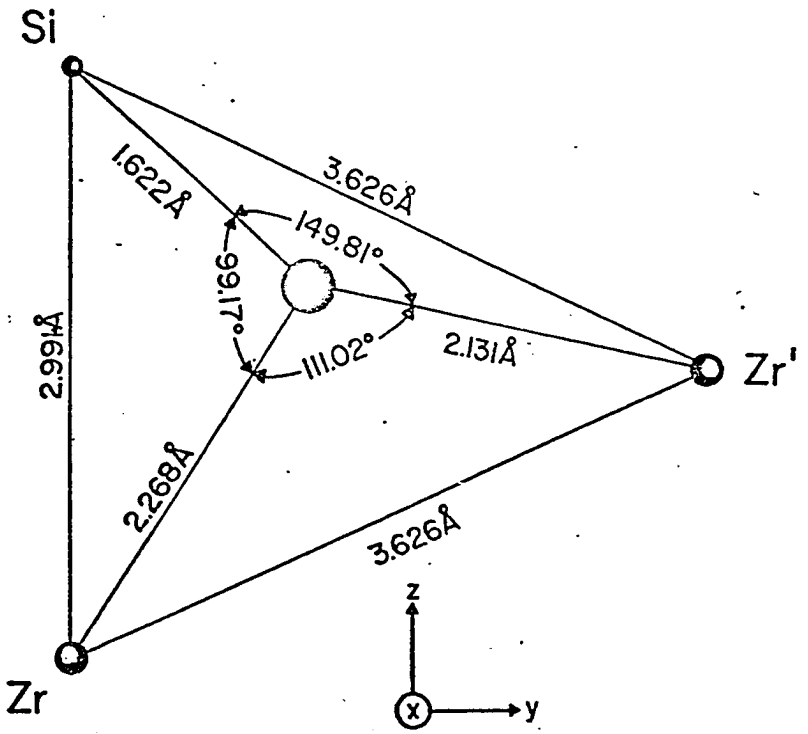

Fig. 9. The coordination, interatomic distances and angles for oxygen (Robinson, et al., 1971).

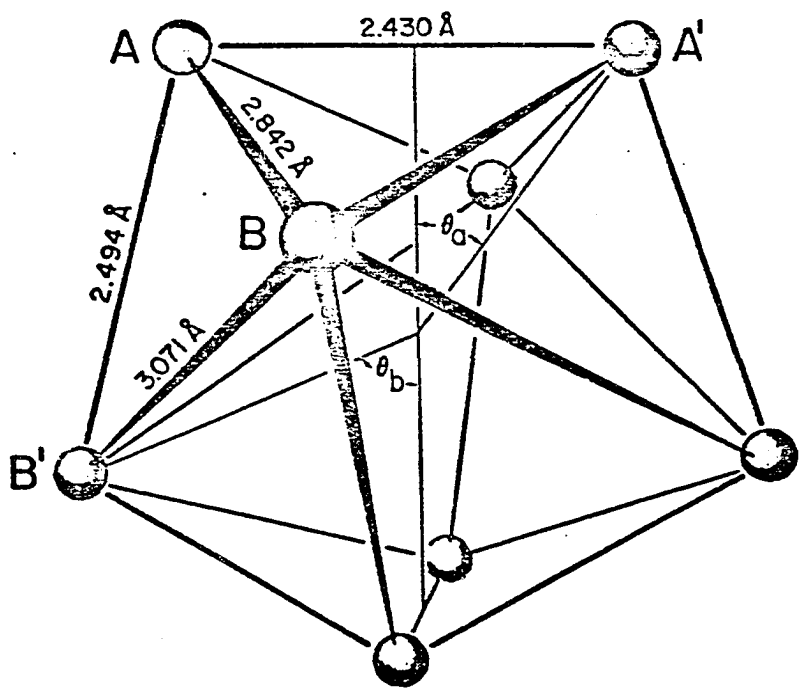

Fig. 10. The ZrO_8 triangular dodecahedron. This volume represents the Zr site in zircon (Robinson, et al., 1971).

TABLE 4

INTERATOMIC DISTANCES (Å) AND ANGLES (DEGREES)
IN A ZIRCON CRYSTAL FROM KRAGERO, NORWAY
(Robinson, et al., 1971)

SiO_4 Tetrahedron			
Si-O	[4][a]		1.622 (1)[b]
O–O Distances			*Angles at Si*
O–O	[2]	2.430 (2)[c]	97.0 (1)
O–O	[4]	2.752 (2)	116.06 (8)
	Mean	2.645	109.71
ZrO_8 Triangular Dodecahedron			
Zr–O(A)	[4]		2.268 (1)
Zr–O(B)	[4]		2.131 (1)
	Mean		2.200
O–O Distances			*Angles at Zr*
O(A)–O(A′)	[2]	2.430 (2)[c]	64.8 (1)
O(A)–(B)	[8]	2.842 (1)	80.41 (2)
O(A)–O(B′)	[4]	2.494 (2)[d]	69.00 (5)
O(B)–O(B′)	[4]	3.071 (2)	92.23 (1)
	Mean	2.770	78.77
Cation—Cation Distances			*Angles at oxygen*
Zr–Zr′		3.626 (2)	111.02 (5)
Zr–Si		2.991 (2)	99.17 (6)
Zr′–Si		3.626 (2)	149.81 (5)

[][a] Multiplicity.
()[b] Estimated standard deviations refer to the last decimal place.
[c] Edge shared between tetrahedron and dodecahedron.
[d] Edge shared between two dodecahedra.

D. Chemistry

The theoretical composition of zircon is 67.1 wt. % ZrO_2 and 32.9 wt. % SiO_2. In most crystalline varieties the content of impurities is low. Metamict varieties show substantial deviation from the theoretical composition with a decrease in Zr and Si and an increase in water and other elements.

Table 5 is a modified compilation by H. Görz (unpublished) of all elements reported in zircons from the literature through 1967. The majority of these chemical analyses of zircons include the elements that are present in zircons as separate phases such as inclusions but are not contained within the crystal lattice of the mineral.

It has been determined that the zirconium site in the zircon lattice is a triangular dodecahedron. This volume is asymmetrical, which suggests that there would be a preference for the transitional elements since they have polarized electron orbits (Lippard, 1967). The evidence for this preference is shown in the fact that the most common elements in zircons are transitional.

An eight-fold oxygen coordinated site requires elements with relatively high valences (+3, +4). In zircon the volume of the zirconium site is relatively small, which would require an element with a small (0.82 Å) ionic radius. Thus, on the basis of valence and ionic radius criteria, all transitional elements except those in columns IIIB and IVB may be eliminated. The valences of scandium and titanium are correct for possible incorporation into the zircon lattice, but they seem to have ionic radii which are too small for an acceptable fit. Because of this process of elimination, it is predictable that zircons are most commonly

TABLE 5

TRACE ELEMENTS IN ZIRCONS
(Modified after H. Görz)

8 coordination ionic radia calculated from the Born equation.

*unreliable or single reported value

Element	Min. reported (ppm)	Max. reported (ppm)	Charge	8-fold Ionic Radium (Å)	Ionization Potential (volts)
Be	1	2000	+2	0.39	18.14
Mg	7	6750	+2	0.79	14.97
Ca	200	30000	+2	1.03	11.82
Sr	15	500	+2	1.38	10.98
Ba	80	10000	+2	1.39	9.95
Ra		100*	+2	1.48	10.10
Na		4375*	+1	1.01	5.14
K		2320*	+1	1.38	4.34
Cr	30	200*	+3	0.65	32.1
Mn	2	12000	+4	0.93	52.0 (?)
Fe	70	100000	+2 (+3)	0.77 (0.66)	16.24
Ni	2	50	+2	0.72	18.13
Cu	1	500	+2	0.75	20.28
Zn	20	6000	+2	0.77	17.89
Ag	1	50*	+1	1.36	7.57
Au		30*	+3	0.88	31.0
W		200*	+4	0.73	61
S	2505	2880*	+4	0.38	47.08
H_2O					
B	10	50*	+3	0.24	37.75
Al	150	40000	+3	0.53	28.31
Sc	10	1000	+3	0.74	24.64
Y	30	85000	+3	0.95	20.6
La	60	8000	+3	1.18	19.2
Rare earths	11	57300			
-Yb	11	1500	+3	0.89	
-Ce	250	5000	+4	0.97	36.7
-Er	900	18400	+3	0.92	
-Gd	150	500	+3	1.01	
-Dy	300	500	+3	0.95	
Hf	40	288000	+4	0.81	31.0
Th	2	100000	+4	1.06	24.4
Pb	1	100000	+4	0.87	43.93
U	10	72900	+4	1.01	
Sn	5	5000*	+4	0.74	40.57
Ti	30	2000	+4	0.70	44.66
P	40	11480	+5	0.36	64.74
V	10	1295	+4	0.65	48.3
Nb	30	7000	+4	0.77	49.3
Ta	110	150*	+5	0.70	44.8
Sb	150	700*	+5	0.64	55.7
Bi	2	5000*	+3	1.00	25.42
Zr			+4	0.82	33.83

composed of Zr, Hf, Y, the rare earth members of the lanthanide series, and some members of the actinide series.

Empirical rules established to predict the behavior of elements state that, generally, elements with the highest charge, the largest ionization potential, and an ionic radius equal to or slightly smaller than the size available at the lattice site will be preferentially incorporated into that site. In discussing ionic radii it is essential to use the radius for the proper coordination number since ionic radius varies as a function of coordination number. This relation is demonstrated in the following reduced version of the Born equation:

$$\frac{r_p}{r_m} = \frac{p^{1/n-1}}{m} \qquad \text{(Wells, 1962)}$$

where r_p and r_m are the apparent radii for coordination number p and m. n is a constant with the value of 9.

Zirconium is the ideal candidate for the triangular dodecahedral site in the zircon lattice, since it has a +4 charge, an ionic radius of 0.82 Å and the highest ionization potential (33.83 volts) of the common candidates for the site. Due to the lanthinide contraction, hafnium, located directly below zirconium, has almost identical properties to zirconium (Cotton and Wilkinson, 1967), with a +4 charge, an ionic radius of 0.81 Å, and an ionization potential of 31.0 volts. It is due to this great similarity that hafnium is the next most abundant element in zircons. HfO_2 content in zircon varies from 0.2 weight percent (Fleischer, 1955) to 31 weight percent (Vlasov, 1966). Both of these values represent extremes. The ratio of Hf/Zr in zircons has been shown to increase with progressive differentiation and increase in SiO_2 of silicate melts (Godfried and Waring,

1964; Kosterin, et al., 1963; Kosterin, et al., 1958; Lyakhovich and Shevaleyvskii, 1962; Lipova and Shevaleyesvkii, 1961; Lipova, et al., 1957; Pavlenko, et al., 1957; Tugarinov, et al., 1956). These studies were often made in areas where consanguity of intrusive phases was obvious chemically and through field relations.

Yttrium is commonly found in chemical analyses of zircons. Dennen and Shields (1956) suggest that Y enters the zircon lattice isostructurally as xenotime (YPO_4). Recent studies involving the use of the electron microprobe for zircon analysis by Görz and White (1970) indicate that isostructural substitution may not always be the case since the amount of Y present in a "spot" was generally higher than the amount of P necessary to form xenotime. They also discovered that the distribution of Y and P varies from "spot" to "spot" in each grain. The atomic properties of yttrium do not necessitate a coupled substitution because of ionic radius of yttrium is 0.92 Å and it has an ionization potential of 20.6 volts which makes Y the third best candidate for the zirconium site. They did not, however, analyze for elements such as cerium and other rare earths which may possibly enter the zircon lattice as phosphates and thus contribute to the degree of variation of Y and P.

Zircons are characteristically high in yttrium earth elements (ΣY = Y + Gd, Tb, Dy, Ho, Er, Tm, Yb, and Lu) and low in the cerium earth elements (ΣCe = Ce, Pr, Nd, Pm, Sm, and Eu) (Vlasov, 1966). Very little is known about the atomic properties of the rare earth elements. In accessory minerals of granitic rocks the $\Sigma Y/\Sigma Ce$ ratio increases with differentiation. Since most of the rare earth elements are locked up in the accessory minerals, the same trend is observed in whole rock analyses for these two

elemental groups (Lyakhovich and Barinskii, 1961; Leonova and Balashov, 1963).

The presence of thorium and uranium in zircons favors their use in radiometric age-determinations. Zircons containing these elements tend to become more metamict with time due to radioactive decay (Holland and Gottfried, 1955). Mumpton and Roy (1961) experimentally showed that the presence of Th in zircons is due to the zircon ($ZrSiO_4$)-thorite ($ThSiO_4$) limited solid solution. The limit of the solid solution was found to be less than 3 mole percent of thorite in zircon at 800°C and 1500 bars. Thorium is a poor candidate for the zirconium site in zircon because of its large (1.05 Å) ionic radius. It is possible that thorium enters the lattice at high temperatures when the zircon lattice is expanded. However, during cooling thorium may become unstable in the shrinking lattice and may, therefore, exsolve as a thorium rock phase or a thorite inclusion. Görz and White (1971), using the electron microprobe and scanning electron microscope to study inclusions in zircons, discovered that Th in addition to Ca, Al and Fe form separate phases in zircon and are not part of the zircon lattice. They have not yet been able to identify this exsolved phase mineralogically.

Uranium behaves in a similar manner to thorium in zircons, since it too has a large ionic radius (1.01 Å). Mumpton and Roy (1961), studying the system ZrO-SiO_2-UO_2, experimentally determined that there exists a limited solid solution of the hypothetical "$USiO_4$" molecule in zircon. During cooling and shrinkage of the zircon lattice, the uranium may exsolve and form a separate phase such as the one described by Görz and White (1971).

The behavior of thorium, uranium, and the rare earth elements in

accessory minerals from granitic rocks have been studied by Lyakhovich and Barinskii (1961). They suggested the increase in Y and U with differentiation and a decrease in Ce and Th content. Since accessory minerals tie up most of the Th, U and rare earth elements, a study by Leonova and Balashov (1963) of the rocks from the Susaniyr batholith showed the same relation between these elements. This relationship also holds for zircon specifically, as shown by Lyakhovich and Shevaleyevskii (1962).

The study of the distribution of elements within individual zircon grains from granites show that both U and Th are concentrated at the periphery of grains (Silver and Deutsch, 1963); however, electron microprobe traverses indicate an increase in the U/Th as well as the Hf/Zr ratio from the center of the grain outward (Veniale, et al., 1968). The average U/Th ratio for zircons from granites is 2.6 (Hurley and Fairbairn, 1957). The Y content of the zircons also increases from the center towards the periphery (Veniale, et al., 1968; Görz and White, 1970).

Although some of the elements with large ionic radii are exsolved from the zircon lattice during cooling, thus forming inclusions, inclusions can also be incorporated into a mineral by capture during crystal growth as has been described by Roedder (1962). Investigation by means of scanning electron microscope and microprobe will shed light on the relationship of elements in reported zircon analyses.

E. Paragenesis

Zircons have been reported from almost all igneous rock types. The discussion of zircon paragenesis in this section will be essentially

limited to the granitic rocks with a few comments on the other rock types.

In rocks of basaltic composition, zirconium is low (10-170 ppm) and is probably contained in the magnesian pyroxenes during the early stages of crystallization (Wager and Mitchell, 1951). During the later stages of crystallization when and if amphiboles replace pyroxenes, the zirconium may become redistributed and form euhedral or subhedral zircons. Some of the zirconium is still contained in the lattice of amphiboles until the biotite begins to replace amphiboles. At this time zirconium again redistributes itself and is contained primarily in zircons (Vlasov, 1966b). When the redistribution occurs during amphibolization and biotitization, some of the zircons may crystallize from the melt directly whereas others may form by the exsolution of zirconium from the lattices of the primary minerals (Vlasov, 1966b).

In alkaline rocks, zircons may begin crystallizing either early or late from a melt and form either euhedral or anhedral zircons. In peralkaline rocks, zircons are supplanted by zircono-silicates which concentrate the zirconium from the cooling melt (Vlasov, 1966).

Most zircon studies have been made in granitic rocks; however there are still questions as to the behavior of zircons in this rock type. There are three divergent views as to the time and range of crystallization of zircons from granitic melts. On the basis of the refractory nature of zircons and the distribution of euhedral zircons throughout the various minerals of granitic rocks, some workers (Wager and Mitchell, 1951; Poldervaart, 1956) have postulated an early and short range of crystallization of zircons from granitic melts. Murthy (1958) supported this view on the basis of the theoretical behavior of zirconium in zircons crystal-

lizing from a granitic melt. The second group suggests that zircon crystallizes late from granitic melts (Moorhouse, 1956). They support their argument with a similar method as the first group, that is, by a statistical study of the incidence of zircon inclusions in different host minerals. The last group considers that zircons crystallize out early in granitic melts, but that they have a long range of crystallization. Their evidence for the early crystallization is that zircons are enclosed in even the most mafic minerals of granitic rocks. The evidence for the long range of crystallization comes from the suggestion that trace element (U, Th, Pb) variation in solid solution forming minor minerals (zircons) is governed by the same petrologic factors (temperature-pressure-bulk composition) that influence major and minor element variation in major elements which crystallize over extended ranges (Silver and Deutsch, 1963). Other studies on the rare earth elements and Hf/Zr ratios of zircons previously mentioned show chemical changes in zircons and their surrounding rock in terms of these elements with progressive differentiation of granitic melts (Lyakhovich and Barinskii, 1961; Leonova and Balashov, 1963; Godfried and Waring, 1964; Kosterin, et al., 1963; others). Microprobe analysis has made possible the study of the chemical zonation of individual zircon crystals. Definite trends are observed in the behavior of elements from the center of zircon grains to their peripheries, such as increase in Y, Th and Hf, and decrease in Zr and U. Uniform chemical change requires time which implies a long period of crystallization.

In summary it can be stated that there seems to be a strong argument for the early crystallization of zircon. Recent chemical data also

overwhelmingly show the long period of crystallization of zircons from granitic melts (Silver and Deutsch, 1963; Godfried and Waring, 1964). It is important to keep these ideas in mind when discussing the statistical studies of zircon population morphologies, since some of the premises on which such studies have been based are not true, as noted above.

V. ZIRCON POPULATION ANALYSIS

Poldervaart (1956) suggests the use of zircon populations in interpreting certain aspects of the petrogenesis of granites. The premise on which such interpretations were made was that zircons crystallize very early and almost instantaneously from granitic melts. The morphology, size, and shape of these zircons were presumed to reflect the physiochemical conditions of the early melt (Buckley, 1951). Since zircons were also considered to be resistant to subsequent chemical changes in the melt, they would be excellent minerals by which to finger print parent magmas. The petrogenetic implications would be that a parent magma with a defined zircon population could differentiate and intrude as a number of separate intrusives of different rock types; however, evidence for the consanguity of these rock types would be preserved in the zircon population.

In order to quanitatively characterize the zircon populations, the length and width of zircon crystals were determined and then the reduced major axis (RMA) and the mean elongation ratio (MER) were calculated. The RMA is a best fit line to the scatter of points representing the length-width dimensions of the crystals on an x-y plot (Larsen and Poldervaart, 1957). It is calculated by dividing the standard deviation of length by the standard deviation of the width of the zircon crystals (Kermack and Haldane, 1950). This may represent the growth trend of the crystals. The MER is the mean of the length/width ratios of the zircon crystals.

In order to index a zircon population by this method it is necessary

to know the slope, position, and length of the RMA on a plot of the length versus the width of zircon crystals. It is also necessary to know the mean elongation ratio. Intrusives from a common magmatic parent would be expected to have zircon populations which exhibit like slopes, positrons and lengths for their RMAs as well as similar MERs.

The RMA and MER data are generally presented graphically and comparisons between zircon populations are usually made. The data can also be treated numerically, which is preferable when doing analyses of variance.

The use of frequency curves for quantitative zircon population studies was proposed by Smithson (1939), who had little success with them in differentiating zircon populations. Veniale, et al. (1968) however used frequency curves in conjunction with RMA and MER data in zircon population analysis with reasonable success.

The Z test (Imbrie, 1956) has been used extensively to show the significance of variation of the RMA and MER of a fossil population. The present study, involving the zircon populations from the Boulder batholith, has used one factor analysis of variance to test the significance of variation between groups (Table 12). The analysis of variance involves the estimation of the variation within a group and between groups and allows for the assessing of differences when more than one comparison is made. This statistical list is most powerful when equal numbers of samples are available from each group.

Several studies using zircon populations have been made on granitic plutons of different crustal levels in Read's granite series. Alper and Poldervaart (1957) studied the epizonal Animas stock and Larsen

and Poldervaart (1957; 1961) studied two mesozonal plutons, the Bald Rock and the Bald Mountain batholiths using zircon populations. The zircon population in the homogeneous Animas stock was the same throughout the entire body. The relatively homogeneous Bald Mountain batholith also showed a similar zircon population throughout the pluton. However the extremely differentiated Bald Rock batholith showed that zircon populations varied with the zoning. They attributed the variation in zircon populations by appealing to an inhomogeneous initial magma. In all the above mentioned studies, the assumption was the early and short duration crystallization of zircon in granitic melts. The plutons were explained in terms of their zircon population rather than the zircon populations interpreted in light of the petrographic, chemical, and structural information available for the various plutons.

VI. DATA PRESENTATION AND DISCUSSION

A. Introduction

The Boulder batholith is one of the best studied composite epizonal batholiths in North America; however, published maps are available for only the northern two-thirds of the batholith. Sampling for this investigation was therefore limited to those portions where maps were available. Chemical data are available for most of the batholith and are particularly abundant for the southern end where there are plutons representative of both the sodic and more potassic or main magma series as defined by R. I. Tilling (personal communication, 1971).

A total of 94 zircon samples were processed for the statistical analysis of zircon populations. Of these, 35 were analyzed by electron microprobe for six elements (Zr, Hf, Y, Th, U, Si), and 17 were analyzed for three elements (Zr, Hf, Y). An average of four to five grains constituted each sample for the microprobe analysis. The choice of elements was made on the basis of previously published information on the major elemental constituents of zircon and their behavior in zircons (see pages 35-43).

Whole rock chemical analyses were made of six samples from the Porphyritic granodiorite stock, using atomic absorption techniques to determine the magmatic affiliation of that pluton.

Data generated in the course of this study are presented and discussed in this section. There are five parts. Part on deals with the chemical and petrographic data on the Porphyritic granodiorite stock and

the Biotite granite respectively, to determine their affiliation to the other plutons of the Boulder batholith. Part two is a general physical description and chemistry of individual zircon crystals, and is composed of three topics: 1) the general physical description of the zircons, their morphology, zoning, and inclusions; 2) chemical analyses of the zircon crystals and correlation of zircon crystal habit to crystal chemistry; 3) behavior of thorium and uranium in zircon crystals from the Boulder batholith. Part three involves the physical description and the estimated chemistry of populations of zircon crystals and emphasizes two topics: 1) the distribution of the three classes of zircon crystal habit within the plutons and 2) the estimated chemistry of zircon populations within the batholith. Part four is a presentation of data from the statistical analysis of zircon populations based on RMA and MER criteria and the discussion of this data in light of the recent literature and the chemical and crystal habit data generated by this study.

B. Petrographic and Chemical Data on the Boulder Batholith

General Statement

Two aspects of the intrusive history and evolution of the Boulder batholith have not been sufficiently explained in the literature. It is essential that the batholith be well understood, since the object of this study is to determine the degree to which zircons, chemically and morphologically, reflect the history of a composite epizonal granitic body. The two aspects of the batholith's history important in the interpretation of this study's zircon data are the relationship of the Biotite granite to the Butte quartz monzonite and the relationship of

the Porphyritic granodiorite stock to the remainder of the plutons of the Boulder batholith. These two relationships were determined by a petrographic and modal analysis of the Biotite granite and whole rock chemical analysis of the Porphyritic granodiorite stock.

Intrusive Position of the Biotite Granite

Knopf (1957) considered the Biotite granite as the fifth and final phase in the intrusive sequence of the northern portion of the Boulder batholith. This conclusion was based on scanty intrusive relations between the Biotite granite and the Butte quartz monzonite and on chemical data which indicated that the Biotite granite is the most differentiated rock type of the area. Becraft, et al. (1963) described the "mla" unit as a facies of the Butte quartz monzonite, which exhibits structural relationships to the Butte quartz monzonite similar to that of the Biotite granite; that is, it has intruded the adjacent units of the Butte quartz monzonite. However the "mla" unit also exhibits gradational contacts. Becraft, et al., (1963) also recognized that the "mla" unit occurs near the periphery of and is almost enclosed by the Butte quartz monzonite, which is also the disposition of the Biotite granite.

The Biotite granite was studied petrographically and mineral modes for it were determined on two samples (MBA-1 and MBA-2) so as to enable its comparison with the published petrographic and modal data on the "mla" unit (Fig. 11). In hand specimen appearance, texturally, and in terms of mineral composition, the Biotite granite and the "mla" unit are similar. Both can be described as medium-grained, light gray rocks with a specific gravity of 2.61 (Knopf, 1957) and 2.63 (Becraft, et al., 1963) respectively. They are both allotromorphic to hypidiomorphic in texture. Tourmaline

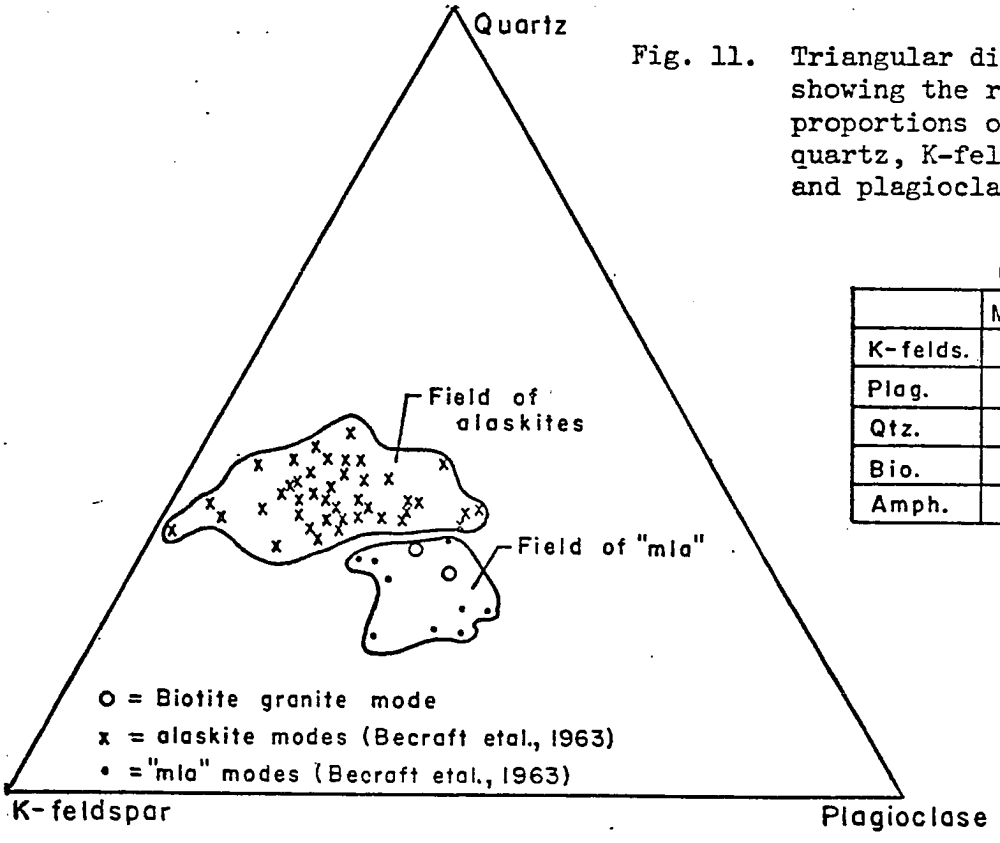

Fig. 11. Triangular diagram showing the relative proportions of modal quartz, K-feldspar and plagioclase.

mode %

	MBA1	MBA2
K-felds.	35	38
Plag.	34	29
Qtz.	26	31
Bio.	4	2
Amph.	1	0

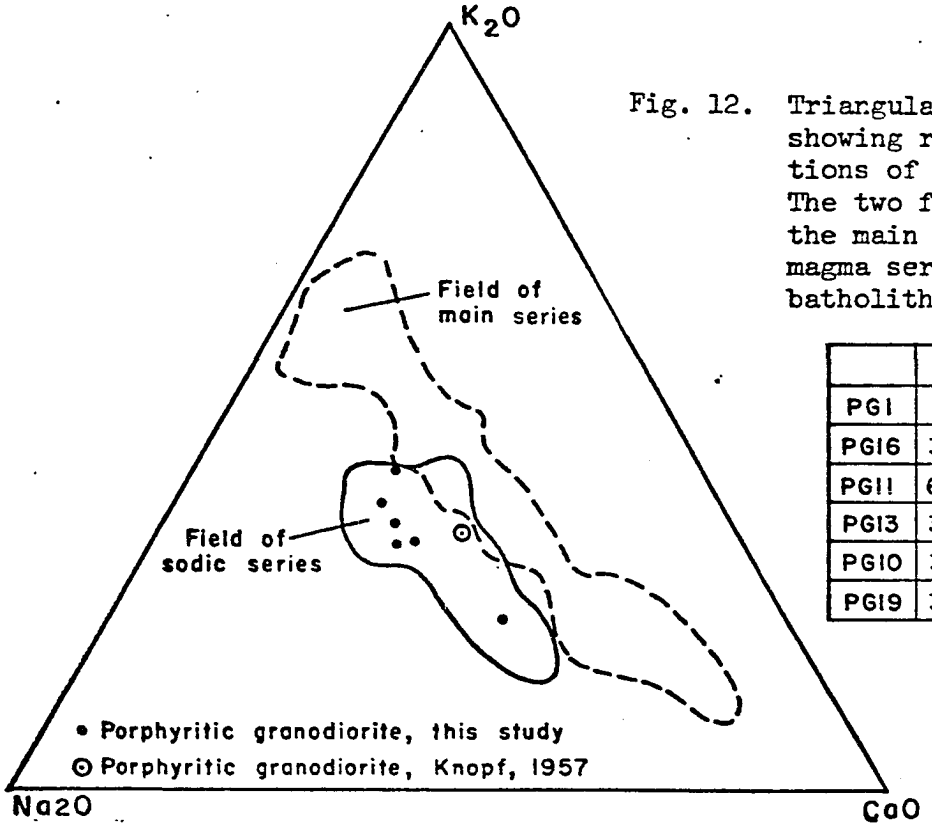

Fig. 12. Triangular diagram showing relative proportions of K_2O-Na_2O-CaO. The two fields represent the main and the sodic magma series of the Boulder batholith (Tilling, unpublished data.

wt. %

	CaO	Na_2O	K_2O
PG1	2.87	4.79	4.65
PG16	3.58	4.58	3.88
PG11	6.30	4.72	3.24
PG13	3.76	5.12	4.29
PG10	3.20	4.79	5.71
PG19	3.28	4.89	4.34

occurs commonly in amounts less than 1 percent but occasionally as much as 4 percent in both. The amount of biotite and amphibole present in the Biotite granite samples falls within the range of these minerals in the "mla" unit (bio. = 2-5%, amph. = 0-7%). They both contain similar proportions of K-feldspar, plagioclase, and quartz as can be seen in Figure 11 since the Biotite granite modes plot within the "mla" field.

The alaskites found in the Boulder batholith have a large range of mineral and textural variation, and some alaskites also contain tourmaline. Figure 11 shows that the two Biotite granite samples plot within the "mla" cluster, therefore rejecting the possibility of Biotite granites being equivalent to the alaskite.

On petrographic evidence, it can therefore be stated that the Biotite granite is equivalent to the "mla" unit, and since the "mla" unit is considered a facies of the Butte quartz monzonite, so can be the Biotite granite. The structural relationship of both of these units with the adjacent Butte quartz monzonite suggests that autointrusion has occurred. The gradational contacts found in the well-exposed "mla" unit may not be as obvious in the poorly exposed northern portions of the batholith from which the Biotite granite has been described.

Magmatic Affiliation of the Porphyritic Granodiorite

The Porphyritic granodiorite stock, consisting of a porphyritic (Kpg) and a non porphyritic (Kgd) phase, was considered by Knopf (1957) to be the third intruded pluton in the intrusive sequence of the northern portion of the batholith. This conclusion was drawn on the basis of the SiO_2 content of the rocks and the anorthite content of the plagioclase. There are no intrusive relations visible between the stock and the rest

of the batholith.

Tilling (personal communication, 1971) suggests, on the basis of Pb and Sr isotope and major element chemical data, that there are two magma series represented in the batholith. The sodic series is represented by the plutons in the southern portion of the batholith, and the more potassic or main series is represented by the remaining bulk of the batholith. Tilling did not place the Porphyritic granodiorite stock into either of the magma series because of insufficient data.

To establish the Porphyritic granodiorite stock as a member of one of the two magma series, whole rock analyses were made on six samples from the stock. The results from the analyses are plotted on a CaO-Na_2O-K_2O diagram (Fig. 12) which contain the fields of the two magma series as defined by Tilling. The analyzed samples fall within the field of the sodic series, as does the single published analysis for the Porphyritic granodiorite (Knopf, 1957). This strongly suggests that the Porphyritic granodiorite is the sole representative of the sodic magma series in the northern part of the batholith.

The above interpretations of the Biotite granite and the Porphyritic granodiorite, in conjunction with the radiometric, Pb-Sr isotope and chemical data, help in refining the general understanding of the intrusive history of, at least, the northern part of the Boulder batholith. It appears that during a relatively short (9 m.y.) period of time, two magma series were simultaneously operating in the small area of the northern part of the batholith. The main magma series, progressively differentiating, was emplaced in sequence as the Unionville granodiorite, the Butte quartz monzonite and the Biotite adamellite. These three plutons are

spatially, temporally, and chemically overlapping. During cooling, differentiation was occurring within each pluton due to the existence of temperature and chemical gradients in the bodies which produced variations in mineralogy and texture in the rocks. This intra-pluton inhomogeneity is in part represented by the Biotite granite or the "mla" unit rock type. Simultaneous with the differentiation and intrusion of the main series, the sodic magma series was also active. In the northern part of the batholith, the Porphyritic granodiorite intruded from the sodic magma series and also differentiated during cooling. Due to the proximity of the two magma series in time and space, a certain amount of mixing of magmas may have occurred.

C. General Physical Description and Chemistry of Individual Zircon Crystals

Physical Description

Zircon populations encountered in granitic rocks have often showed that several crystal habits occur. These various habits have been recognized by Larsen and Poldervaart (1961) and Tomita and Karakida (1958); however, neither of these references have described the crystal habits in any detail. Figure 6 shows some common zircon crystal habits.

In the study of zircons from the Boulder batholith, a variety of euhedral zircon crystal habits were recognized (Fig. 13a). All the habits possess combinations of the simple forms published in Dana (1932, Table 6).

Due to the fact that the interfacial angle measurements on the zircons were made in this study orthographically on photos of crystals lying on the {110} prism face, it is not possible to distinguish between forms {331}, {311} and {131}. Therefore, the ensuing description of the

Fig. 13a. Examples of the three classes of zircon habits recognized from the Boulder batholith. Magnification approximately 450x.

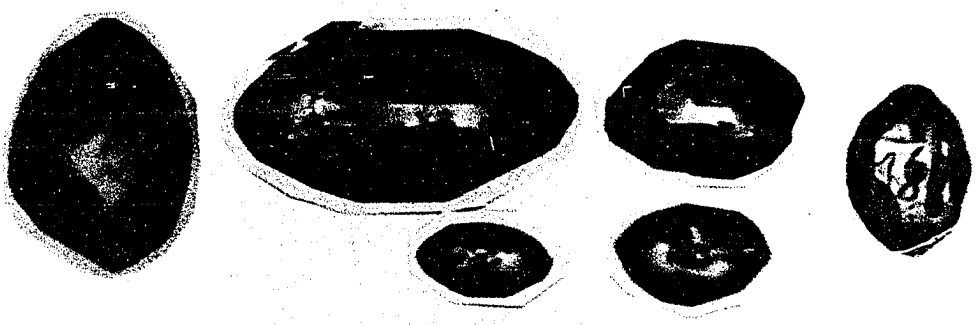

class I

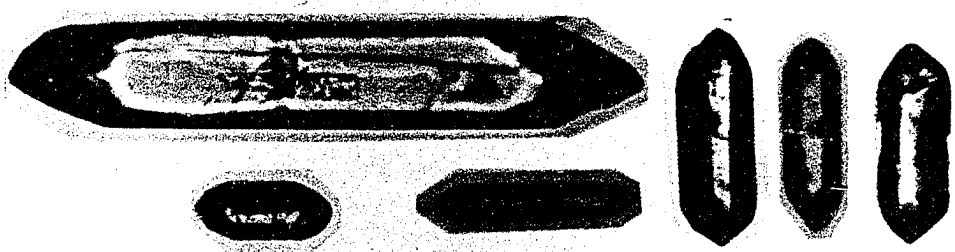

class II

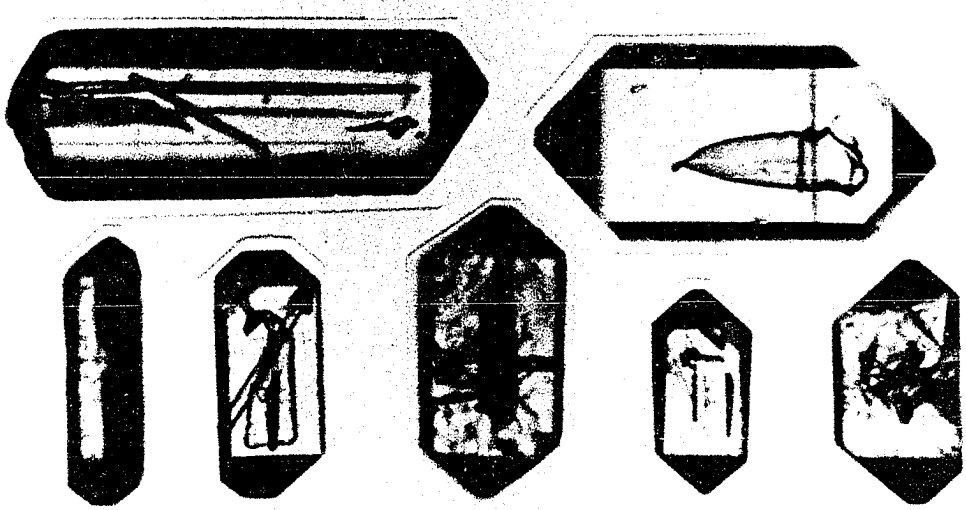

class III

crystal habits will refer to form {331} with the understanding that the form may be either one of the three forms with a 3 in its Miller index.

The three crystal habit classes to be described are transitional in nature. Very few crystals, though, have an exactly equal number of attributes from two classes such that classification is impossible. Generally if two habits are present in a zircon crystal, one habit predominates, and thus the crystal is classified into that crystal habit class.

Class III zircons consist of crystals with the simplest crystal habit containing relatively few faces. They have large {110} prism form and a well developed {111} pyramid form. If a {001} form develops, it is very small. Form {331} does not appear in this crystal habit. If a {100} form occurs it is small. The mean length/width ratio of this class of zircon crystal habit is 2.38.

Class II zircons consist of crystals whose complexity of crystal habit is intermediate. This class has a well developed {110} prism form and a {111} pyramid form. If form {001} develops, it is very small. Form {331} occurs in zircons of this class, but the form is not distributed on all sides of the crystal. The {100} form is developed but it is about half the size of the {110} form. The mean length/width ratio is 2.16.

Class I consists of zircons with the most complex habit. The {110} prism form is small in this class but the {331} form is large and it is distributed on all sides of the crystal. There is always an intermediate sized {111} form and it is the same size as the {001}form. This particular combination of faces gives the zircon crystal a very rounded or football shaped appearance. The mean length/width ratio is 1.47. Figure 13a shows

examples of the three zircon crystal habit classes.

The zircons from the Priest's Pass leucomonzonite are all anhedral. Thin section studies show that they are molded around and between the feldspar crystals and form inclusion zones in the biotite, parallel to the enclosing minerals outline (Fig. 13b-f). Two samples from the Butte quartz monzonite (BS9 and JC6) also contain anhedral zircons which have abundant opaque inclusions. These individual grains are not representative of the zircon populations from the two samples. Due to the abundance of inclusions, the density and the paramagnetic properties of these grains were altered, therefore not providing a high quality, clean separate in the heavy liquid and Frantz isodynamic separator. These anhedral zircons are called class 0.

Due to the high index of refraction of the zircons it is virtually impossible to see the interior of zircon crystals, particularly the crystals with small prism faces. If compositional zoning is present, it is difficult to see for this reason. In some cases growth zones are visible due to opaques which adhered to the surfaces of the crystal during growth. For the same reason, inclusions are also difficult to see. In crystals of habit class III where there is a large prism face, inclusions can be readily observed. No attempt was made by this study to determine the composition of the included phases. Anhedral inclusions such as irregular bubbles consisting of one, two or three phases are present. Solid, opaque phases are generally anhedral also and are possibly composed in part of elements which exsolved from the zircon lattice during cooling. Other inclusions were probably trapped during crystal growth. In general all zircon crystals from the Boulder batholith are clear.

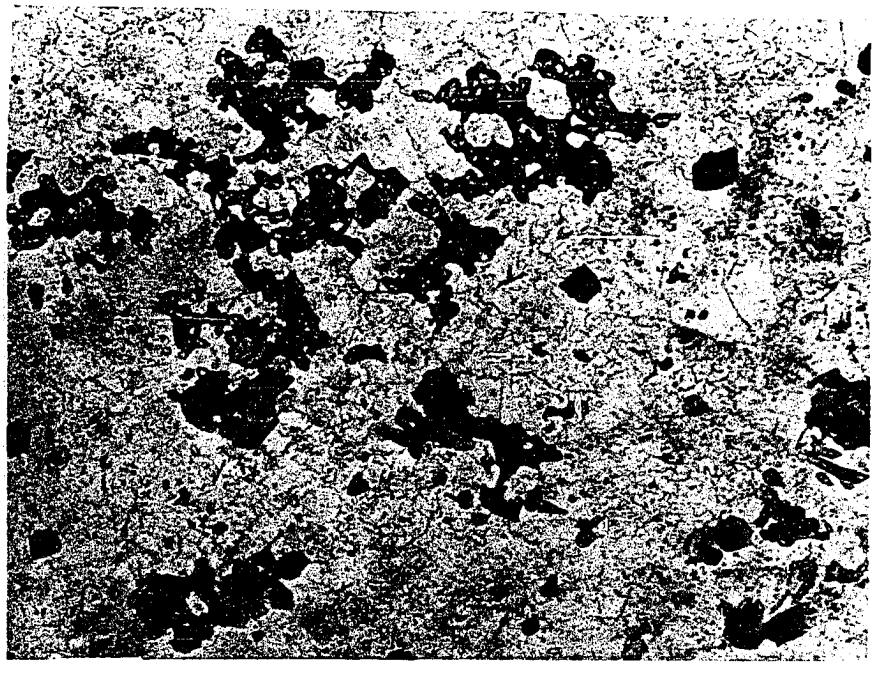

Fig. 13b.

Fig. 13c.

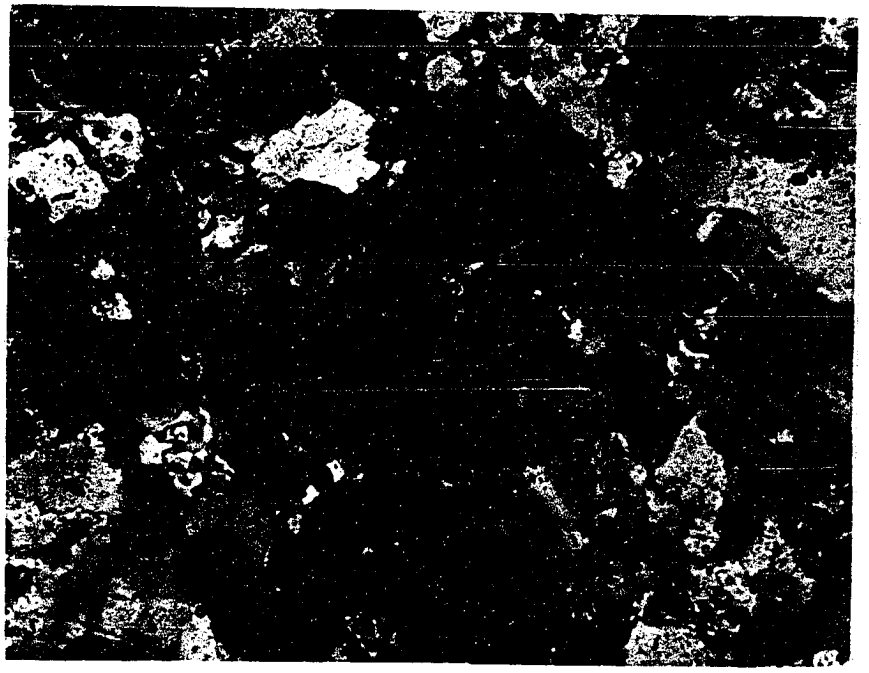

Fig. 13d.

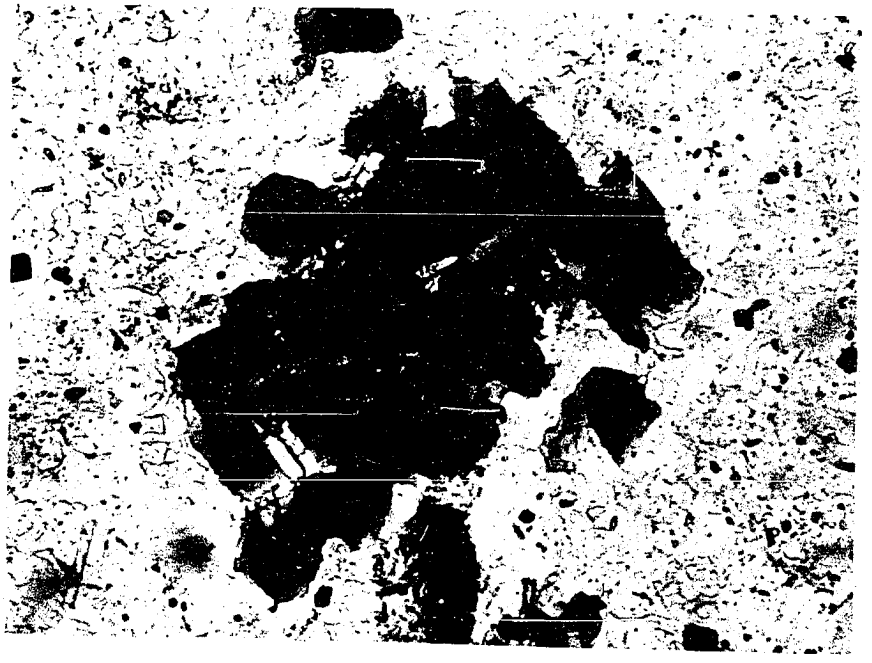

Fig. 13e.

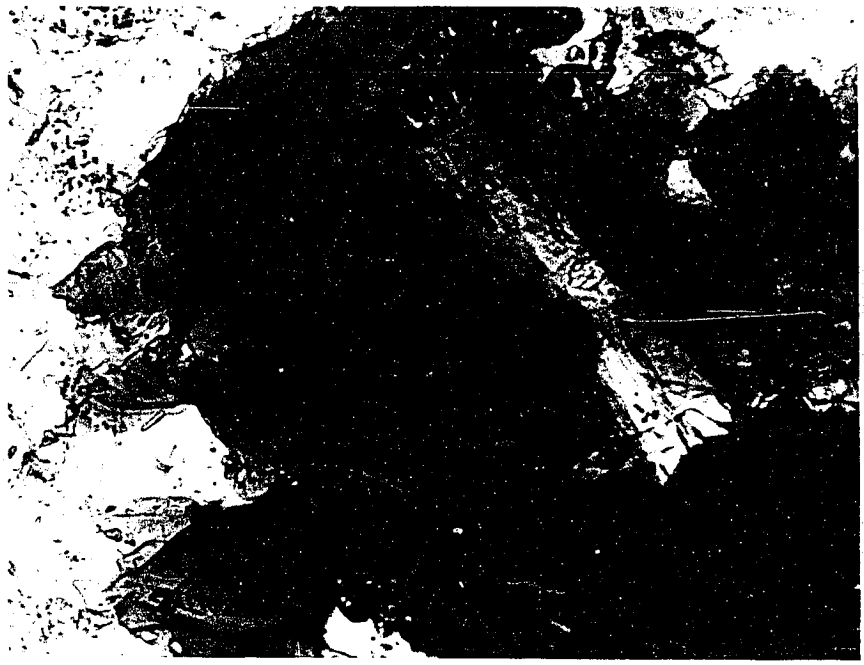

Fig. 13f.

Fig. 13b - Photomicrograph showing anhedral zircons between feldspar grains suggesting late crystallization of these zircons. From Priest's Pass leucomonzonite. Uncrossed nicols.

Fig. 13c - Close up Fig. 16b. Uncrossed nicols.

Fig. 13d - Photomicrograph showing zone of anhedral zircons in a biotite phenocryst. Biotite is surrounded by feldspar grains. Crossed nicols.

Fig. 13e - Same as above. Uncrossed nicols.

Fig. 13f - Close up of portion of biotite flake froms Figs. 13e and f showing the anhedral habit of the zircon.

ZIRCON $ZrSiO_4$ TETRAGONAL – 0.64037				
	hKl	φ	ρ	
c	001	—	0°	
a_1	100	90° 00′	90° 00′	
a_2	010	0	90° 00′	
m	110	45° 00′	90° 00′	
u	331	45° 00′	69° 47.5′	
p	111	45° 00′	42° 10′	
e	101	90° 00	32° 38′	
x	311	71° 34′	63° 43′	
	131	18° 26′	63 43′	

TABLE 6. List of idealized forms, their Miller indices and their (phi) and (rho) angles (F. Koucky, after Dana, 1932).

Correlation of Zircon Crystal Habit with Crystal Chemistry

Due to the small size of individual zircon crystals, there is little data in the literature on the chemistry of specific grains. The procedure in the past has been to separate a large zircon crop from the rock and to analyze the entire crop spectrometrically. With the advent of microprobe techniques, it has become possible to study minute single grains. All zircon chemical data on Zr, Hf, Y, Th, U and Si in this study were generated by electron microprobe analysis of single zircon crystals and are presented in Table 7 in weight percent.

Since three crystal habit classes were defined in the course of this study, an effort was made during microprobe analysis to probe zircons from each class in order to determine if there was any chemical correlation with crystal habit in these zircons. Plots of various combinations of elements were therefore made. The plot of Hf/Zr-Th/Zr-Y/Zr proved to best show the relation of crystal habit to zircon chemistry. Figures 14b-f show the relative proportions of these three components for individual zircon grains from Knopf's (1963) five intrusive phases. Figure 14a is a composite of these three components for all individual zircon grains from the main magma series as defined by R. I. Tilling (personal communication, 1971).

In figures 14a-f it is observed that the fields defining the three crystal habit classes are concentrated in the region of the Hf/Zr corner due to the fact that the hafnium content of zircons is so much greater than the thorium and yttrium contents. The crystal habit fields in Figures 14e-h, which are summarized in Figure 14a, are distributed in a manner indicating a progressive increase of (Y + Hf)/Th ratio from class

TABLE 7

CHEMICAL ANALYSES OF ZIRCONS FROM THE BOULDER BATHOLITH

Ident.	Zr	Hf	Y	Th	Si	O	Hf/Zr	Y/Th	Class
UG 1-1	45.76	1.24	0.15	0.01	14.95	37.89	0.027	--	II
UG 1-2	47.53	1.19	0.07	0.16	14.84	36.21	0.025	0.43	III
UG 1-3	47.23	1.42	0.17	0.10	15.44	35.64	0.030	1.70	III
UG 1-4	48.13	1.29	0.07	0.04	15.03	35.44	0.027	1.75	III
UG 1-5	48.53	1.34	0.10	0.16	15.02	34.85	0.028	0.62	III
UG 3-1	48.03	1.40	0.07	0.04	15.23	35.23	0.029	1.75	III
UG 3-2	48.61	1.43	0.07	0.10	15.02	34.77	0.029	0.70	III
UG 3-3	49.17	1.58	0.15	0.13	15.01	33.96	0.032	1.15	III
UG 3-4	48.76	1.44	0.12	0.01	15.10	34.57	0.030	--	I
UG 5-1	48.96	1.08	0.07	0.0	15.86	34.03	0.022	0.00	III
UG 5-2	49.84	1.15	0.12	0.0	15.78	33.11	0.023	0.00	II
UG 5-3	49.30	1.18	0.17	0.22	15.85	33.28	0.024	0.77	I
UG 5-4	47.50	1.25	0.16	0.11	15.81	35.17	0.026	1.45	III
UG 5-5	48.41	1.20	0.14	0.11	15.74	34.40	0.025	1.27	III
UG 6-1	43.79	1.21	0.12	0.01	14.49	40.38	0.028	--	II
UG 6-2	45.12	1.23	0.15	0.13	14.66	38.71	0.027	1.15	III
UG 6-3	45.08	1.30	0.03	0.10	14.62	38.87	0.029	0.30	III
UG 6-4	44.43	1.26	0.10	0.0	14.59	39.62	0.028	0.00	II
UG 6-5	45.01	1.18	0.17	0.07	14.56	39.01	0.026	2.42	III
UG 9-1	44.40	1.25	0.23	0.17	14.12	39.83	0.028	1.35	I
UG 9-2	43.30	1.30	0.11	0.13	14.20	40.96	0.030	0.84	III
UG 9-1	42.83	1.15	0.08	0.26	13.03	42.65	0.027	0.30	I
UG 9-2	41.90	1.24	0.01	0.51	13.29	43.05	0.030	0.02	I
UG 9-3	43.40	1.34	0.11	0.20	13.17	41.78	0.031	0.55	I
UG 9-4	45.04	1.13	0.16	0.01	13.15	40.51	0.025	--	II
UG 9-5	43.93	1.16	0.25	0.14	13.25	41.27	0.026	1.78	I
UG 10-1	48.02	1.43	0.17	0.09	15.58	34.71	0.030	1.88	III
UG 10-2	49.91	1.20	0.14	0.11	15.93	32.71	0.024	1.27	III
UG 10-3	49.49	1.25	0.23	0.13	15.82	33.08	0.025	1.76	III
UG 10-4	50.41	1.20	0.19	0.31	15.82	32.07	0.024	0.61	I
PG 2-1	49.01	1.05	0.07	0.25	14.94	34.68	0.021	0.28	I
PG 2-2	49.11	1.18	0.23	0.26	14.94	34.28	0.024	0.88	III
PG 2-3	48.78	1.21	0.07	0.13	14.89	34.92	0.025	0.53	I
PG 2-4	48.43	1.28	0.08	0.11	14.63	35.47	0.026	0.72	II
PG 6-1	46.02	1.21	0.16	0.05	14.64	37.92	0.026	3.20	II
PG 6-2	45.22	1.15	0.08	0.07	14.75	38.73	0.025	1.14	III
PG 6-1	48.22	1.25	0.07	0.11	14.78	35.57	0.026	0.63	II
PG 6-2	49.70	1.24	0.16	0.20	14.93	33.77	0.025	0.80	III
PG 6-3	48.80	1.27	0.02	0.14	15.03	34.74	0.026	0.14	I
PG 6-4	49.60	1.27	0.20	0.14	14.90	33.89	0.026	1.42	III
PG 6-5	49.36	1.15	0.06	0.10	15.06	34.27	0.023	0.60	I
PG 9-1	47.20	1.08	0.30	0.05	14.05	37.32	0.023	6.00	II
PG 9-2	46.30	1.18	0.18	0.0	14.31	38.03	0.025	0.00	II
PG 9-3	47.25	1.23	0.16	0.11	14.31	36.94	0.026	1.45	II

TABLE 7 (CON'T)

Ident.	Zr	Hf	Y	Th	Si	O	Hf/Zr	Y/Th	Class
PG 9-1	49.90	1.41	0.01	0.10	15.19	33.39	0.028	0.10	I
PG 9-2	49.05	1.52	0.13	0.0	15.31	33.99	0.031	0.00	II
PG 9-3	47.51	1.79	0.13	0.05	14.63	35.89	0.038	2.60	II
PG10-1	42.67	1.24	0.15	0.07	13.76	42.11	0.029	2.14	II
PG10-2	43.21	1.11	0.26	0.05	13.89	41.48	0.026	5.20	II
PG10-3	41.25	1.11	0.11	0.0	13.07	44.46	0.027	0.00	II
PG10-4	43.40	1.05	0.30	0.0	13.89	41.36	0.024	0.00	II
PG11-1	48.70	1.51	0.66	0.25	15.59	33.29	0.031	2.64	II
PG11-2	48.67	1.12	0.59	0.25	15.68	33.69	0.023	2.36	II
PG11-3	49.32	1.29	0.58	0.16	15.69	32.96	0.026	3.62	III
PG16-1	43.96	1.13	0.41	0.14	13.65	40.71	0.026	2.92	II
PG16-2	45.28	1.26	0.02	0.0	13.53	39.91	0.028	0.00	II
PG16-3	43.19	1.18	0.12	0.17	13.83	41.51	0.027	0.70	III
PG16-4	45.73	1.21	0.03	0.10	13.31	39.62	0.026	0.30	I
PG18-1	50.19	1.27	0.10	0.17	15.12	33.15	0.025	0.58	III
PG18-2	52.34	1.33	0.02	0.17	15.41	30.73	0.025	0.11	I
BMA 2-1	49.84	1.37	0.20	0.14	15.01	33.44	0.027	1.42	III
BMA 2-2	49.86	1.44	0.08	0.0	15.08	33.54	0.029	0.00	II
BMA 2-3	49.26	1.53	0.10	0.0	15.00	34.11	0.031	0.00	II
BMA 2-1	49.68	1.39	0.01	0.05	15.03	33.84	0.028	0.20	II
BMA 2-2	48.55	1.40	0.03	0.04	15.01	34.97	0.029	0.75	II
BMA 2-3	48.67	1.53	0.01	0.0	14.97	34.82	0.031	0.00	II
BMA 2-4	49.70	1.31	0.06	0.13	14.46	34.34	0.026	0.46	III
BA 2-1	47.87	1.26	0.06	0.09	15.47	35.25	0.026	0.66	III
BA 2-2	49.28	1.20	0.18	0.18	15.74	33.42	0.024	1.00	III
BA 2-3	48.21	1.32	0.11	0.0	15.88	34.48	0.027	0.00	II
BA 2-4	49.36	1.56	0.05	0.0	15.86	33.17	0.032	0.00	II
MBA 1-1	49.31	1.31	0.06	0.20	15.88	33.24	0.027	0.30	II
MBA 1-2	49.13	1.39	0.06	0.0	15.82	33.60	0.028	0.00	II
MBA 1-3	49.11	1.22	0.06	0.0	15.94	33.67	0.025	0.00	II
MBA 1-4	48.74	1.17	0.44	0.20	15.90	33.55	0.024	2.20	I
MBA 1-5	49.65	1.38	0.03	0.0	16.08	32.86	0.028	0.00	II
LM 6-1	47.80	1.30	0.13	0.22	15.55	35.00	0.027	0.59	0
LM 6-2	47.98	1.21	0.21	0.11	15.25	35.24	0.025	1.90	0
LM 6-3	46.68	1.60	0.10	0.02	15.30	36.30	0.034	5.00	0
LM 6-4	47.51	1.18	0.15	0.0	15.36	35.80	0.025	0.00	0
LM 8-1	49.50	1.18	0.06	0.16	15.06	34.04	0.024	0.37	0
LM 8-2	48.46	1.07	0.22	0.22	15.11	34.92	0.022	1.00	0
LM 8-3	48.67	1.30	0.13	0.33	15.04	34.53	0.027	0.39	0
LM 8-4	47.79	1.37	0.11	0.42	14.96	35.35	0.029	0.26	0
SD 1-1	47.38	1.02	0.11	0.05	14.52	36.92	0.022	2.20	II
SD 1-2	47.31	1.00	0.13	0.13	14.34	37.09	0.021	1.00	III
SD 1-3	46.85	1.05	0.07	0.05	14.40	37.58	0.022	1.40	II
SD 1-4	46.43	0.99	0.22	0.04	14.20	38.12	0.021	5.50	II
SD 1-5	46.89	0.95	0.07	0.01	14.25	37.83	0.020	7.00	II

TABLE 7 (CON'T)

Ident.	Zr	Hf	Y	Th	Si	O	Hf/Zr	Y/Th	Class
CL 1-1	47.10	1.20	0.16	0.04	13.43	38.07	0.025	4.00	III
CL 1-2	42.28	1.19	0.05	0.20	11.51	44.77	0.028	0.25	I
CL 1-1	48.65	1.48	0.13	0.0	14.63	35.11	0.030	0.00	II
CL 1-2	47.59	1.44	0.05	0.0	14.87	36.05	0.030	0.00	II
CL 1-3	48.30	1.43	0.17	0.14	14.73	35.23	0.030	1.21	III
CL 2-1	45.68	1.16	0.15	0.0	14.55	38.46	0.025	0.00	III
CL 2-2	45.15	1.61	0.13	0.11	14.49	38.51	0.036	1.18	II
CL 2-3	44.30	1.14	0.26	0.01	14.40	39.89	0.026	--	II
CL 2-1	49.50	1.24	0.17	0.36	15.81	32.92	0.025	0.47	I
CL 2-2	50.38	1.26	0.09	0.0	15.83	32.44	0.025	0.00	II
CL 2-3	50.30	1.37	0.11	0.0	15.69	32.53	0.027	0.00	II
CL 2-4	49.87	1.35	0.08	0.09	15.90	32.71	0.027	0.88	III
CL 3-1	47.73	1.25	0.03	0.0	15.71	35.28	0.026	0.00	II
CL 3-2	48.73	1.20	0.02	0.0	15.91	34.14	0.025	0.00	II
CL 3-3	48.48	1.21	0.05	0.13	15.61	34.52	0.025	0.38	I
CL 4-1	45.70	1.11	0.15	0.04	14.80	38.20	0.024	3.75	III
CL 4-2	44.52	1.25	0.07	0.0	14.29	39.87	0.028	0.00	II
CL 4-3	44.86	1.16	0.03	0.04	14.58	39.33	0.026	0.75	III
CL 4-4	42.23	1.14	0.01	0.05	13.39	43.18	0.027	0.20	III
NE 1-1	48.17	1.36	0.07	0.02	14.58	35.80	0.028	3.50	II
NE 1-2	47.59	1.27	0.11	0.0	14.56	36.47	0.027	0.00	II
NE 1-3	47.53	1.34	0.07	0.0	14.64	36.42	0.028	0.00	II
NE 1-4	47.40	1.27	0.08	0.0	14.63	36.62	0.027	0.00	II
NE 1-5	46.26	1.38	0.12	0.0	14.52	37.72	0.030	0.00	II
NE12-1	48.94	1.39	0.10	0.0	15.02	34.55	0.028	0.00	II
NE12-2	48.04	1.32	0.05	0.0	15.03	35.56	0.027	0.00	II
NE12-3	49.35	1.29	0.14	0.04	16.10	33.08	0.026	3.50	III
NE12-4	49.11	1.42	0.06	0.08	14.87	34.46	0.029	0.75	III
NE12-5	49.13	1.20	0.02	0.0	15.24	34.41	0.024	0.00	II
JC 1-1	49.77	1.30	0.03	0.01	15.25	33.64	0.026	3.00	II
JC 1-2	49.59	1.32	0.09	0.04	16.30	32.66	0.027	2.25	III
JC 1-3	48.48	1.34	0.05	0.19	15.09	34.85	0.028	0.26	I
JC11-1	47.23	1.42	0.08	0.13	14.92	36.22	0.030	0.61	III
JC11-2	49.28	1.39	0.10	0.20	15.53	33.50	0.028	0.50	III
JC11-3	49.71	1.40	0.12	0.0	15.53	33.24	0.028	0.00	II
JC11-4	48.64	1.34	0.07	0.07	15.28	34.60	0.028	1.00	II
JC11-5	48.67	1.52	0.15	0.04	15.20	34.42	0.031	3.75	III
JC 6-1	45.12	3.29	0.18	0.14	13.98	37.29	0.073	1.28	0
JC 6-2	45.38	2.16	0.25	0.01	14.13	38.07	0.048	--	0
JC43-1	48.97	1.34	0.08	0.0	14.99	34.62	0.027	0.00	II
JC43-2	49.67	1.32	0.10	0.0	15.33	33.58	0.027	0.00	II
EP10-1	50.29	1.26	0.12	0.08	15.32	32.93	0.025	1.50	III
EP10-2	49.78	1.32	0.02	0.0	15.38	33.50	0.027	0.00	II
EP10-3	49.83	1.19	0.06	0.0	15.42	33.50	0.024	0.00	II
EP10-4	50.27	1.25	0.05	0.10	15.45	32.88	0.025	0.50	III
EP10-5	49.90	1.29	0.08	0.0	15.37	33.36	0.026	0.00	II

TABLE 7 (CON'T)

Ident.	Zr	Hf	Y	Th	Si	O	Hf/Zr	Y/Th	Class
BO15-1	47.42	1.32	0.02	0.16	15.61	35.47	0.028	0.12	I
BO15-2	47.76	1.23	0.03	0.0	14.80	36.18	0.026	0.00	II
BO15-3	47.32	1.34	0.07	0.0	15.49	35.78	0.028	0.00	II
BO15-4	46.96	1.34	0.13	0.0	14.39	37.18	0.029	0.00	II
BO15-5	46.96	1.28	0.10	0.0	14.51	37.15	0.027	0.00	II
BS14-1	50.67	1.29	0.12	0.0	16.30	31.62	0.025	0.00	II
BS14-2	49.37	1.28	0.06	0.10	15.44	33.75	0.026	0.60	III
BS14-3	49.84	1.20	0.13	0.0	15.21	33.62	0.024	0.00	I
BS14-4	49.27	1.28	0.02	0.0	15.18	34.25	0.026	0.00	II
DM 1-1	48.60	1.31	0.07	0.04	15.02	34.96	0.027	1.75	II
DM 1-2	48.97	1.33	0.11	0.0	14.97	34.62	0.027	0.00	II
DM 1-3	46.67	1.30	0.05	0.0	15.15	36.83	0.028	0.00	II
DM 1-4	48.24	1.26	0.11	0.0	16.30	34.09	0.026	0.00	II
DM 1-5	47.36	1.28	0.06	0.0	15.01	36.29	0.027	0.00	II
EH 2-1	44.68	1.24	0.12	0.0	13.69	40.27	0.028	0.00	II
EH 2-2	46.04	1.27	0.02	0.0	13.92	38.75	0.028	0.00	II
EH 2-3	45.34	1.18	0.02	0.0	13.95	39.51	0.026	0.00	II
EH 2-4	43.36	1.26	0.02	0.0	13.03	42.33	0.029	0.00	II
EH 2-5	42.70	1.25	0.02	0.0	14.09	41.94	0.029	0.00	II
EH 6-1	49.12	1.40	0.03	0.0	16.24	33.21	0.029	0.00	II
EH 6-2	49.28	1.33	0.03	0.0	16.22	33.14	0.027	0.00	II
PG 1-1	49.86	1.23	0.12				0.025		II
PG 1-2	49.44	1.07	0.20				0.0222		III
PG 1-3	49.12	1.34	0.03				0.027		II
PG 1-4	49.64	1.23	0.15				0.025		III
BA 1-1	47.96	1.49	0.0				0.031		III
MBA 2-1	48.08	1.31	0.08				0.027		I
MBA 2-2	47.31	1.33	0.01				0.028		I
LM 1-1	49.14	1.17	0.21				0.024		III
CL 8-1	48.59	1.37	0.12				0.028		?
L 8-2	50.22	1.30	0.12				0.026		?
NE15-1	47.15	1.28	0.02				0.027		II
NE15-2	48.88	1.26	0.02				0.026		III
NE15-3	48.73	1.28	0.03				0.026		II
NE15-4	48.67	1.25	0.0				0.026		II
NE15-5	48.52	1.42	0.0				0.029		II
JC13-1	48.35	1.42	0.01				0.029		II
JC13-2	47.85	1.30	0.07				0.027		III
JC13-3	47.67	1.37	0.01				0.029		II
JC19-1	49.87	1.29	0.27				0.026		II
JC19-2	49.17	1.37	0.10				0.028		III
JC19-3	49.30	1.24	0.13				0.025		II
JC19-4	50.40	1.31	0.10				0.026		I
JC19-5	48.58	1.71	0.13				0.035		III
JC29-1	48.08	1.39	0.06				0.029		I
JC29-2	47.53	1.26	0.07				0.027		

TABLE 7 (CON'T)

Ident.	Zr	Hf	Y	Hf/Zr	Class
JC29-3	47.21	1.39	0.0	0.029	II
JC29-4	47.73	1.46	0.01	0.031	II
JC29-5	47.23	1.40	0.06	0.030	I
JC37-1	47.75	1.27	0.07	0.027	II
JC37-2	48.54	1.16	0.08	0.024	I
JC37-3	47.43	1.25	0.06	0.026	I
JC37-4	46.88	1.19	0.02	0.025	III
JC37-5	47.51	1.24	0.07	0.026	II
JC51-1	47.38	1.55	0.20	0.033	II
JC51-2	47.20	1.20	0.08	0.025	II
JC51-3	47.64	1.29	0.01	0.027	II
JC51-4	49.27	1.30	0.05	0.026	II
JC51-5	48.79	1.31	0.05	0.027	II
EP 6-1	47.50	1.38	0.12	0.029	II
EP 6-2	47.58	1.16	0.17	0.024	II
EP 6-3	47.50	1.30	0.06	0.027	II
EP 6-4	48.10	1.26	0.03	0.026	III
EP 6-5	48.45	1.26	0.01	0.026	II
EP18-1	48.13	1.34	0.02	0.028	III
EP18-2	48.02	1.29	0.08	0.027	II
EP18-3	47.52	1.38	0.06	0.029	II
EP18-4	49.27	1.42	0.08	0.029	II
EP18-5	47.29	1.37	0.10	0.029	II
BO12-1	47.29	1.30	0.03	0.027	II
BO12-2	36.98	1.42	0.01	0.038	II
BO12-3	48.94	1.38	0.06	0.028	III
BO12-4	49.42	1.40	0.02	0.028	II
BO12-5	49.84	1.56	0.07	0.031	II
BS 1-1	47.35	1.16	0.07	0.024	I
BS 1-2	47.70	1.29	0.06	0.027	II
BS 1-3	47.20	1.24	0.0	0.026	II
BS 1-4	47.72	1.24	0.01	0.026	I
BS 1-5	47.54	1.29	0.02	0.027	II
BS 9-1	47.05	3.02	0.35	0.064	0
BS 9-2	41.09	1.53	1.33	0.037	0
BS 9-3	46.37	1.58	0.58	0.034	0
BS 9-4	46.55	1.86	0.62	0.040	0
BS 9-5	43.68	1.67	1.26	0.038	0
DM 3-1	48.30	1.20	0.01	0.025	II
DM 3-2	46.87	1.25	0.03	0.027	I
DM 3-3	47.71	1.37	0.06	0.029	II
DM 3-4	47.23	1.31	0.02	0.028	II
DM 3-5	47.12	1.14	0.01	0.024	I
DL12-1	47.40	1.44	0.06	0.030	II
DL 12-1	47.61	1.40	0.07	0.029	II
DL12-3	47.14	1.24	0.06	0.026	III

TABLE 7 (CON'T)

Ident.	Zr	Hf	Y	Hf/Zr	Class
EH 2-1	44.68	1.24	0.12	0.028	II
EH 2-2	46.04	1.27	0.02	0.028	II
EH 2-4	43.36	1.26	0.02	0.029	II
EH 2-5	42.70	1.25	0.02	0.029	II

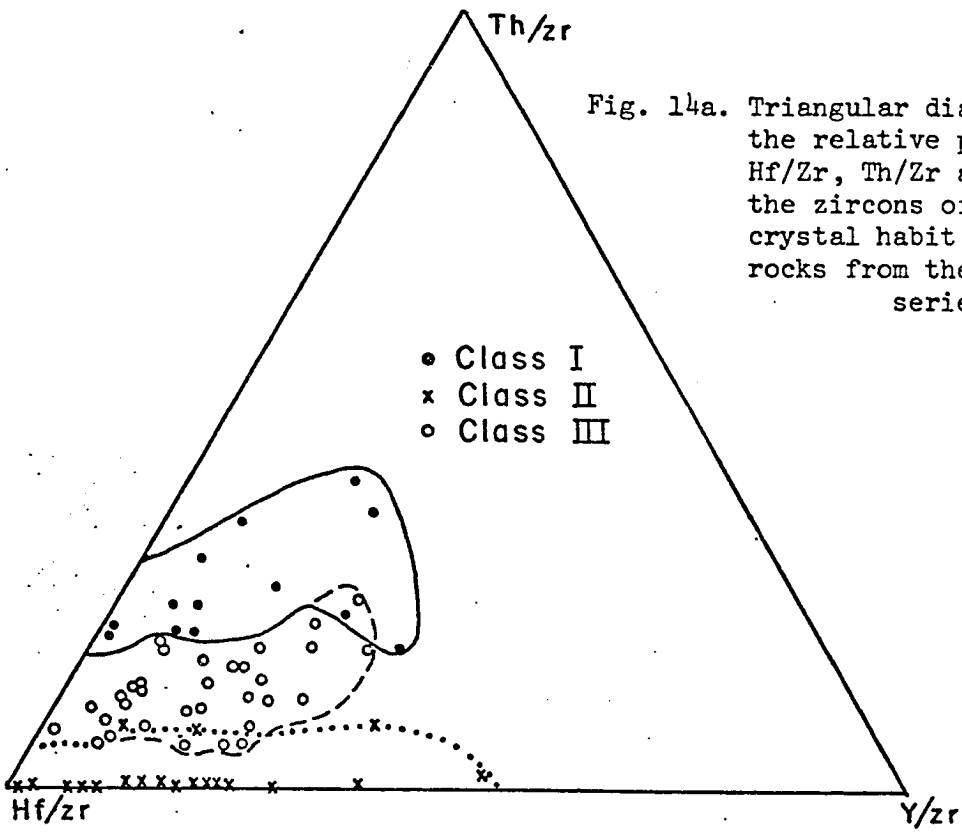

Fig. 14a. Triangular diagram showing the relative proportions of Hf/Zr, Th/Zr and Y/Zr for the zircons of the three crystal habit classes of rocks from the main magma series.

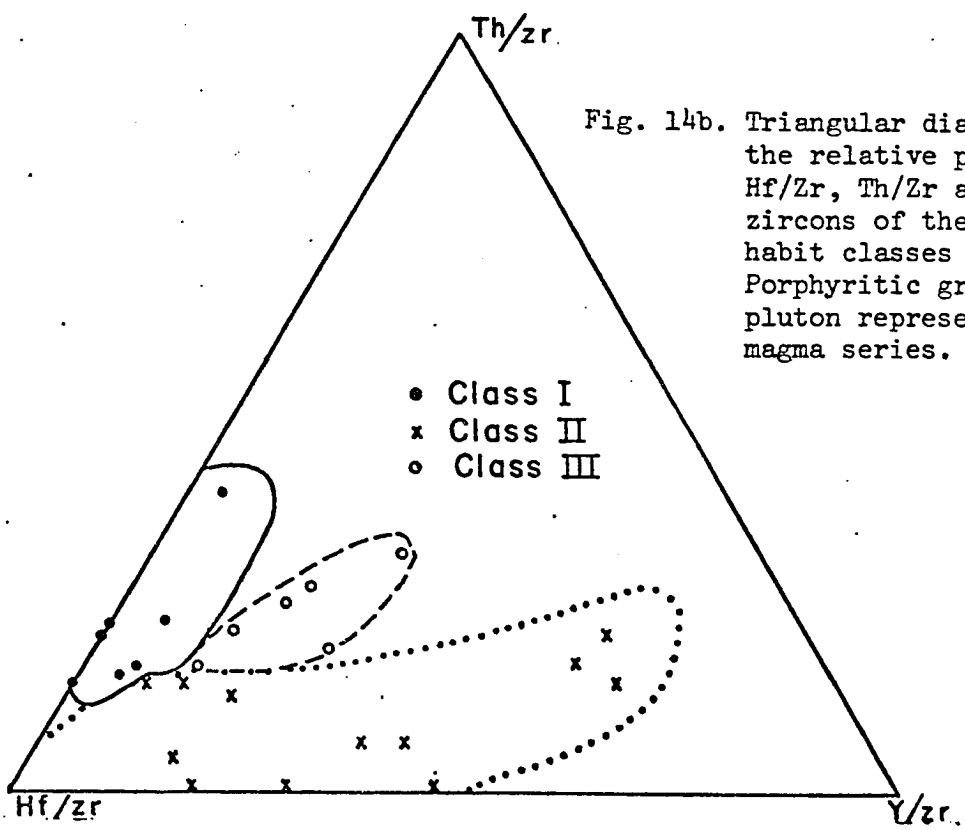

Fig. 14b. Triangular diagram showing the relative proporations of Hf/Zr, Th/Zr and Y/Zr for the zircons of the three crystal habit classes of the Porphyritic granodiorite, a pluton representing the sodic magma series.

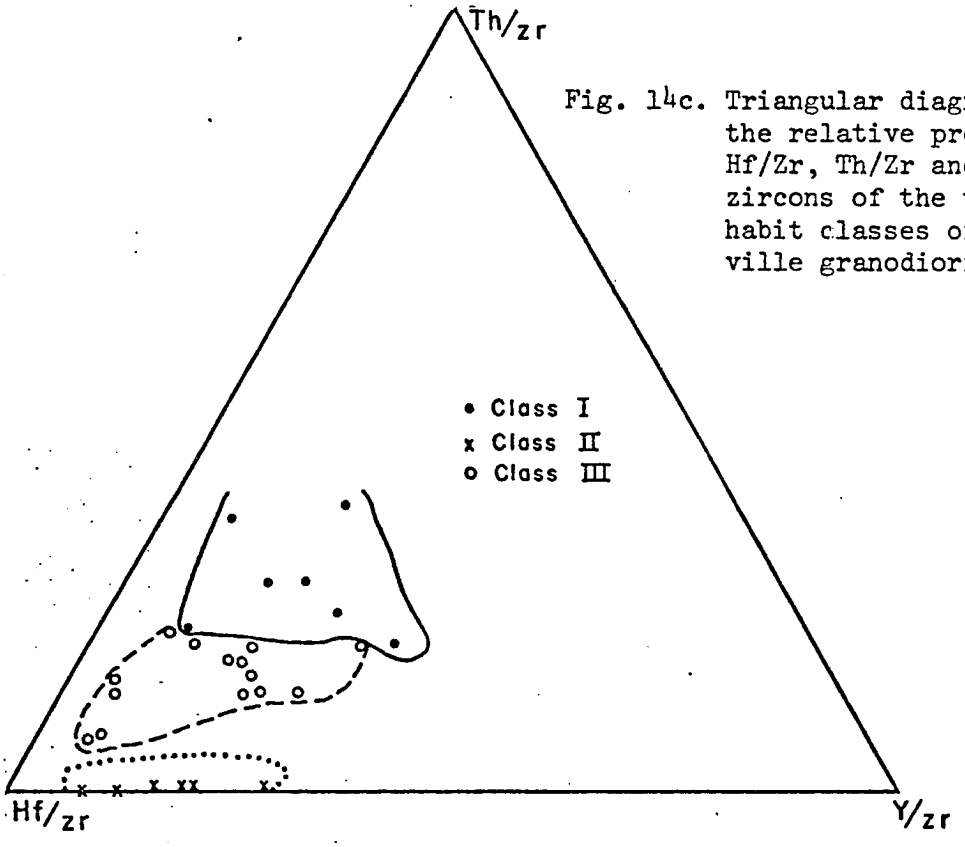

Fig. 14c. Triangular diagram showing the relative proporations of Hf/Zr, Th/Zr and Y/Zr in zircons of the three crystal habit classes of the Unionville granodiorite.

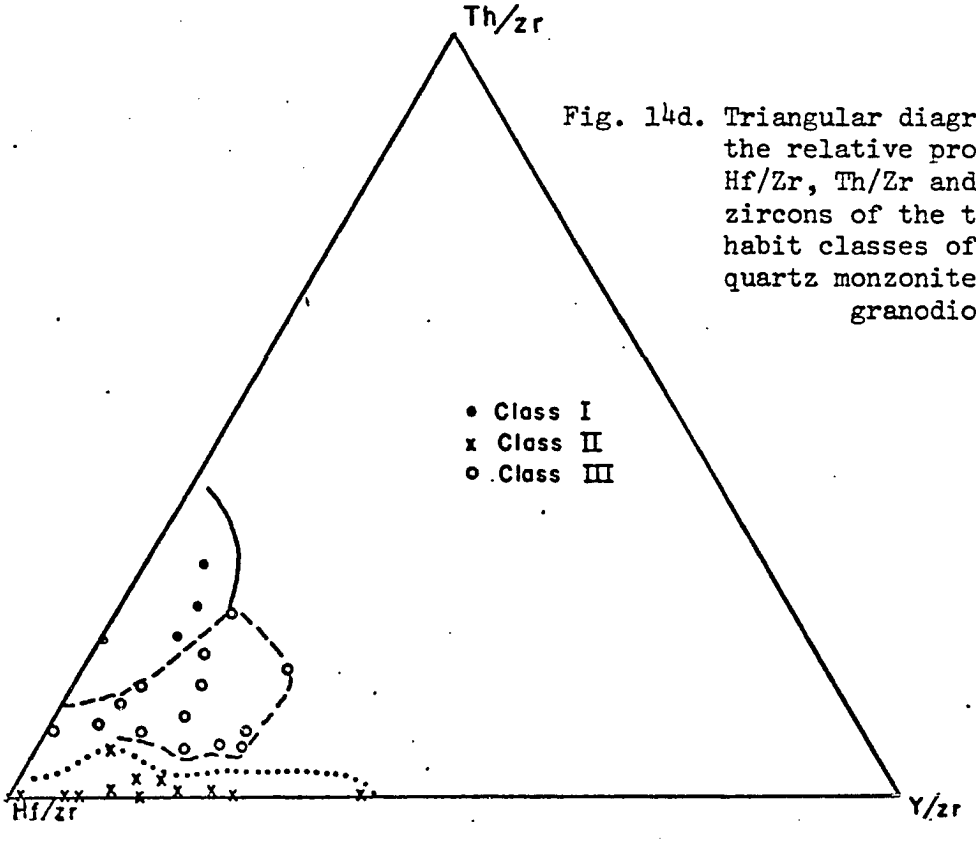

Fig. 14d. Triangular diagram showing the relative proporations of Hf/Zr, Th/Zr and Y/Zr in zircons of the three crystal habit classes of the Butte quartz monzonite (Clancy granodiorite).

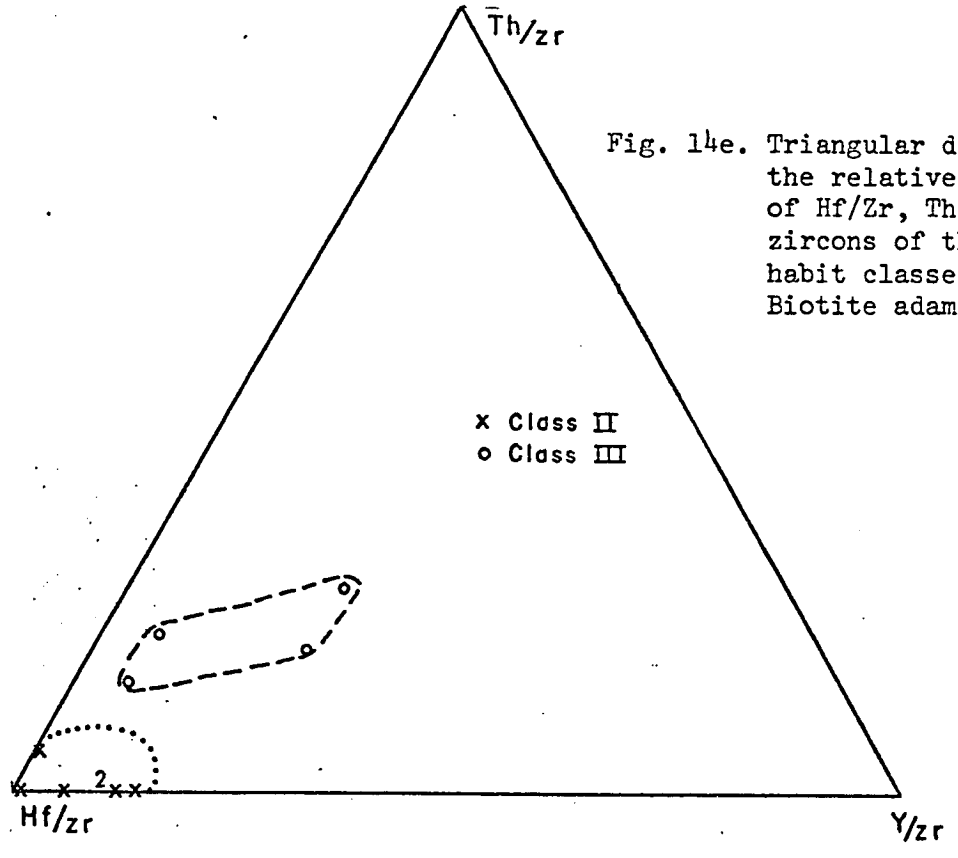

Fig. 14e. Triangular diagram showing the relative proporations of Hf/Zr, Th/Zr and Y/Zr in zircons of the three crystal habit classes from the Biotite adamellite.

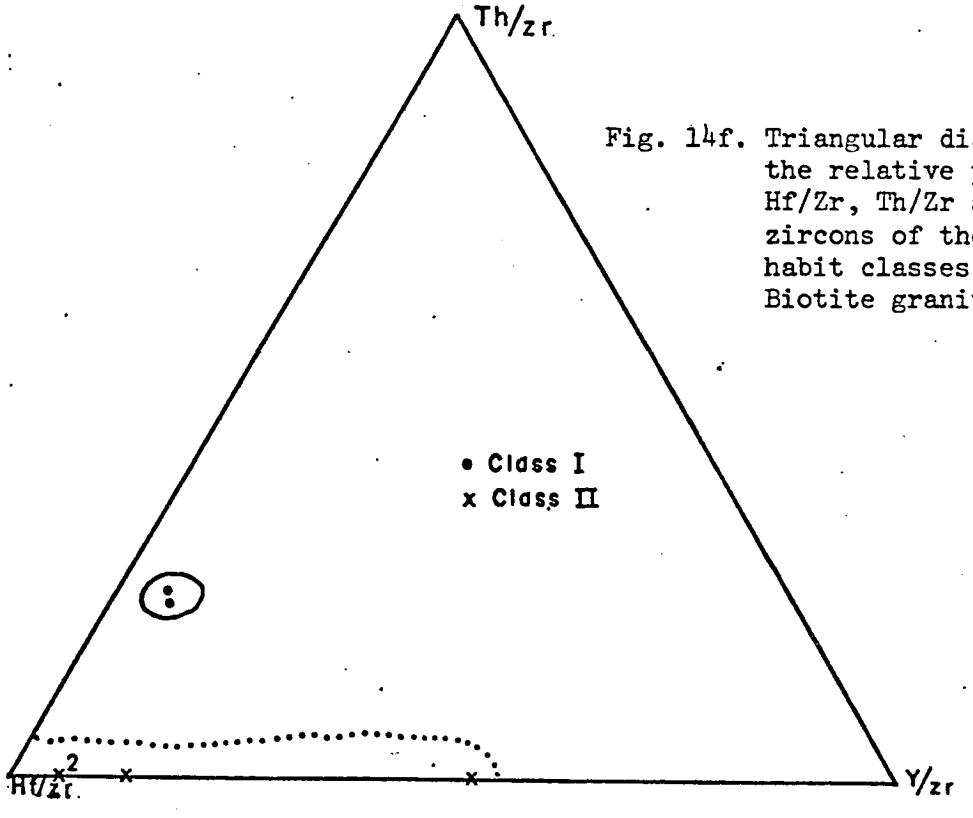

Fig. 14f. Triangular diagram showing the relative proportions of Hf/Zr, Th/Zr and Y/Zr in zircons of the three crystal habit classes from the Biotite granite.

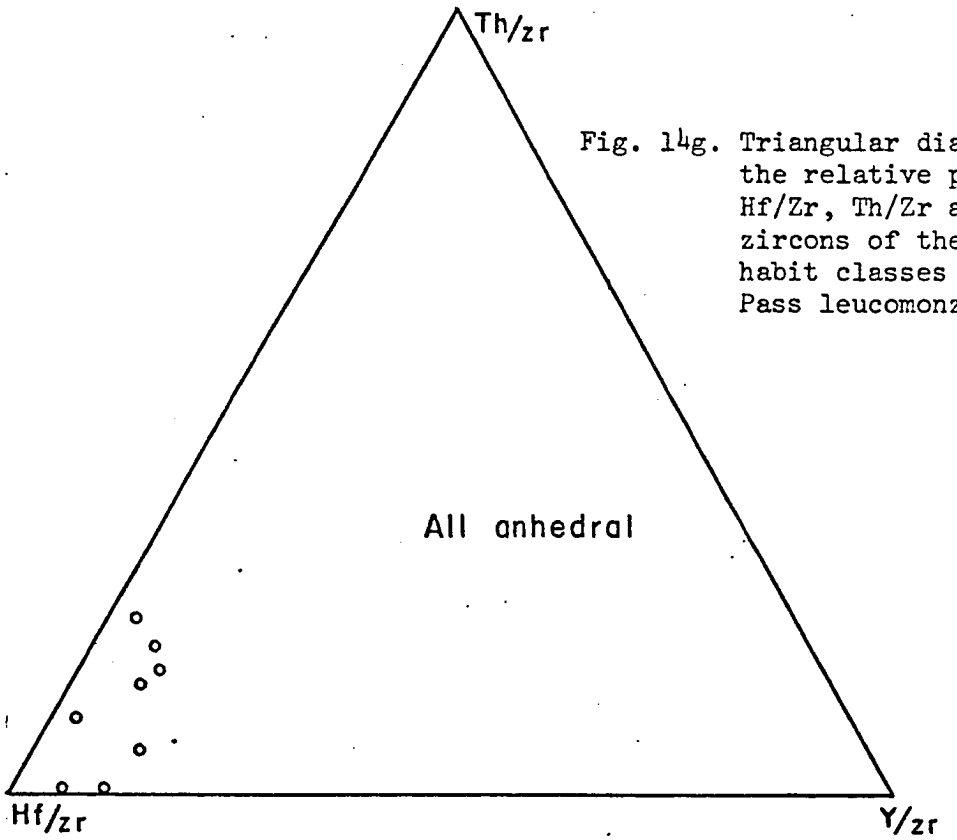

Fig. 14g. Triangular diagram showing the relative proportions of Hf/Zr, Th/Zr and Y/Zr in zircons of the three crystal habit classes from the Priest Pass leucomonzonite.

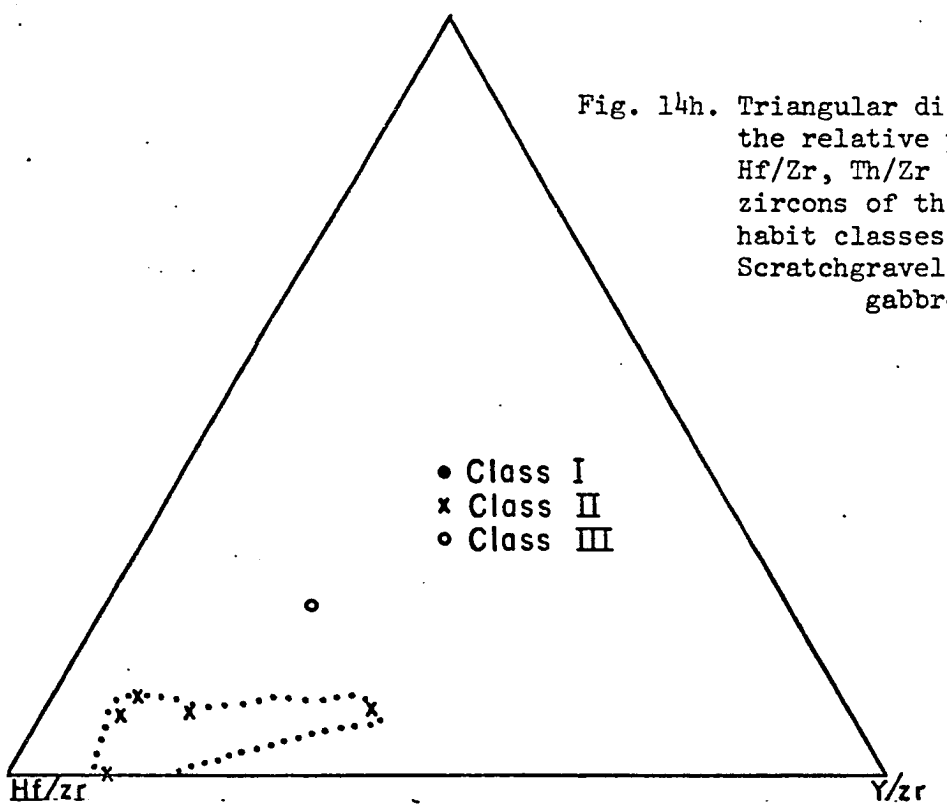

Fig. 14h. Triangular diagram showing the relative proportions of Hf/Zr, Th/Zr and Y/Zr in zircons of the three crystal habit classes from the Scratchgravel Hills' syeno-gabbro.

I to class III to class II. Zircons from the Porphyritic granodiorite stock (Fig. 14b) representing the sodic magma series, however, do not show a similar distribution of crystal habit class fields. In this case, the fields are much larger and they are distributed in a manner so that class I field is juxtaposed against the class III as well as the class II fields.

Buckley (1951) has experimentally demonstrated that minor variations in the crystal chemistry of a mineral controls crystal habit. It can therefore be suggested that the (Y + Hf)/Th ratio controls the crystal habit classes of these zircons.

The role of thorium in controlling the crystal habit of these zircons is strongly inferred since the crystal habit class fields are arranged almost parallel to the side line opposite the Th/Zr corner (Fig. 14a). The configuration of the crystal habit class fields (Fig. 14a) does not, however, indicate the individual roles of hafnium and yttrium in controlling crystal habit class. Due to the great similarity of hafnium and zirconium, because of the lanthanide contraction, the presence of hafnium in the zirconium site of zircon is not expected to affect the crystal lattice to any large extent. The substitution of hafnium for zirconium may, therefore, not be expected to cause a change in crystal growth behavior resulting in a variation of habit (Buckley, 1951). Yttrium on the other hand does not possess ionic properties suitable for the zirconium site in zircon as does hafnium. It is therefore expected that the presence of yttrium in the zirconium site effects the growth behavior of the crystal, thus producing a variation in crystal habit. The critical factor controlling the crystal habit class in zircon may therefore be the Y/Th ratio rather than the (Y + Hf)/Th ratio.

Lyakhovich and Shevaleyskii (1961) in studying the hafnium and zirconium content of zircons from several plutons have concluded on empirical grounds that the amount of hafnium in zircons did not affect the crystal habit. Since they had not analyzed for any other elements, they did not speculate as to which elements did affect the habit. Their study appears to support the argument presented above for the crystal habit variation of zircons from the Boulder batholith.

A possible explanation for the differences in the crystal habit fields of the main magma series (Fig. 14a) and the Porphyritic granodiorite (Fig. 14b) is that other elements not analyzed in this study may exert some influence on crystal habit. These other elements are perhaps the yttrium and cerium earths which are closely associated chemically with yttrium and thorium. A difference in rare earth composition for the two magma series is possible because of their inconsanguity. Also differences in the bulk chemistry of the two magma series may affect the partitioning of the elements influencing crystal habit.

There are numerous factors, both chemical and physical, that control crystal growth. The interrelationship of all these factors is complex and not well understood. If chemical control is important in determining crystal habit of zircons, then a variation in chemistry will cause a crystal habit variation by enhancing or suppressing growth of certain faces. Controlled experiments may be the solution in providing a better understanding of the correlation of crystal chemistry to crystal habit. Until then all conclusions along these lines are tentative.

Since zircon crystal habit appears to depend on zircon chemistry, it is essential to explain the reason for the distribution of the zircon

crystal habit fields classes on Figures 14a-h. As reviewed in previous sections, there is little argument as to the early start of crystallization of zircons from granitic melts. Evidence for this conclusion is petrographic, such as zircon's euhedral habit and its presence in minerals representing a wide range of crystallization; other evidence is from U-Pb isotope studies (Silver and Deutsch, 1963). The duration of the range of crystallization, however is a subject of debate. The arguments for both long and short durations of crystallization from granitic melts have been previously reviewed.

Zircon crops separated from rock samples the size of hand specimens generally contain crystals representing two or three of the three crystal habit classes. Figures 14a-h show that these classes represent a range of (Hf+ Y)/Th ratios. It is difficult to conceive of a melt so heterogeneous on the hand specimen scale, that it would instantaneously crystallize out zircons of such a large range of (Y + Hf)/Th ratios. A range in the chemistry of minerals suggests a duration in the crystallization period of that mineral particularly in viscous granitic melts where reactions are slow. A range in the chemistry of a mineral from a single small sample precludes instantaneous crystallization from a melt.

Additional support for the argument that zircon crystallizes over a duration of time is that there is a range of Hf/Zr ratios for the zircon crystals as shown in Figure 15. It is well established that the Hf/Zr ratio of zircons increases with differentiation of a melt (Gottfried and Waring, 1964; Lyakhovich and Shevaleyevskii, 1962). The differentiation of a melt requires time as well. The possibility of the crystallization of three separate unrelated zircon populations consisting entirely of

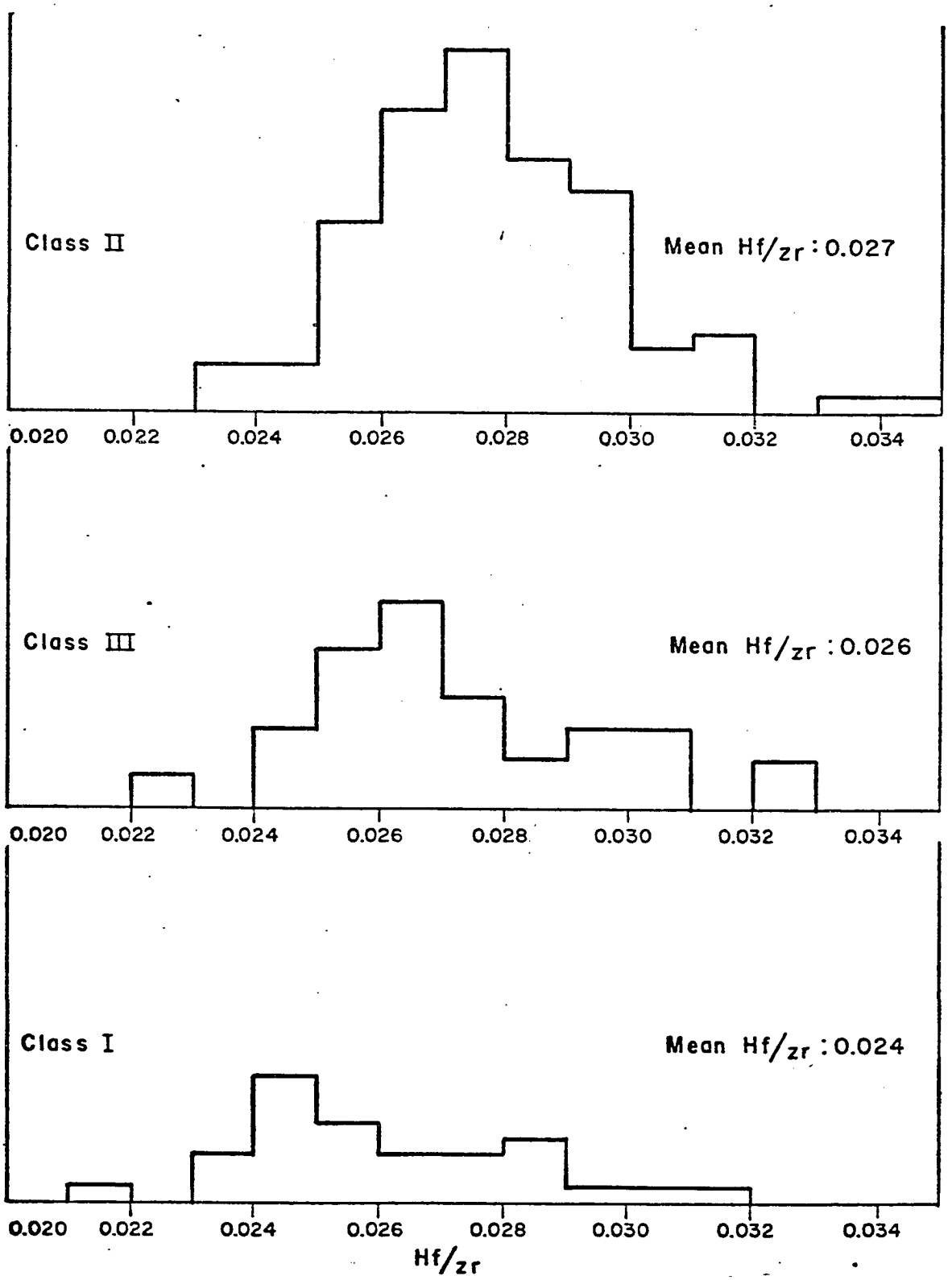

Fig. 15. Histogram showing the distribution of Hf/Zr in the three crystal habit classes of zircon. Each unit on abcissa represents one grain.

each one of the three classes and subsequent mixing of these three populations is precluded by the transitional nature of the crystal habits of their chemistry.

With the establishment of the idea that zircons begin to crystallize from the melt at an early time and continue to do so over a duration, it is necessary to determine the change in their chemistry during this range of crystallization. Three considerations aid in determining the chemical change in zircons during crystallization. 1) Thorium has an ionic radius of 1.06 Å which is much larger than the ionic radius of Y which is 0.92 Å. Thorium would therefore be a better candidate for the zircon lattice at higher temperature, because at elevated temperatures the lattice expands and allows for larger atoms to enter the structure. Yttrium is a better candidate for entering the zircon lattice at lower temperatures. 2) Figures 14a-h show that hafnium along with yttrium increases to the expense of thorium from crystal habit class I to III to II. Table 8 also shows that the Hf/Zr of zircon grains generally increases from class I to III to II. This relation is shown graphically in Figure 15. The increase of Hf/Zr ratio with differentiation of a melt is well established in the literature which is reviewed in earlier sections. 3) Using electron microprobe techniques Pigorini, et al. (1968) report changes in the concentrations of certain elements in zircons from the center to the periphery of a grain. They report an increase in hafnium and yttrium from the center of the zircon towards the periphery and a coupled decrease in the thorium and zirconium.

Taking the above three considerations into account, it can be inferred that during crystallization of zircons from a melt there is a

TABLE 8

AVERAGE Hf/Zr RATIOS FOR CRYSTAL HABIT CLASSES IN EACH SAMPLE

Sample No.	Class I	Class III	Class II
UG 1		0.027	0.027
UG 3	0.029	0.030	
UG 5	0.023	0.023	0.024
UG 6		0.027	0.028
UG 9	0.028	0.030	
UG 10	0.024	0.026	
PG 1		0.023	0.026
PG 2	0.023	0.024	0.026
PG 6	0.025	0.025	0.026
PG 9	0.028	0.029	
PG 11	0.026	0.027	
PG 16	0.026		0.027
PG 18	0.025	0.025	
BMA 2		0.027	0.030
BA 2		0.025	0.029
SD 1	0.021		0.021
CL 1	0.028	0.028	0.030
CL 2	0.025	0.026	0.028
CL 3	0.025		0.025
CL 4		0.025	0.028
NE 12	0.024	0.027	0.027
NE 15		0.026	0.027
JC 1		0.027	0.027
JC 13		0.027	0.029
JC 19	0.026	0.026	0.026
JC 29	0.028		0.029
JC 73	0.025	0.025	0.026
EP 6		0.026	0.027
EP 10		0.025	0.026
EP 18		0.028	0.029
BO 12		0.028	0.029
BO 15	0.028		0.028
BS 1	0.025	0.027	0.027
DM 3	0.027		0.027
DL 12		0.026	0.030

change in the chemistry of zircons from lower to higher Y/Th ratio which in turn may cause the variation of zircon crystal habit class from class I to class III to class II. This variation is accompanied by an increase in the Hf/Zr ratio of the zircons.

Not all rocks encountered from the Boulder batholith contain zircons that began crystallizing early from a melt. Zircons from the Priest's Pass leucomonzonite are anhedral and interstitial to feldspars and form inclusion zones in the biotite parallel to the enclosing mineral's periphery. These intermineralic relations suggest the crystallization of zircon during the crystallization of biotite (Fig. 13b-f); Figure 14f shows that these anhedral zircons plot in the same vicinity on the diagram as do the euhedral zircons from the main magma series, suggesting that although zircon crystallization began late in this silica undersaturated melt, it may have followed the same trend chemically as did its euhedral counterparts. The late crystallization of zircon has been reported by Vlasov (1966) from other silica undersaturated rocks similar to the Priest's Pass leucomonzonite.

Behavior of Thorium and Uranium in Zircons

The zircons from the Boulder batholith are unusual in that they contain large amounts of thorium (mean thorium is 0.07%) but contain uranium in amounts below the detection limit of the microprobe. Generally, the thorium content of zircons from granitic rocks is 0.05% and the uranium content is 0.13% yielding a U/Th ratio of 2.6 (Hurley and Fairbairn, 1957).

The abundance of thorium in these zircons can be possibly ascribed to two factors. First, the Boulder batholith has a much higher thorium,

as well as uranium, content than most calc alkaline plutons (Tilling and Gottfried, 1969), thus making more thorium available to zircon during crystallization. Second is the absence of thorite ($ThSiO_4$) in the heavy mineral separates from the rocks of the Boulder batholith. This factor suggests that thorium partitioned in favor of zircon and other thorium bearing mineral phases rather than forming thorite.

The deficiency of uranium in these zircons from a relatively radioactive batholith is not easily explained. Pitchblende (U_2O_3), associated with chalcedony veins, is present in the batholith in quantities sufficient to have been considered economic (Becraft, 1956). The uranium in the melt may have partitioned in favor of minerals other than zircon or more probably uranium partitioned in favor of the fluid phase which eventually formed the pitchblende bearing chalcedony veins. The reasons for this particular behavior of uranium and thorium is not understood.

D. Physical Description and Estimated Chemistry of Populations of Zircons

Physical Description of Zircon Populations

The proportions of the three crystal habit classes of zircon (defined in the previous section) within each sample was determined, and a study of the distribution of the various populations of zircons was made within each pluton. Due to an insufficient number of samples for some of the plutons, it was impossible to show any trends in the variation of the proportions of the crystal habit classes of a zircon population as a function of the location. There were, however, sufficient samples from both the Unionville granodiorite and Porphyritic granodiorite to show a trend (Figs. 16 and 17).

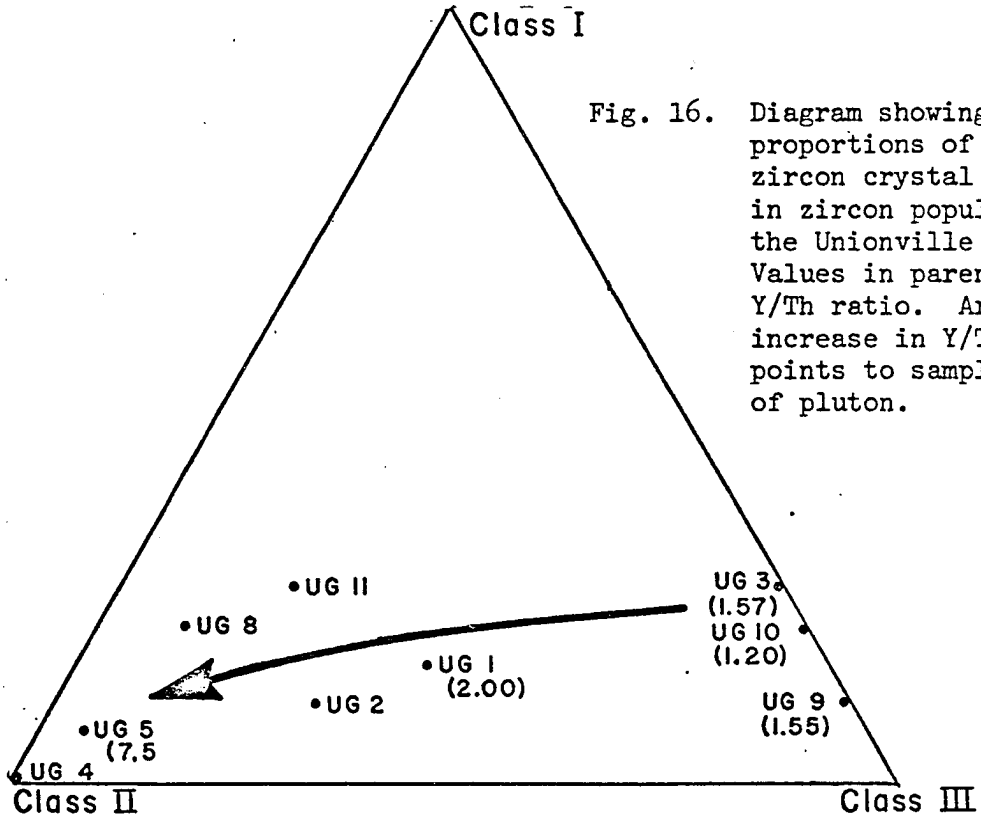

Fig. 16. Diagram showing the relative proportions of the three zircon crystal habit classes in zircon populations from the Unionville granodiorite. Values in parentheses show Y/Th ratio. Arrow shows increase in Y/Th ratio and points to samples at center of pluton.

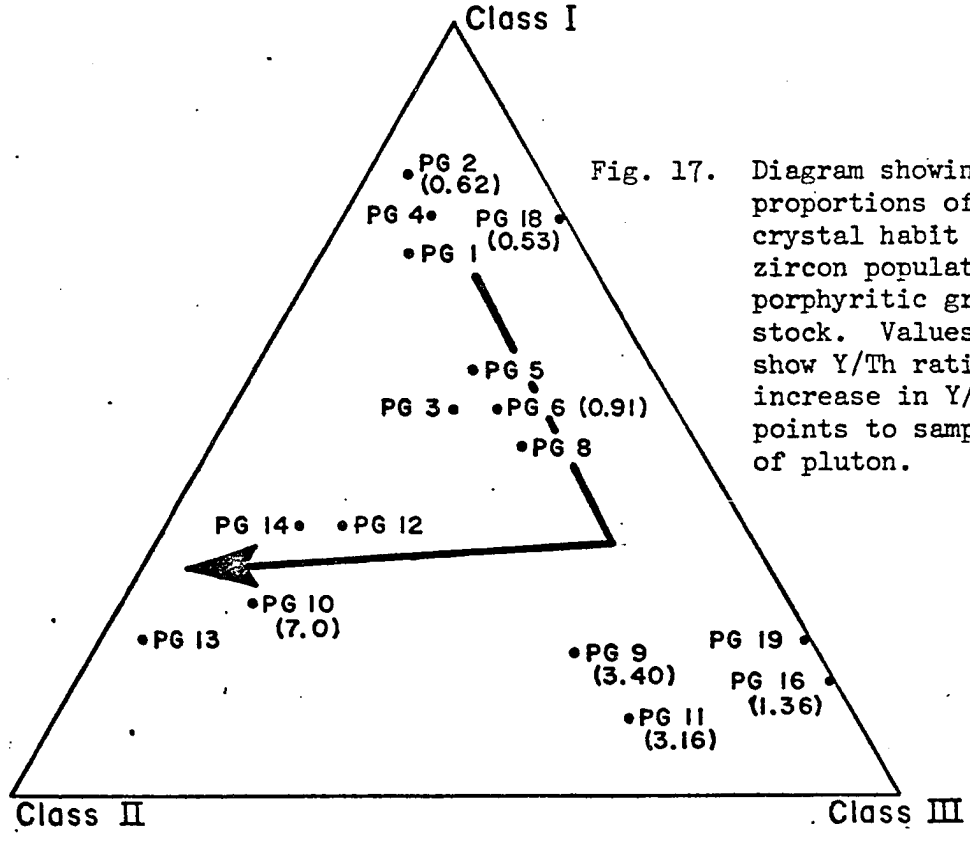

Fig. 17. Diagram showing the relative proportions of three zircon crystal habit classes in zircon populations from the porphyritic granodiorite stock. Values in parentheses show Y/Th ratio. Arrow shows increase in Y/Th ratio and points to samples at center of pluton.

The trend of the variation of the proportions of the crystal habit classes of zircon as a function of location in the Unionville granodiorite shows an increase of class II zircons at the expense of class I and III zircons from the periphery towards the center of the pluton as indicated by the arrow on Figure 16. A similar trend is observed for the crystal habit classes of zircons from the Porphyritic granodiorite (Fig. 17). However, there is a modification in the trend of the latter pluton, since in going from the periphery towards the center, the proportion of class III increases at the expense of class I zircons, and then there is an increase in the proportion of class II zircons at the expense of class III zircons. The reason for the initial lack of variation between class I and class III zircon crystal habits in the Unionville granodiorite may be due to the fact that samples were not obtained from as close to the periphery of this pluton as they were for the Porphyritic granodiorite stock.

The Chemistry of Zircon Crystal Populations

This section will present and discuss data on the Y/Th ratio zonation of the Unionville granodiorite and the Porphyritic granodiorite and the distribution of the three crystal habit classes in samples from these plutons in light of the estimated zircon chemistry data. Data on the Hf/Zr ratio of zircon populations from the various plutons of the Boulder batholith will also be presented and discussed. The chemistry of zircon populations was estimated by taking weighted averages of the chemistry of three crystal habit classes of zircon based on their relative proporation in a sample (Table 9). An estimate of the total chemical composition by

TABLE 9

AVERAGE ESTIMATED CHEMICAL COMPOSITIONS OF ZIRCON POPULATIONS, BOULDER BATHOLITH, MONTANA

	% Crystal Habit			Wt %				Ratios	
	Class								
Sample	I	II	III	Zr	Hf	Y	Th	Hf/Zr	Y/Th
UG 1	15	48	37	46.21	1.24	0.12	0.06	0.027	2.00
UG 3	25	0	75	48.64	1.26	0.11	0.07	0.029	1.57
UG 5	8	88	4	48.73	1.15	0.15	0.02	0.028	7.50
UG 6	25	25	50	44.60	1.24	0.12	0.06	0.028	2.00
UG 9	10	0	90	43.33	1.29	0.14	0.09	0.030	1.55
UG 10	20	0	80	49.39	1.27	0.18	0.15	0.026	1.20
PG 1	70	20	10	49.50	1.26			0.025	
PG 2	80	15	5	48.54	1.25	0.08	0.13	0.025	0.62
PG 6	50	20	30	47.91	1.22	0.10	0.11	0.026	0.91
PG 9	19	27	54	47.92	1.37	0.17	0.05	0.028	3.4
PG 10	25	60	15	42.63	1.13	0.21	0.03	0.027	7.0
PG 11	10	25	65	49.13	1.30	0.60	0.19	0.026	3.16
PG 16	15	0	85	44.38	1.19	0.15	0.11	0.027	1.36
PG 18	75	0	25	50.73	1.28	0.09	0.17	0.025	0.53
BMA 2	35	55	10	49.33	1.44	0.07	0.06	0.030	1.40
BA 1	40	0	60	47.96	1.49			0.031	
BA 2	19	33	48	48.21	1.32	0.10	0.08	0.026	1.25
MBA 1	30	67	3	49.13	1.28	0.17	0.10	0.025	1.70
MBA 2	12	85	3	47.70	1.32			0.028	
LM 1	0	0	0	49.14	1.17			0.024	
LM 6	0	0	0	47.76	1.23	0.15	0.09	0.026	1.67
LM 8	0	0	0	48.60	1.23	0.13	0.28	0.026	0.46
SD 1	70	30	0	47.01	1.00	0.12	0.07	0.021	1.71
CL 1	35	55	10	46.04	1.35	0.09	0.08	0.030	1.13
CL 2	35	62	3	48.23	1.30	0.15	0.15	0.025	1.00
CL 3	60	30	10	48.39	1.22	0.04	0.08	0.024	0.50
CL 4	40	45	15	44.43	1.21	0.07	0.05	0.026	1.40
CL 8	50	45	5	49.41	1.34			0.027	
NE 1	15	80	5	47.39	1.32	0.09	0	0.028	
NE 12	15	70	15	48.69	1.33	0.08	0.01	0.027	8.00
NE 15	35	45	20	48.49	1.29			0.027	
JC 1	10	75	15	49.62	1.31	0.04	0.04	0.027	1.00
JC 11	15	85	0	48.71	1.41	0.10	0.09	0.029	1.11
JC 13	20	70	10	47.96	1.38			0.028	
JC 19	15	80	5	49.69	1.29			0.026	
JC 6	0	0	0	45.38	2.76	0.22	0.08	0.061	2.75
JC 29	55	35	10	47.55	1.38			0.029	
JC 37	35	40	25	47.57	1.22			0.024	
JC 43	15	65	20	49.16	1.31	0.08	0.01	0.027	8.00
JC 51	30	60	10	52.02	1.33			0.028	
EP 6	20	65	15	47.74	1.30			0.026	
EP 10	30	40	50	50.04	1.27	0.07	0.04	0.025	1.75
EP 18	35	60	5	48.04	1.37			0.029	
BO 12	10	85	5	45.94	1.42			0.029	

TABLE 9 (CON'T)

BO 15	35	60	5	47.32	1.31	0.06	0.06	0.028	1.00
BS 1	25	60	15	47.67	1.25			0.026	
BS 9	0	0	0	44.42	1.66			0.037	
BS 14	15	55	30	49.73	1.26	0.08	0.04	0.026	2.00
DM 1	25	60	15	47.48	1.34	0.07	0.01	0.028	7.00
DM 3	25	70	5	47.41	1.26			0.027	
DL 12	25	50	25	47.37	1.36	0.029			
EH 2	20	80	0	44.42	1.24			0.028	
EH 6	15	80	5	49.28	1.37	0.03	0	0.028	

this method can be justified on the assumption that the three crystal habit classes are real in so far as they represent definite chemical ranges.

The behavior of Y, Th and some other rare earth elements in accessory minerals in differentiated granitic masses has been reported in the literature and reviewed in previous sections. It has been suggested that with differentiation of a granitic pluton there is an increase in the yttrium content and a decrease in the thorium content in the rocks as well as the accessory minerals (Lyakhovich and Barinskii, 1961; Leonova and Balashov, 1963). Since zircon populations contain a large proportion of the yttrium and thorium present in granitic rocks, the inverse relationship between these two elements should be revealed in the estimated chemical analyses of the zircon populations.

If it is assumed that upon intrusion into cooler rocks, the melt will cool and crystallize from the periphery towards the general center of the body, and if differentiation of a melt occurs in conjunction with progressive crystallization, and if the yttrium-thorium relationship suggested in the literature is true, then it would be expected to find lower Y/Th ratios for zircons at the periphery of a pluton and higher Y/Th ratios as the center of the pluton is approached. Since the chemical analyses for zircon populations were estimated on the basis of the proportions of the three zircon crystal habit classes, and since it has been suggested that it is the Y/Th ratio of zircons which may control their crystal habit, then it would be expected that there will be a close relation between the proportions of the crystal habit classes and the Y/Th ratio.

Only two plutons from the Boulder batholith were sufficiently sampled to show a relation between yttrium and thorium. The two plutons are the Unionville granodiorite and the Porphyritic granodiorite stock. Figures 16 and 17 show the relative increase of class III at the expense of class I and then class II at the expense of class III from the periphery to the center of these two plutons as indicated by the arrow. The values in the parentheses on Figures 16 and 17 represent estimated Y/Th ratios. It can be observed from these two figures that the Y/Th ratios increase from periphery of the plutons to the center as predicted in the previous paragraph. This zonation in terms of the Y/Th ratio is consistent with that suggested in the literature.

Figure 18 is a contour map of the Y/Th ratios in the Unionville granodiorite and the Porphyritic granodiorite stock. The contours are drawn on the basis of the estimated Y/Th ratio and the anticipated Y/Th ratio inferred from the proportions of the three zircon crystal classes. The contours indicate an increase in the Y/Th ratio from periphery towards the center as predicted in the literature. The Y/Th ratio contours, as drawn, cut across the Kpg-Kgd contact, which corresponds with the interpretation of the Porphyritic granodiorite stock, stating that the two portions of the stock merely represent textural and mineralogic variations of the same mass of magma.

Although the estimated values of Y/Th ratios are probably not equal to the whole rock Y/Th ratio, the trends indicated by the estimated values are consistent with those presented in the literature.

In summary it can be said that the relative proportions of the three crystal habit classes in a zircon population is reflected by the

Fig. 18. Map of the northwest portion of the Boulder batholith showing location of electron microprobe samples (o) and samples in which the proportions of the three crystal habit classes were determined (o). Solid and dashed lines infer Y/Th contours of 2.0 units. Arrowhead pattern represents volcanic rocks, dotted pattern represents sediments.

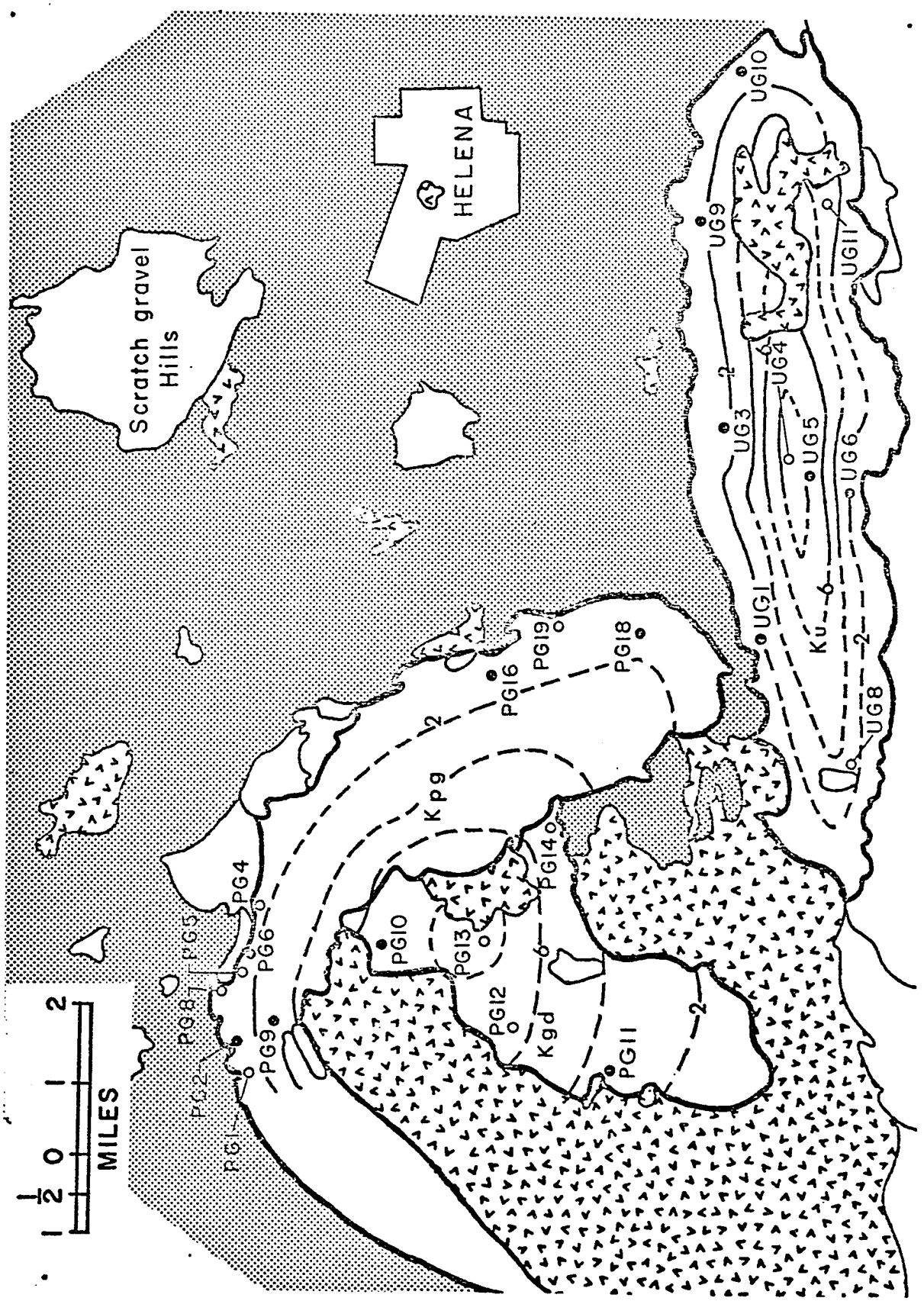

Y/Th ratio of the population. The Y/Th ratio of crystals changes as a function of the changing chemical and temperature conditions of the melt from which the zircons crystallize.

The estimated hafnium and zirconium contents of the zircon populations from the Boulder batholith, as shown on the Hf versus Hf/Zr plot (Fig. 19) reflect the preferred interpretation of the batholith's history. The first point observed in Figure 19 is the overlapping of the fields defining the Hf/Zr ratio of the various plutons. This overlap is expected because the plutons were intruded in a very close succession temporally (9 m.y.) during which time differentiation was occurring simultaneously on the pluton and on the batholith scale. Progressively, silicic plutons, due to the intratelluric differentiation, were being intruded while more mafic earlier plutons in the sequence were still in the process of crystallizing and differentiating. Previous studies, discussed earlier, have established that Hf/Zr ratio increases with differentiation of melts. Since a rapid intrusive succession coupled with differentiation on various scales exists in the batholith, overlapping Hf/Zr fields are inevitable.

An example of this overlap occurs between the Unionville granodiorite and the Butte quartz monzonite (Fig. 19). While the earlier more mafic Unionville granodiorite was cooling and differentiating, it was progressively varying in its Hf/Zr ratio. Sometime during this process, the more silicic Butte quartz monzonite intruded with an initial Hf/Zr ratio similar to that of some differentiated portions of the Unionville granodiorite. This caused the strong overlap in the Hf/Zr fields of these two plutons.

Two trends can be observed in the distribution of the Hf/Zr fields in Figure 19. The dominant trend consists of an almost linear distribution

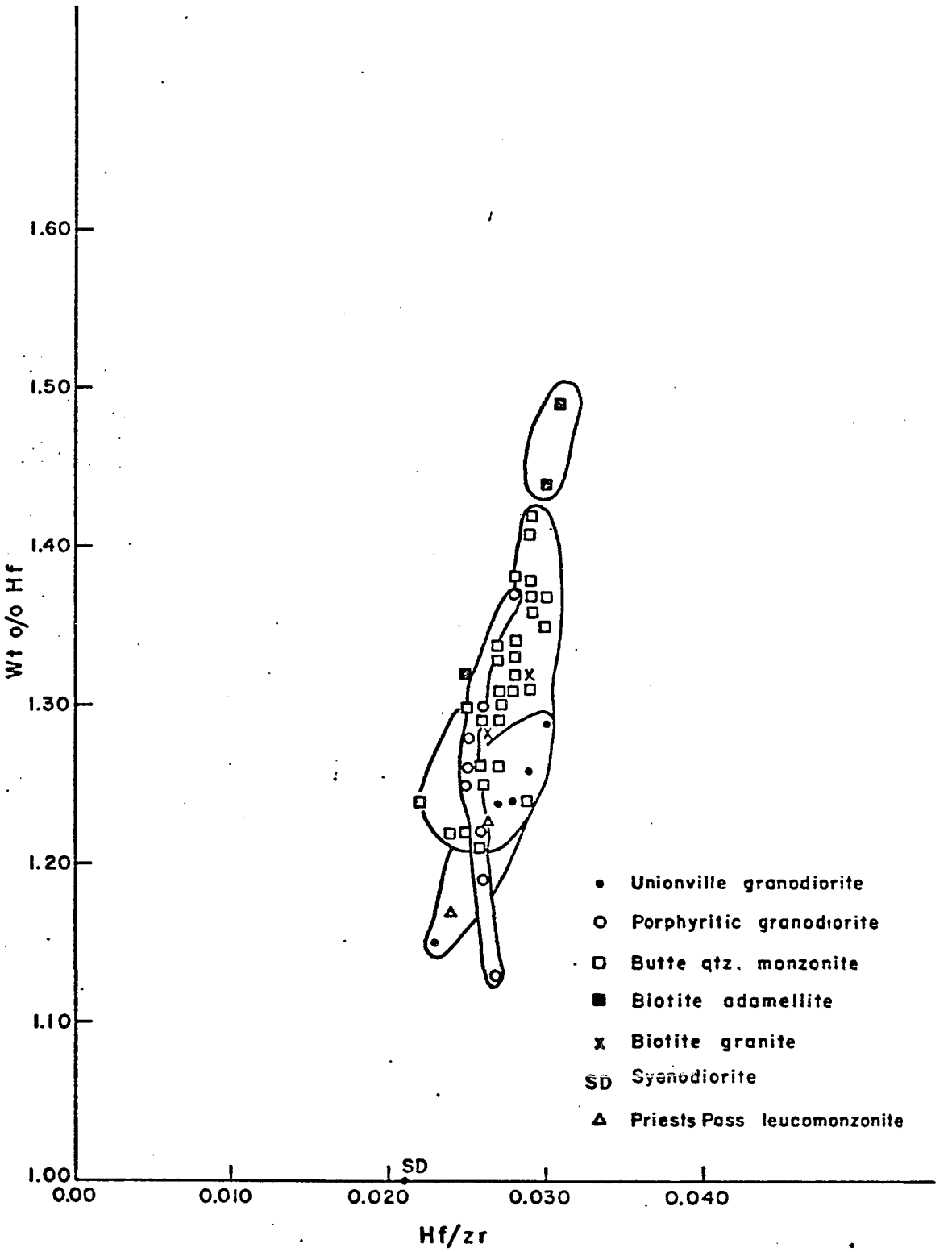

Fig. 19. Diagram showing Hf vs Hf/Zr ratios of zircon populations from plutons of the Boulder batholith.

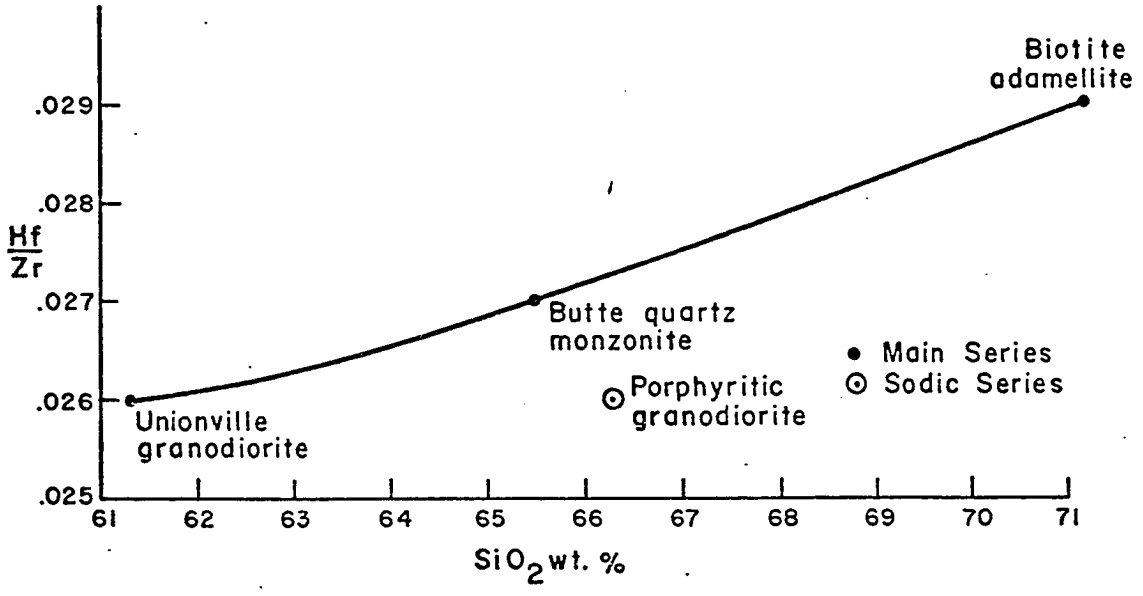

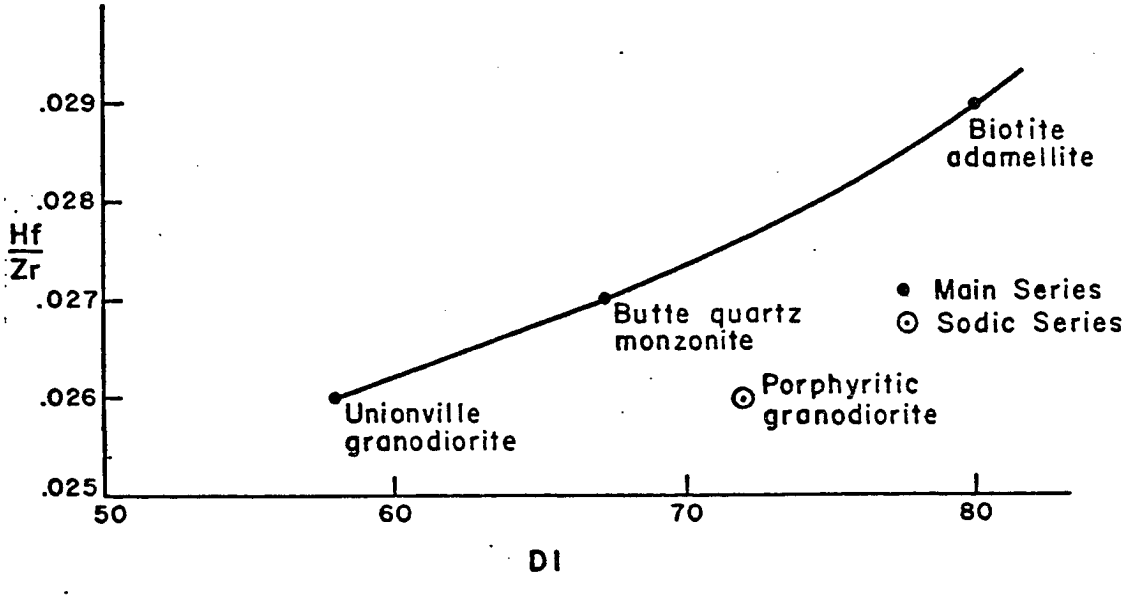

Fig. 20. a. Mean Hf/Zr for zircon populations plotted against SiO_2 content from Knopf analyses (1963).

b. Mean Hf/Zr for zircon populations plotted against Knopf differention index (DI) (1963).

of Hf/Zr fields of the Unionville granodiorite, the Butte quartz monzonite, and the Biotite adamellite. The other trend is followed by the samples from the Porphyritic granodiorite stock. The dominant trend is crosscut by the latter in the low hafnium region, but in the higher hafnium region, the latter trend parallels the dominant trend with a relatively lower Hf/Zr ratio (Fig. 19). The parallelism of the dominant trend of the samples from the Porphyritic granodiorite stock in the high hafnium region (Fig. 19) may represent a mixing of the two magma series, which is a possibility. However there is no other evidence to suggest such an occurrence.

The presence of two trends in the estimated Hf/Zr ratios of the zircon populations from the Boulder batholith compliments the idea of the plutons of the batholith representing two magma series (R. I. Tilling, personal communication, 1971). The Porphyritic granodiorite stock is a representative of the sodic magma series, and it would be expected that the zirconium and hafnium in a magma of this composition might partition differently between the zircon and a melt than in a magma from the main series. The difference in the behavior of the Hf/Zr ratio in the melts from the two magma series may be implied from Figures 20a and b, which show the relationship of mean Hf/Zr ratio for a pluton and its mean SiO_2 content (Fig. 20a) and its differentiation index (DI) (Fig. 20b) (Knopf, 1963). For a given SiO_2 content on a given level of differentiation, the Hf/Zr ratio of the sodic series is lower than the Hf.Zr ratio of the main series. If the Hf/Zr ratio of a zircon population can be equated to a differentiation index for that mineral, and if it is assumed that the amount and proportions of hafnium and zirconium are the

same for the original melts of the two magma series, it can be suggested that zircons begin to crystallize out of a melt later in more sodic melts than in potassic melts. This implies that zirconium is more soluble in a sodic melt over a larger temperature-pressure range than in a potassic melt. That is, more sodic melts must cool and differentiate farther than potassic melts in order to begin crystallizing zircons. This seems to be supported by experimental data on solubility of zircons in granitic melts (L. H. Larsen, personal communication, 1972).

The position of the Biotite granite samples in the Butte quartz monzonite field on Figure 19 is expected because the Biotite granite is probably merely a facies of the Butte quartz monzonite. Because of this relationship, both should therefore have similar Hf/Zr ratios.

The field of the Biotite adamellite does not overlap the field of the Butte quartz monzonite (Fig. 19) because the Biotite adamellite was probably not sampled sufficiently to show the entire range in its Hf/Zr ratios. Sample BA 2 from the Biotite adamellite does not plot in the Biotite adamellite field but plots in the Butte quartz monzonite field on Figure 19. The deviation of this sample from its prescribed field is probably due to the fact that it was collected close to the Biotite adamellite - Butte quartz monzonite contact and is therefore mislocated and represents a sample from the Butte quartz monzonite. Mislocation of this sample is due to the poor exposure in the northern portion of the batholith which has led to some lattitude of interpretation as to the positions of the contacts during mapping.

Two satellite bodies sampled for this study are poorly under-

stood in context of the batholith's history. The Scratchgravel Hills consist of predominantly syenodiorite presumably intruded early in the sequence. Zircons from only one sample were analyzed from this stock. The analysis plots in the lower hafnium and low Hf/Zr ratio region of Figure 19. The low hafnium content in these zircons is expected since Hf/Zr ratios are always low in mafic rock types. The Scratchgravel Hills sample is in line with the trend of the Hf/Zr ratio fields of the main magma series (Fig. 19). This is consistent with R. I. Tilling's interpretation as to the magma series affiliation of the syenodiorite (personal communication, 1971).

The Priest's Pass leucomonzonite, the second and more minor of the satellitic plutons studied, is even less well understood than the syenodiorite. It has been classified by Knopf (1963) as an aberrant intrusion since there is no other rock type in the batholith that is similar to it. Part of the problem with the proper understanding of this silica undersaturated body is that it is very narrow and is located at the contact with country rock along its entire length, which makes it quite susceptible to contamination by assimilation thus resulting in a loss of original identity. The zircon samples from the Priest's Pass leucomonzonite plot within the Unionville granodiorite and part of the Butte quartz monzonite Hf/Zr ratio fields on Figure 19. These samples also plot close to the area where the Porphyritic granodiorite crosscuts the main magma series trend in the Hf/Zr ratio fields. Without a better understanding of this pluton, it is impossible to draw any conclusions attempting to explain the behavior of the estimated Hf/Zr ratio in its zircon population.

In summary it can be said that the estimated Hf/Zr ratios for the

zircon populations from the plutons of the Boulder batholith reflect the intrusive history and evolution of the batholith.

E. Statistical Analysis of Zircon Populations

Statistical studies of zircon populations based on the reduced major axis (RMA) and the mean elongation ratio (MER) have been used in the past to provide evidence for petrogenetic interpretation in granitic masses (Larsen and Poldervaart, 1957; Larsen and Poldervaart, 1951; Spotts, 1962). The basic assumption in all these studies was that zircons crystallize early and only for a short duration from a granitic melt. The granitic bodies studied were representative of all of the Granite Series of Buddington (1959). However, none of them were composite in nature. As a well-studied eqizonal composite batholith, the Boulder batholith was chosen to test the variation of zircon populations based on RMA and MER on a pluton and batholith scale.

The techniques of the statistical analysis were those suggested by Larsen and Poldervaart (1957), and are summarized in the Appendix. An average of 176 doubly terminated zircons were measured from twenty-two samples from the northern part of the Boulder batholith. The northern part of the batholith consists of a number of plutons from both magma series and, therefore, provides an excellent base for such a study. The RMA and MER were calculated for each sample and each of the crystal habit classes of each sample (Tables 10, 11). Analysis of variance was used to determine the significance of variation of the RMA and MER of the zircon populations within and between plutons.

As a precaution, mean length, mean width, MER, and RMA of the

TABLE 10

SUMMARY DATA ON ZIRCON POPULATION ANALYSIS BOULDER BATHOLITH, MONTANA

Sample	$\bar{X}$ mm	$\bar{Y}$ mm	Sx	Sy	r	MER	RMA	Dd
UG 1	0.15161	0.06136	0.05110	0.02070	0.17175	2.8047	22.06	70.96
UG 4	0.06920	0.02861	0.01678	0.0040	0.38536	2.4581	16.11	19.59
UG 8	0.15358	0.06794	0.04842	0.01398	0.30554	2.4024	21.40	61.29
UG 10	0.14131	0.05917	0.05464	0.01991	0.39782	2.5437	20.02	63.83
UG 11	0.04618	0 .02929	0.01156	0.00552	0.56557	1.5951	25.53	11.94
CL 2	0.05580	0.03249	0.02179	0.01038	0.71795	1.7412	25.47	18.12
CL 3	0.05577	0.03278	0.02306	0.09212	0.53862	1.7331	21.78	23.85
CL 5	0.10197	0.05032	0.05217	0.02805	0.51171	2.1312	28.27	58.53
CL 8	0.10196	0.06895	0.02821	0.02211	0.74548	1.5335	38.09	25.58
PG 5	0.08164	0.04749	0.02258	0.01450	0.41465	1.8479	32.71	29.03
PG 11	0.11722	0.05874	0.03758	0.01592	0.36766	2.0845	24.00	44.02
PG 13	0.06899	0.03470	0.03411	0.01061	0.64371	1.9953	17.28	30.15
PG 16	0.06941	0.03283	0.02185	0.00887	0.49184	2.1665	22.11	23.77
PG 19	0.07567	0.03214	0.02665	0.00893	0.55291	2.4141	18.52	26.58
BA 1	0.04826	0.02586	0.02139	0.00723	0.64024	1.8743	18.68	19.15
BA 2	0.07551	0.03230	0.04187	0.01014	0.41063	2.4049	13.61	46.77
BMA 1	0.05978	0.03174	0.02979	0.01113	0.65346	1.9040	20.48	26.48
BMA 2	0.05296	0.02894	0.02514	0.00986	0.79975	1.8256	21.42	17.09
BWS 1	0.05470	0.02979	0.02356	0.03635	0.11759	2.0526	32.95	
MBA 1	0.06111	0.03302	0.01533	0.00772	0.55237	1.8915	26.72	16.24
MBA 2	0.05840	0.03303	0.01485	0.00851	0.66227	1.8097	29.81	14.07
MBA 3	0.06648	0.03756	0.02089	0.01065	0.68720	1.8111	27.02	18.55

TABLE 11

SUMMARY DATA FOR ZIRCON POPULATION ANALYSIS BASED ON CRYSTAL HABIT CLASSES

	CLASS I				CLASS II				CLASS III			
Sample	$\bar{X}$ mm	$\bar{Y}$ mm	MER	RMA	$\bar{X}$ mm	$\bar{Y}$ mm	MER	RMA	$\bar{X}$ mm	$\bar{Y}$ mm	MER	RMA
UG 1	0.136	0.093	1.47	33.4	0.162	0.061	2.77	21.8	0.162	0.060	3.00	19.3
UG 11	0.050	0.032	1.61	65.5	0.052	0.031	1.63	20.6	0.068	0.025	2.76	6.2
UG 4	-	-	-	-	0.067	0.027	2.51	12.5	-	-	-	-
UG 8	0.157	0.086	1.84	21.9	0.166	0.065	2.88	22.1	0.156	0.060	2.74	29.9
UG 10	0.067	0.050	1.34	11.8	-	-	-	-	0.162	0.068	2.43	20.5
CL 5	0.061	0.039	1.57	35.3	0.110	0.042	2.67	18.6	0.186	0.083	2.23	53.5
CL 3	0.046	0.031	1.53	41.6	0.051	0.028	1.83	19.5	0.067	0.040	1.71	38.7
CL 8	0.127	0.091	1.40	31.9	0.098	0.060	1.65	24.7	0.120	0.070	1.78	60.0
CL 2	0.058	0.039	1.49	30.5	0.072	0.036	1.93	18.6	0.082	0.038	2.12	18.1
PG 19	0.058	0.040	1.45	33.5	0.081	0.033	2.48	21.5	0.139	0.030	4.94	17.9
PG 5	0.069	0.053	1.33	38.2	0.098	0.052	2.00	32.1	0.099	0.039	2.66	54.2
PG 13	0.053	0.039	1.33	22.7	0.063	0.035	1.84	23.2	0.077	0.031	2.59	16.6
PG 11	0.122	0.054	2.50	20.0	0.142	0.059	2.50	24.7	0.106	0.059	1.87	31.1
PG 16	0.052	0.036	1.46	30.0	-	-	-	-	0.091	0.037	2.54	14.4
BA 2	0.045	0.030	1.49	32.2	0.082	0.035	2.37	18.2	0.066	0.033	2.15	27.6
BA 1	0.043	0.027	1.59	20.7	-	-	-	-	0.063	0.029	2.21	20.8
BMA 2	0.044	0.028	1.55	29.5	0.059	0.031	1.95	26.8	0.084	0.041	2.08	26.7
BMA 1	0.040	0.031	1.29	40.0	0.055	0.029	1.93	21.0	0.066	0.033	1.95	29.1
MBA 3	0.056	0.038	1.44	24.8	0.063	0.033	1.94	30.7	0.073	0.037	1.97	23.2
MBA 2	0.052	0.035	1.48	23.7	0.060	0.033	1.88	29.3	0.047	0.024	1.95	27.7
MBA 1	0.056	0.042	1.36	47.5	0.58	0.031	1.90	22.8	0.053	0.024	2.26	22.2

zircon population were recalculated from weighted means of the same parameters of the three crystal habit classes. A linear regression of the measured parameters from a zircon population on the calculated values for these parameters from the crystal habit classes showed that there was good correlation. The table below summarizes the results:

	Correlation coefficient	Slope of line	Y intercept
Mean Length	0.97	1.03	0.00
Mean Width	0.97	1.16	0.01
MER	0.90	0.77	0.43
RMA	0.90	1.00	1.72

There are several interpretations as to the interrelations of the various plutons in the northern part of the batholith; therefore the zircon populations, defined on the basis of their RMA and MER, were tested in light of all of the possible interpretations. The RMA and MER of the zircon populations was tested first against Knopf's (1957) interpretation of five separate intrusive phases generated from a single differentiating magma source. Figure 21 graphically shows the RMA and MER of the five phases on a length versus width of zircon plot. It is usually demonstrated that separation of the five phases is impossible. In order to determine the significance of variation of the RMA and MER of zircon populations within and between plutons, one-factor analysis of variance was used. Using Knopf's interpretation of the plutons, the null hypothesis had to be accepted indicating that the variation of these two parameters within a pluton was greater than the variation of these parameters between plutons (Table 12a).

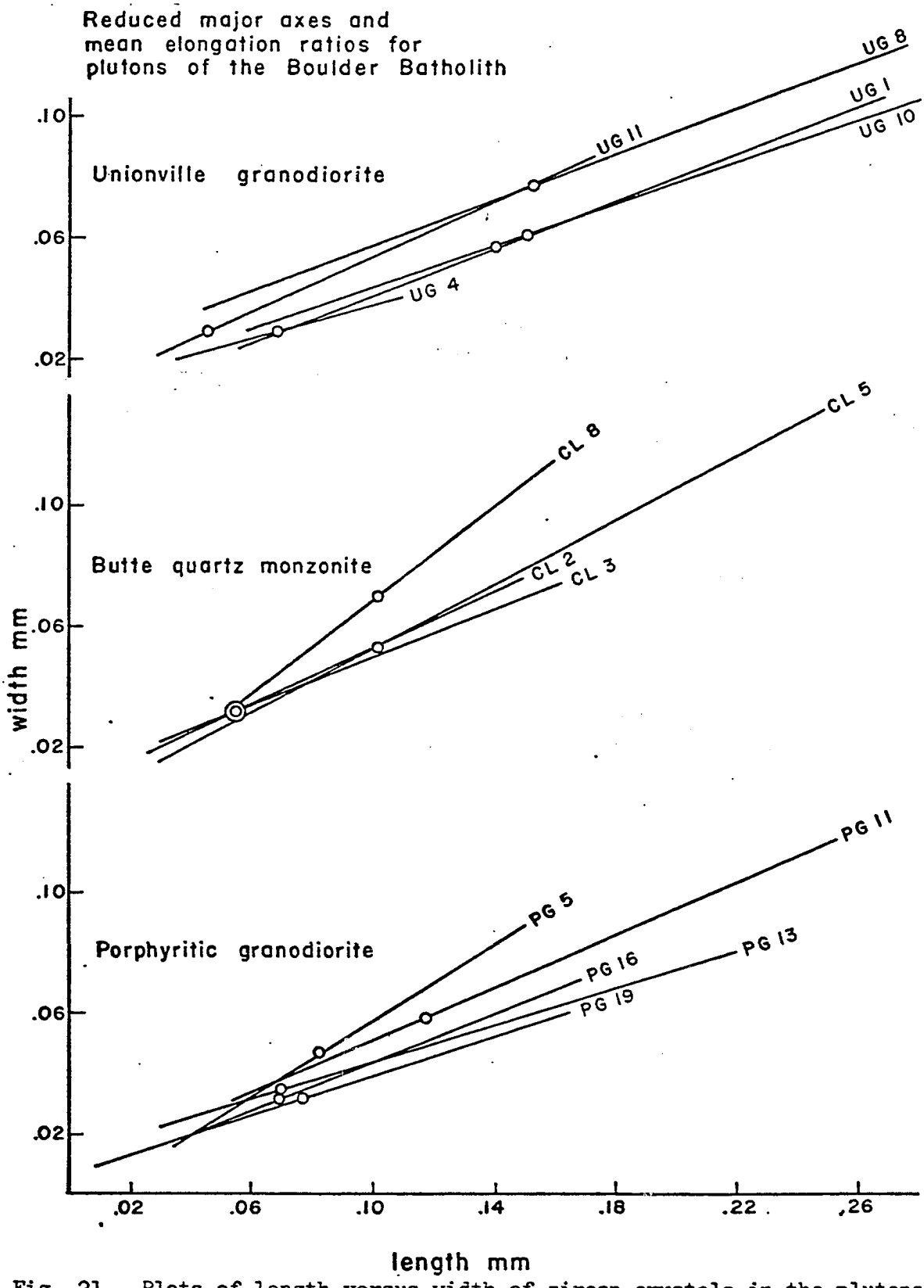

Fig. 21. Plots of length versus width of zircon crystals in the plutons of the Boulder batholith. Lines represent the calculated reduced major axes and points represent the mean elongation ratio.

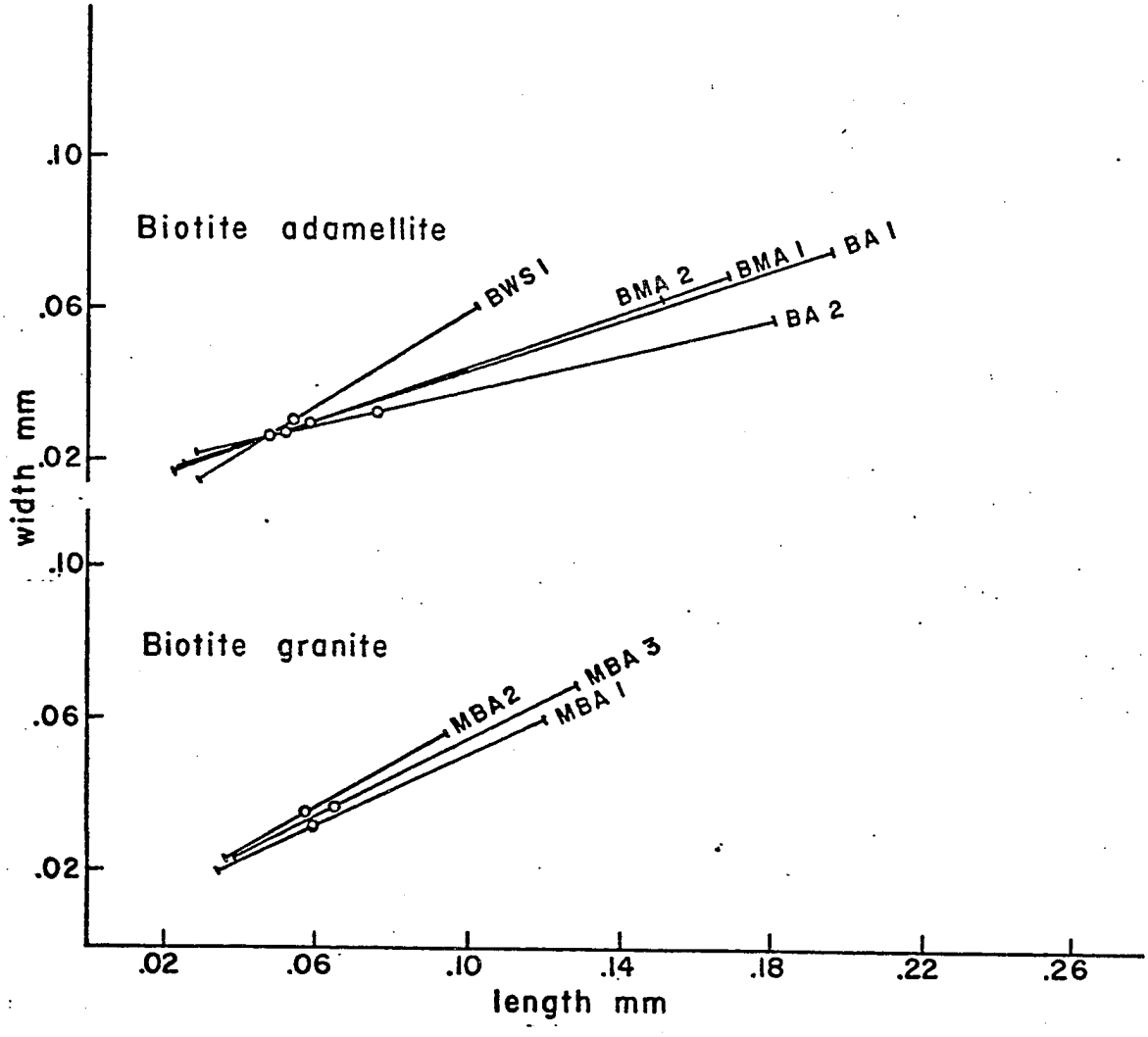

Fig. 21 (Continued)

The length of the line represents the range in length/width ratios of the zircon crystals.

TABLE 12

SUMMARY TABLE OF VARIANCE

Tables show results for one factor analysis of variance, to determine significance of variation of zircon populations in the intrusive phases of the Boulder batholith, Montana. Tables occur in pairs testing RMA and MER. Each pair of tables tests an interpretation of the batholith's intrusive history.

Σ^2 = sum of squares
df = degrees of freedom
F exp = F ratio, experimental
$F_{.95}$ = F ratio at the 95% confidence level

		source of variation	Σ^2	df	mean^2	F exp
(a) Knopf's intrusive phases -	RMA	between intrusive	212.42	4	70.81	2.62
		within intrusive	379.08	14	27.08	
					$F_{.95}$ (4,14) = 3.11	
	MER	between intrusive	0.91	4	0.23	2.48
		within intrusive	1.84	20	0.09	
					$F_{.95}$ (4,20) = 2.87	
(b) Knopf's intrusive phases subdivided into zircon classes						
	Class I - RMA	between intrusive	39.04	4	9.76	0.054
		within intrusive	3054.73	17	179.69	
					$F_{.95}$ (4,17) = 2.96	

Table 12 - Continued

Class II - RMA	between intrusive	165.58	4	41.39	1.51
	within intrusive	494.48	18	27.47	
				$F_{.95}(4,18) = 2.93$	
Class III - RMA	between instrusive	1231.63	4	307.91	1.712
	within intrusive	2693.74	15	179.78	
				$F_{.95}(4,15) = 3.06$	
Class I - MER	between intrusive	0.07	4	0.02	1.025
	within intrusive	0.26	15	0.02	
				$F_{.95}(4,15) = 3.06$	
Class II - MER	between instrusive	0.88	4	0.22	1.85
	within intrusive	2.14	18	0.12	
				$F_{.95}(4,11) = 3.36$	
(c) Knopf's intrusive phases excluding Biotite granite					
RMA	between intrusive	222.53	4	74.18	3.46
	within intrusive	257.25	12	21.44	
				$F_{.95}(4,12) = 3.49$	
MER	between intrusive	0.73	3	0.26	2.60
	within intrusive	1.62	16	0.10	
				$F_{.95}(3,16) = 3.24$	

Rable 12 - Continued

(d) Knopf's intrusive phases excluding Biotite granite subdivided into zircon classes

Class I - RMA	between intrusive	126.40	3	42.13	0.27
	within intrusive	1255.44	8	156.93	

$F_{.95}(3,8) = 4.07$

Class II - RMA	between intrusive	58.42	3	19.47	0.91
		170.67	8	21.33	

$F_{.95}(3,8) = 4.07$

A modification of Knopf's interpretation was next considered. This modification considers that the three crystal habit classes represent contamination of a given zircon population consisting of a single class by assimilation of other classes, either from other intrusives or the country rock. Thus each class may represent a separate population. The RMA and MER of each crystal habit class from all five of Knopf's intrusive phases were compared (Table 12b). Again the null hypothesis had to be accepted. The variation of the RMA and MER of the crystal habit classes was greater within each intrusive than between intrusive phases.

The next interpretation considered is the one suggested by this study, in which the Biotite granite is merely a facies of the Butte quartz monzonite. This implies that there are only four separate plutons. The results from the one factor analysis of variance indicate that again the null hypothesis must be accepted, since the variation of the RMA and MER was greater within intrusives than between (Table 12c).

The final interpretation against which the zircon populations was tested is the one involving the two magma series as suggested by Tilling (personal communication, 1971). In this case the zircon populations from samples of the Porphyritic granodiorite stock, representing the sodic magma series, were compared to the zircon populations from the Unionville granodiorite pluton, a representative from the main magma series. Since each pluton represents a separate magma series, and if zircons crystallized intratellurically, they should be represented by different individual populations based on RMA and MER because of the separate physiochemical conditions under which they crystallized from the melt. The one factor

analysis of variance shows that the variation of zircons based on their RMA and MER was greater within each of the two plutons than the zircon populations variation between the two (Table 12d).

In all the cases cited above, the variation of the RMA and MER of the zircon populations was greater within a pluton than between plutons as determined by one factor analysis of variance. The results from the one factor analysis of variance may represent two situations. The first is that all zircons and crystal habit classes belong to one uniform zircon population which exists throughout the batholith. For this reason it is impossible to fingerprint plutons or magma series on the basis of the RMA and MER of their zircon populations and crystal habit classes. The alternative situation is that each sample contains its individual zircon population and crystal habit classes defined in terms of their RMA and MER. This means that the batholith may be represented by an almost infinite number of zircon populations. Prior to drawing any conclusions, it is important to determine which of these situations exist in the batholith.

Previous zircon population workers, who assumed that zircons crystallize from a melt early and only for a short duration, may have predicted the behavior of the zircon populations for the plutons of the Boulder batholith in the following manner. In Knopf's one magma series interpretation it would have been predicted that all the zircons of the batholith represent one zircon population. With the crystal habit modification it would be expected that each crystal habit class in the entire batholith be characterized by similar RMA and MER. In the two magma series interpretation, it would have been expected that each magma

series be represented by its own individual zircon population. If the crystal habit modification is considered, then there should exist two populations of each crystal habit class of zircons. Another possibility is that each pluton may contain its own individual zircon population, and each crystal habit class in each pluton will be defined by the same RMA and MER.

The variation of RMA and MER acceptable in defining a zircon population has never been mentioned in the literature. However it is possible to get an idea of the amount of acceptable variation by looking at the Animas stock (Alper and Poldervaart, 1957) and the Bald Mountain batholith (Larsen and Poldervaart, 1957). Table 13 shows what these authors considered the variation of RMA and MER in defining a specific zircon population. Also included on Table 13 is the variation of the zircon populations and the crystal habit classes for the possible combinations of plutons, representing the predicted behavior of the zircon population by previous zircon workers who assumed the zircons crystallize early and for a short duration from a melt. As can be seen from Table 13, variation of the RMA and MER is greater than the limits set up by the Animas stock and Bald Mountain batholith. This suggests that the results from the analyses of variance must be interpreted with the model, which suggests that each sample in effect behaves as a single population in terms of the RMA and MER of its zircons and their crystal habits.

It is necessary to attempt an explanation as to why the Boulder batholith does not behave in the fashion predicted by previous studies.

First it is necessary to say that the original assumption made by

TABLE 13

TABLE SHOWING MEAN RMA, RANGE OF RMS, MEAN MER, RANGE OF MER OF ZIRCON POPULATIONS FROM THREE GRANITIC BODIES

Source	Mean RMA	Range of RMA	Mean MER	Range of MER
Animas stock	20.7°	5.0°	2.09	0.36
Bald Mtn. bath.	27.0°	2.5°	1.74	0.11
Boulder bath. one magma	23.8°	24.5°	2.09	1.27
Class I	31.7°	53.7°	1.09	1.21
Class II	22.1°	19.6°	2.03	1.25
Class III	27.8°	48.0°	2.39	3.23
Boulder bath. main series	24.1°	24.5°	2.02	1.27
Class I	32.6°	53.7°	1.59	0.55
Class II	21.2°	18.2°	2.13	1.25
Class III	28.2°	47.0°	2.22	1.29
Porphyritic granod.	22.9	14.2°	1.88	0.57
Class I	28.8°	18.2°	1.41	1.17
Class II	25.3°	9.6°	2.20	0.66
Class III	26.8°	37.6°	2.93	3.07
Unionville granod.	21.0°	9.4°	2.36	1.24
Class I	33.1°	53.7°	1.56	0.50
Class II	19.5°	9.6°	2.45°	1.25°
Class III	18.6°	23.7°	2.74	0.57
Butte qtz. mon.	28.4°	16.31°	1.76	0.60
Class I	34.8°	11.1°	1.49	0.17
Class II	20.7°	6.1°	2.02	1.02
Class III	42.5°	41.9°	1.66	0.52

the early zircon workers has been shown to be incorrect. Although zircons do begin to crystallize early from a melt, they crystallize over a long period and not for a short duration as was earlier assumed. It has been suggested earlier in this study that the Y/Th ratio of zircons varies with differentiation of a melt. The Y/Th ratio may control the crystal habit in zircons, which affects the RMA and MER of the zircon population. The RMA and MER of each of the crystal habit classes may also be affected by their Y/Th ratio, since the classes are chemically and morphologically transitional. The reason for the uniformity of zircon populations in the Animas stock and the Bald Mountain batholith is related to the differentiation of these bodies. Both of these bodies are very homogeneous mineralogically and chemically. In inhomogeneous bodies the zircon populations will not be uniform throughout the pluton as demonstrated in the strongly zoned Bald Rock batholith (Larsen and Poldervaart, 1961). Unfortunately, since the authors had made the assumption that zircons crystallize early and for a short period, they did not explain the differences of zircon populations between the zones of the Bald Rock batholith as reflecting the changes in the differentiating pluton. They rather suggest that the zircons are different in the zones due to inhomogeneity in the original undifferentiated magma.

Second is that although certain plutons of the Boulder batholith have been mapped as homogeneous, they are not, as can be observed in the chemical and mineralogic data presented earlier. This variation will affect the chemistry of the crystallizing zircons, which may affect the criteria defining the zircon populations such as RMA and MER, since zircon crystal habit may be dependent on zircon chemistry. It is for

these reasons that zircon populations for the Boulder batholith failed to behave as predicted.

VII. CONCLUSIONS

In summary, this investigation has resulted in a number of new interpretations as to the intrusive history of the Boulder batholith and the degree to which zircons, morphologically and chemically, reflect the evolution of this composite, epizonal batholith.

It is concluded, on the basis of mineralogical and textural information, that the Biotite granite of Knopf (1957) is the equivalent of the "mla" facies of the Butte quartz monzonite and does not represent a separate pluton. On the basis of major element chemical data, it is also determined that the Porphyritic granodiorite stock is a member of the sodic magma series as defined by Tilling (personal communication, 1971). The northern portion of the Boulder batholith therefore represents an area in which two magma series, a sodic and a more potassic or main series, were operating simultaneously. In this area the sodic magma series is represented by the Porphyritic granodiorite stock and the main series by a succession of three progressively silicic intrusions (Unionville granodiorite, Butte quartz monzonite, and the Biotite adamellite).

Based on the ranges of zirconium, hafnium, yttrium and thorium content of individual zircons and the distribution of these zircons in minerals representing a large temperature range, it is concluded that zircons begin crystallizing early and continue to crystallize for a long duration. This conclusion is supported by Pb-U isotope studies in zircon by Silver and Deutsch (1963). Further, crystal habit variation in zircon is related to the Y/Th ratio in the crystal. The Y/Th

ratio and the Hf/Zr ratio of zircon crystals increase with the differentiation of a granitic melt. The zircons from this batholith are enriched in thorium but are very low in uranium content, possibly due to thorium entering the lattice of zircon and other thorium bearing minerals. Thorite is absent. The low uranium content in the zircons may be due to uranium partitioning in favor of other minerals and the fluid phase, rather than entering the zircon lattice.

The Hf/Zr ratio of zircon populations reflects the intrusive history of the Boulder batholith as interpreted from data generated by this study. The proportions of the three crystal habits of zircon, vary systematically as a function of location within a pluton. The variation of the proportions of the crystal habit classes in a zircon population is reflected in the Y/Th ratio of the population, which increases from the periphery to the center of the pluton.

Zircons in silica undersaturated rocks such as the Priest's Pass leucomonzonite are anhedral and begin to crystallize during biotite formation and continue until complete crystallization of the melt occurs.

The relationship of the differentiation index (DI) and the silica content with the Hf/Zr ratio in zircon populations and the assumption that the zirconium and hafnium content of the two magma series of the batholith are similar suggest possibly that zircons tend to crystallize earlier in the course of differentiation of potassic melts than they do in sodic melts.

Zircon population studies based on the reduced major axis (RMA) and the mean elongation ratio (MER) of zircons is not an effective way

to index magmatic sources since the morphology of all zircons does not reflect the physiochemical conditions of the original melt, but rather the morphologies may reflect the chemical evolution of the melt.

VIII. APPENDIX OF TECHNIQUES

A. Introduction

A brief summary of the techniques used in this study is presented in this section. The techniques are presented in five parts. Part one involves the physical separation of zircons from the enclosing rock. Part two is a description of the techniques used in the description and measurement of zircons for the statistical analysis of zircon population. Part three involves the techniques used in defining the three crystal habit classes of zircon recognized in this study. Part four is a list of equations used in the statistical analysis of zircon populations. Part five involves the techniques used in the preparation of the sample for microprobe analysis and the method used in making the matrix corrections to get true concentration values for the elements analyzed.

B. Zircon Separation

To obtain significant data on zircons, it is first essential to remove the zircons from the rocks. Due to the high specific gravity (4.7) of zircon, the most efficient separation technique, in terms of time and quality of zircon concentrate, is through use of heavy liquids (Larsen and Poldervaart, 1957).

In brief, the separation method consists of grinding the bulk rock to minus 60 mesh, which assures release of the zircons from the minerals which contain them, but does not damage the zircons themselves. Fraction plus and minus 120 mesh are then obtained by sieving the sample.

The coarser fraction is placed in a separatory funnel containing acetylene tetrabromide (sp. gr. 2.96), while the finer fraction is centrifuged in acetylene tetrabromide to expedite separation. "Heavies" from both fractions are washed with acetone, then combined and placed in a separatory funnel containing methylene iodide (sp. gr. 3.32). The "heavies" from the methylene iodide are again washed with acetone and are subjected to a strong magnetic field to remove magnetite and iron filings introduced during grinding. The non-magnetic fraction is then run through the Frantz isodynamic separator at 0.5, 1.0 and 1.75 amperes at a dip of 20° and a plunge of 40°. The most non-magnetic portion is then placed in clerici solution (sp. gr. 4.6) in which zircons sink, effecting final separation. The zircons are then washed with distilled water and are ready for study.

C. Zircon Description and Measurement

Once the zircon crop was obtained, data collection began. As euhedral microphenocrysts, zircons were studied as individual crystals and as populations of crystals.

The crystals were placed in methylene iodide immersion media (index of refraction 1.738) and photomicrographs were made. Individual crystals were described with reference to crystal habit, zoning, and inclusions. In addition to the description, the individual zircon crystals were measured along the long (c-axis) and short (a_1 or a_2 axis) dimension. The measurement was done by placing a glass plate with a photographically printed grid on the photomicrograph or on the negative image which was projected on a wall screen using a film strip projector.

The latter technique proved to be less time consuming. In this manner both dimensions of a crystal could be measured with one manipulation.

Data from the measurements was then used to calculate the reduced major axis (RMA) and mean elongation ratio (MER), mean and standard deviations of length, width, and length/width ratio, the correlation coefficients of length, width, and length/width ratio, and the relative dispersion (Dd) (Imbrie, 1956) and to plot frequency curves and length versus width x-y plots in an attempt to define or compare zircon population parameters. These tedious and time consuming calculations and plots are facilitated by use of the computer program Zircon Statistics Version IV (I. Effimoff and R. J. Starmer, in preparation).

An average of 176 zircon crystals were measured in each sample for the population study based on RMA and MER. Samples consisted of a minimum of 152 and a maximum of 200 crystals each. In determining the RMA and MER for the crystal habit classes 40 crystals from each class were measured.

To determine the significance of variation of the RMA and MER of the zircon populations between the various plutons, one-factor analysis of variance with equal sample-number was used. When an insufficient number of samples was available for a group (pluton), a random numbers table was used to duplicate samples and thus generate a situation where equal number of samples were present in each group. The calculations for one factor analysis of variance were made using a program written for the Wang 500 by Dr. L. H. Lattman.

D. Definition of Crystal Habit Classes

The measurement of interfacial angles and the determination of crystal habits in minerals with the minute size of zircons found in this study was not possible using conventional methods such as optical goniometers. The spindle stage recommended for working with small crystals is inaccurate due to difficulties involved in orientation of the sample.

To circumvent these difficulties in obtaining angular measurements on small crystals, a technique suggested by Dr. F. Koucky was adopted. This technique involves making enlargements of zircon photomicrograph negatives onto 9"x9" extremely fine-grained airphoto film. The image on the airphoto film is a positive and provides an orthographic projection of the crystal which is almost always lying on its {110} face.

Most gnomonic projections for tetragonal minerals are published with the c-axis normal to the horizontal plane (Fig. 22). Since all the interfacial measurements on the zircons were made with the c-axis parallel to the horizontal plane, it was necessary to rotate the c-axis of the gnomonic projection onto the horizontal plane as well (Fig. 23). Once the rotation of the published zircon's gnomonogram was accomplished, the gnomonic projection with the measured angles was superimposed on it, and the indices of the faces were directly read from the published zircon's gnomogram. This is a rapid and accurate way of indexing faces on an orthographic projection.

There is one serious limitation to this technique, and that is the orthographic projection only enables the measurement of faces on the

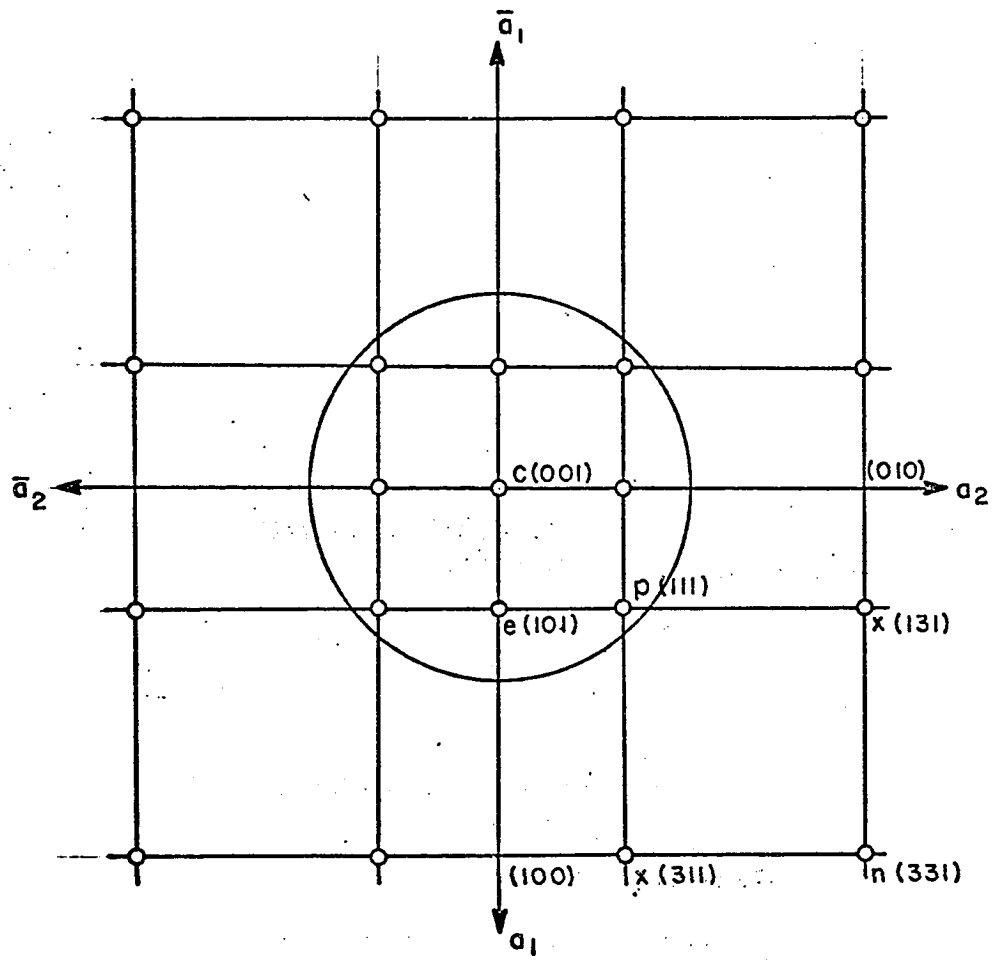

Fig. 22. Gnomonic projection of zircon with c normal to the horizontal plane.

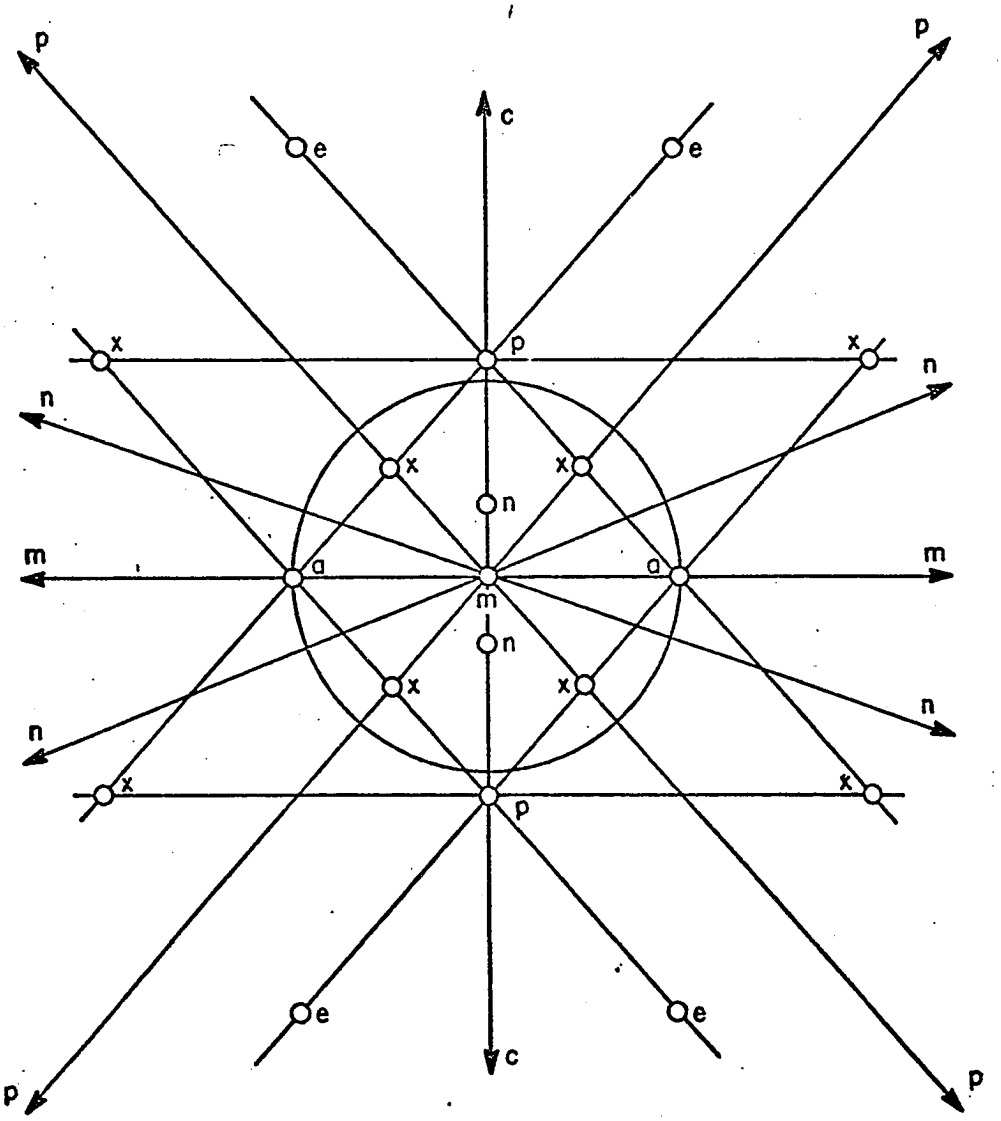

Fig. 23. Gnomonic projection of zircon on (110) face.

periphery of the projected image. The faces in the center of the image cannot be measured.

The interfacial angles for twenty-two euhedral zircon crystals from the three crystal habit classes were measured and plotted gnomonically. The descriptions of the classes are found in earlier sections of this paper. Figure 24 shows a summary diagram illustrating the distribution of the various combination of simple faces in the three crystal habit classes of zircon and comparing them to the ideal zircon with all the sample faces present.

E. Zircon Statistics Calculations

The following is a list of equations used in the calculation of parameters in zircon population studies. Unless specified to the contrary, all the equations are from Imbrie (1956).

Reduced major axis:

$$a = Sy/Sx \qquad \text{where}$$

a = tangent of angle of slope of the RMA

Sy = standard deviation of y (length)

Sx = standard deviation of x (width)

RMA is given in degrees from the horizontal.

Mean elongation ratio:

$$MER = \frac{\Sigma(Y/X)}{n} \qquad \text{where}$$

MER = mean elongation ratio

Σ = sum of all quantities indicated in parentheses

Y = length

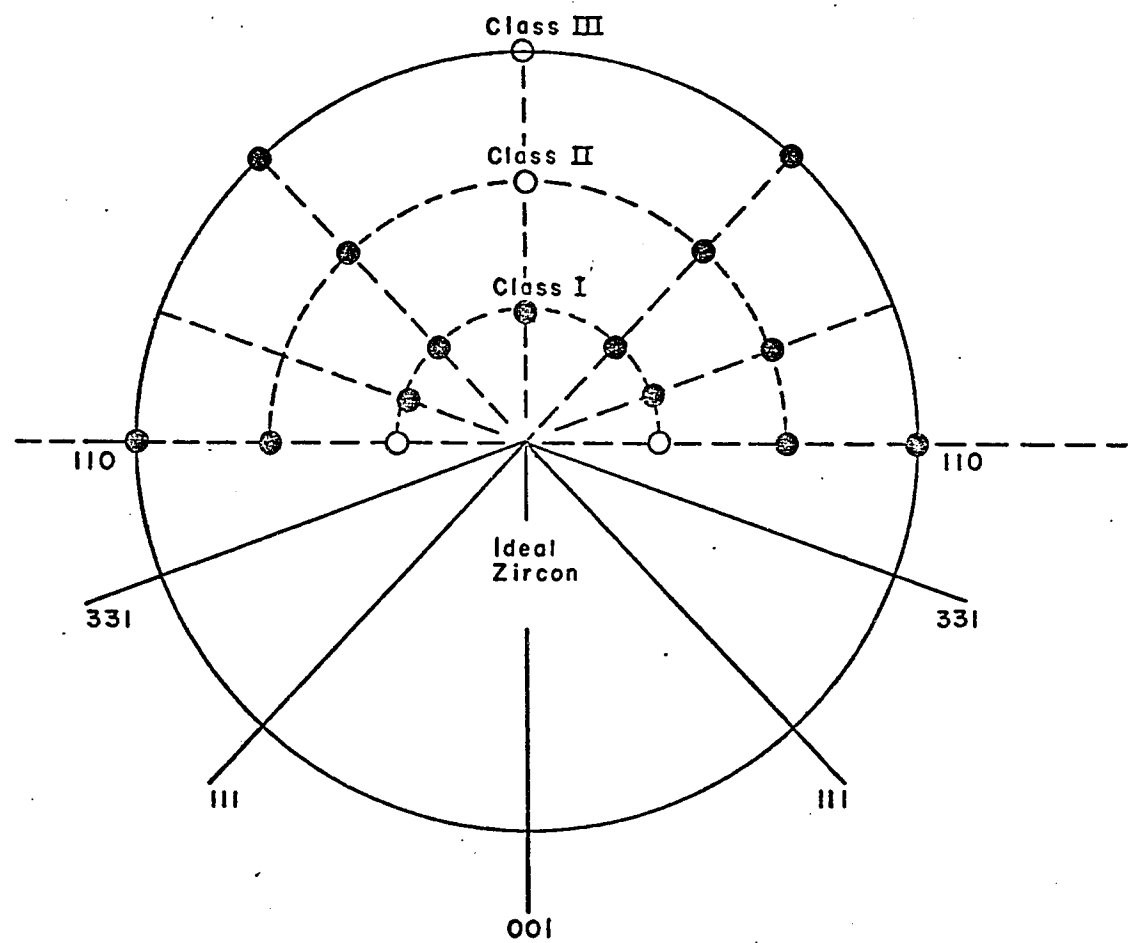

○ Well developed face
● Sometimes present or small face

Class III (100) very small if present
Class II (100) well developed
Class I (100) ?

Fig. 24. Summary diagram showing distribution of faces in the three classes of crystal habits as compared to the ideal zircon from Dana (1932).

X = width

n = number of individuals in sample.

Mean of length, and width:

$$\bar{z} = \frac{\Sigma(z)}{n}$$ where

$\bar{z}$ = mean of z (length or width)

Σ = sum of all quantities indicated in parentheses

n = number of individuals in sample.

Standard deviation:

$$s = \sqrt{\frac{(dz^2)}{n-1}}$$ where

s = standard deviation

d = $(z - \bar{z})$, the difference between any observation z and its mean.

z = length or width.

Correlation coefficient:

$$r = \frac{\Sigma((dx)\ (dy))}{\sqrt{\Sigma(dx^2)\ \Sigma(dy^2)}}$$

r = correlation coefficient

Σ = sum of all quantities indicated in parentheses

dx = $(x - \bar{x})$, the difference between any observation x and its mean

dy = $(y - \bar{y})$, the difference between any observation y and its mean

x = length

y = width.

Coefficient of dispersion:

$$Dd = 100\sqrt{\frac{2\,(1-r)\,(Sx^2 - Sy^2)}{x^2 + \bar{y}^2}}$$ where

Dd = coefficient of relative dispersion of points about the RMA

c = correlation coefficient of x on y

Sx = standard deviation of x (length)

Sy = standard devision of y (width)

$\bar{x}$ = mean of x

$\bar{y}$ = mean of y.

The following is a Table of Variance used in presenting results from analyses of variance. The appropriate equations are written in the proper positions.

Source of variation	Sum of squares	Degrees of freedom	Mean Square	F
between group	$\Sigma_i n_i (\bar{x}_i - \bar{x})^2$	c-1	$\frac{1}{c-1}\Sigma_i n_i (\bar{X} - \bar{X})^2$	$\frac{msb}{msw}$
within group	$\Sigma_i \left[\Sigma_j (X_{ij} - \bar{X}_i)^2\right]$	N-C	$\frac{1}{N-C}\Sigma_i \left[\Sigma_j (X_{ij} - \bar{X}_i)^2\right]$	

where n_i = number of observations in group i

c = groups

X_{ij} = value of the jth observation in group i

$\bar{X}_i$ = mean of group i

$\bar{X}$ = grand mean of all observations.

N = total number of observations in the entire analysis.

msb = mean square between groups

msw = mean square within groups.

(Simpson, et al., 1960).

F. Microprobe Analysis

This section discusses three phases of the electron microprobe analysis of zircons. The first phase involves the preparation of the sample for the analysis, the next phase involves the actual details of the analysis, and finally the data reduction necessitated by matrix effects in order to obtain true elemental concentrations.

In all phases of sample preparation for electron microprobe analysis, care was taken to reduce all factors which would be sources of error and result in inaccurate analysis.

The initial step was to mount the selected zircon grains onto a glass slide using epoxy cement. The sample was then ground, using 400 and 900 size alumina grit, to the point where the cross-section of the zircon grains were exposed. A large exposed area was necessary in order to provide the maximum probing area as well as to make available an area representative of a zoned crystal's chemistry. The grain mounts were then polished using 6, 1, and 0.5 micron diamond paste sequentially. To remove any adhered diamond paste, the mount was washed with water in a sonic cleaner.

Prior to probing, it was necessary to carbon coat the mounts and the standards using a vacuum evaporator because zircon is an insulator electrically. Conductivity in the specimens was further enhanced by painting a conductive path, using silver paint, from an area close to the grains to the brass specimen holder.

Analyses were performed on an ARL, three channel electron microprobe interfaced with a teletype output. Thirty-five samples were

probed for zirconium, hafnium, yttrium, thorium, uranium and silica. Seventeen additional samples were analyzed for zirconium, hafnium, and yttrium only. An average of four to five grains constituted each sample.

The following table shows the elements analyzed, the standards used and the conditions under which analyses were made.

Element	Zr	Hf	Y	Th	U	Si
Standard	Zr metal	Hf metal	Y foil	ThO_2	U metal	Quartz
Accelerating voltage	20Kv	20 Kv	20 Kv	20 Kv	20 Kv	20 Kv
Strongest line	L	M	X	M	M	K
Wave length of line	6.07Å	7.539Å	6.448Å	4.138Å	3.910Å	7.126Å
Analyzing crystal	C	LIF	ADP	LIF	LIF	KAP

The average size of the "spot" was approximately 1.5 microns. Inclusions were avoided during the probe analysis. The analysis of each zircon grain represents the average of four irradiated spots.

Precision of readings (reproducability) was determined on the standard for each element, since the standards were more homogeneous than the zircon crystal. The following table shows the statistics on the precision of readings.

	Mean counts/100 sec.	Variance	Standard deviation	Relative error
Zr	21,578	36,352	190	± 0.88%
Hf	46,222	152,917	391	± 0.85%
Y	14,517	9,344	96	± 0.66%
Th	6,801	1,864	43	± 0.63%
Si	68,835	421,888	649	± 0.94%

After all the raw data was obtained, it was necessary to make the appropriate matrix corrections and reduce it to values representing elemental concentrations. The MAGIC II program written by Colby (1968) which transforms K values to actual weight percent compositions using binary compounds or single element standards was used. Beaman and Isasi (1970) consider MAGIC II to be among the outstanding programs for quantitative electron microprobe analysis available to date.

The input to MAGIC II consists of raw data in counts per second for elements in the unknown and the standard, their atomic numbers and weights, the spectral lines used in their analysis, the accelerating voltage, the take off angle (52.5° in this instance). One element can be calculated by difference so the same information is necessary for it. In this study oxygen was determined by difference.

The output consists of a listing of the input data, the back-scatter factor, excitation potential, absorption jump ratio, fluorescence yield, calculated weight percent and atomic percent of elements analyzed and determined by difference, the K value, and peak to background ratio.

Although this is a very useful computer program, it is also very expensive to run. Due to the large number of grains analyzed, the expense involved in data reduction, raw data from forty-one grains analyzed for six elements was input into the MAGIC II program. Calibration curves for the six elements were established from the program's output, since both K value and the actual concentration in weight percent were presented (Fig. 25a-e). K values for the remaining analyses were calculated with a Wang 500, program written for that purpose using

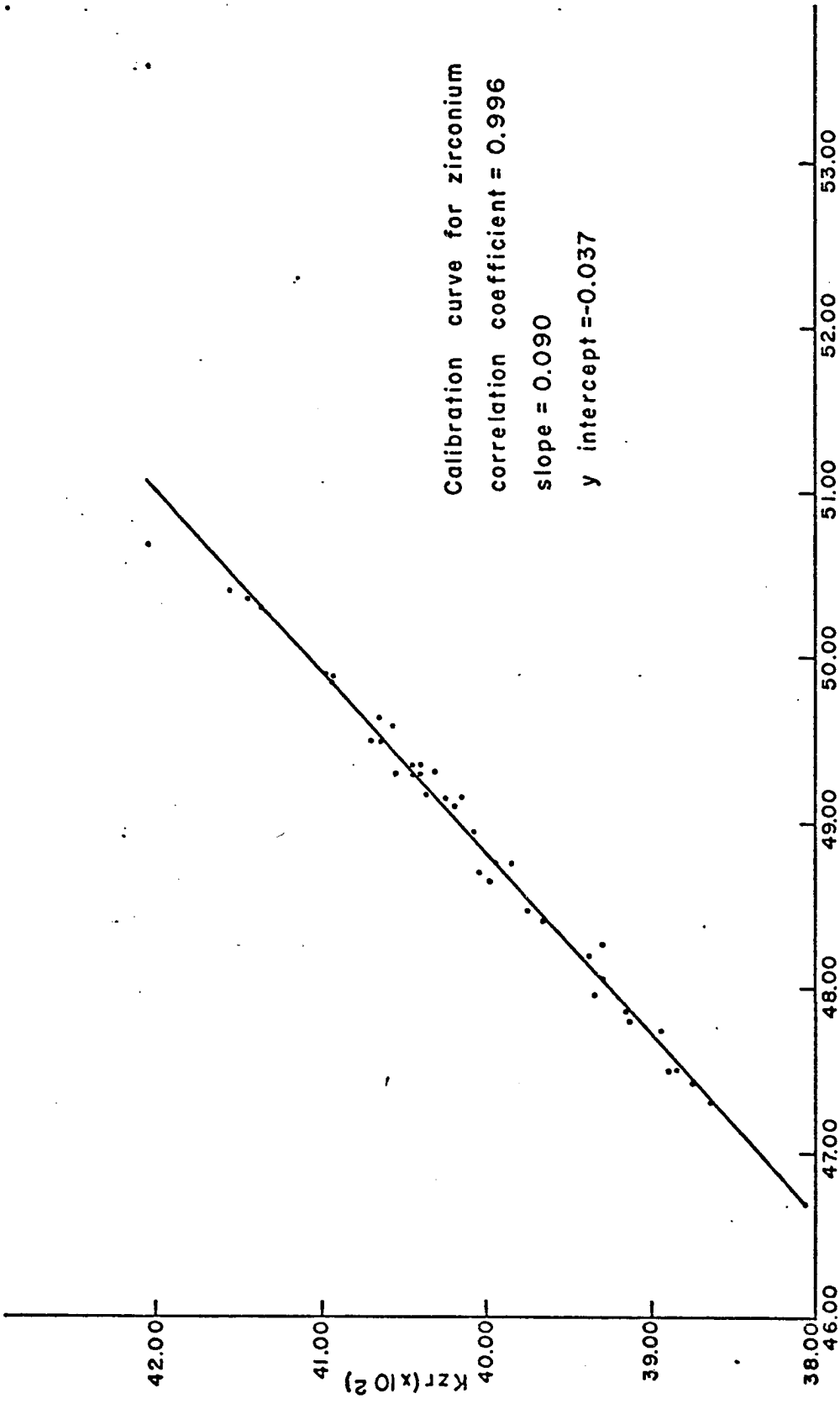

Fig. 25a.

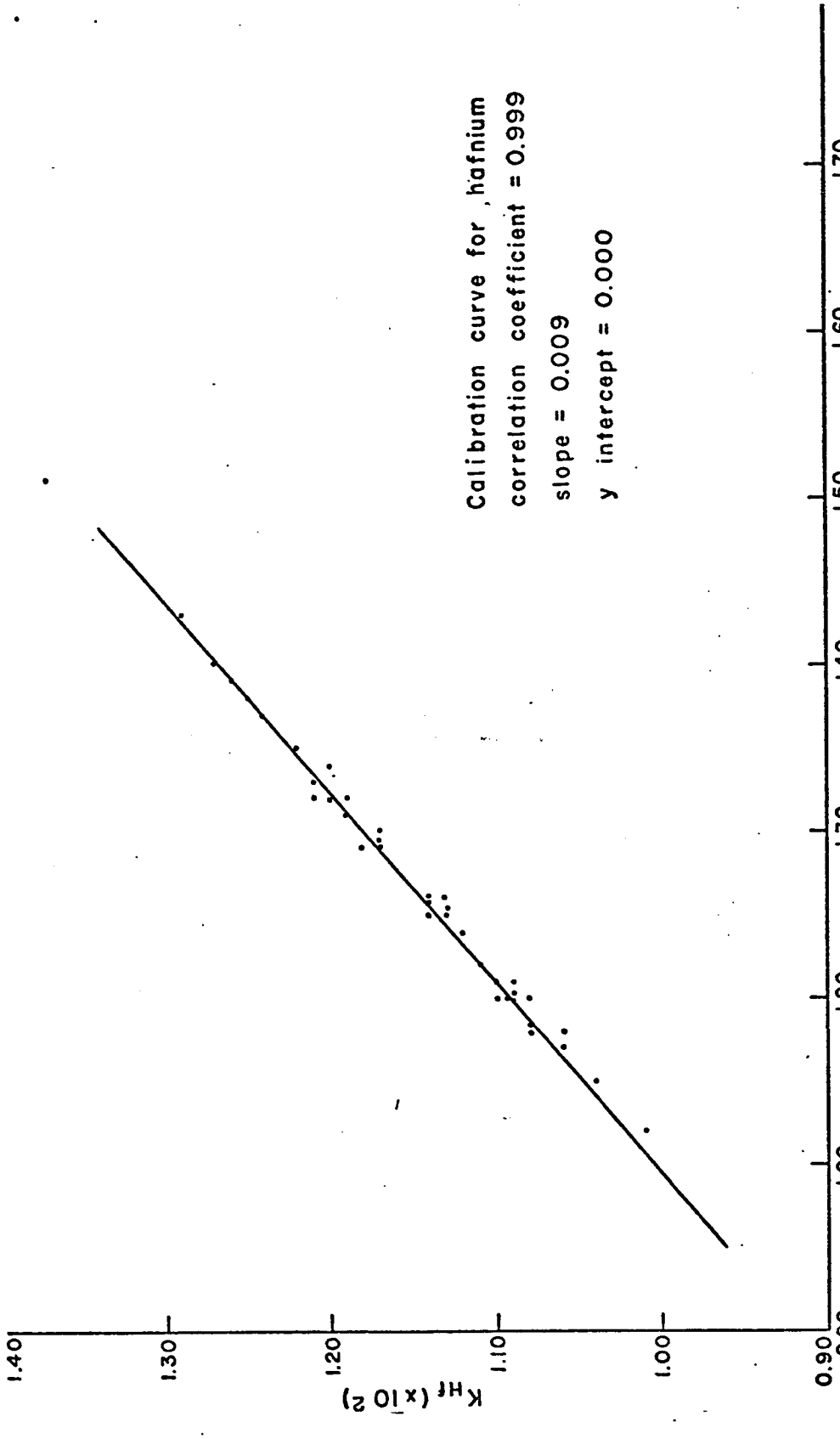

Fig. 25b.

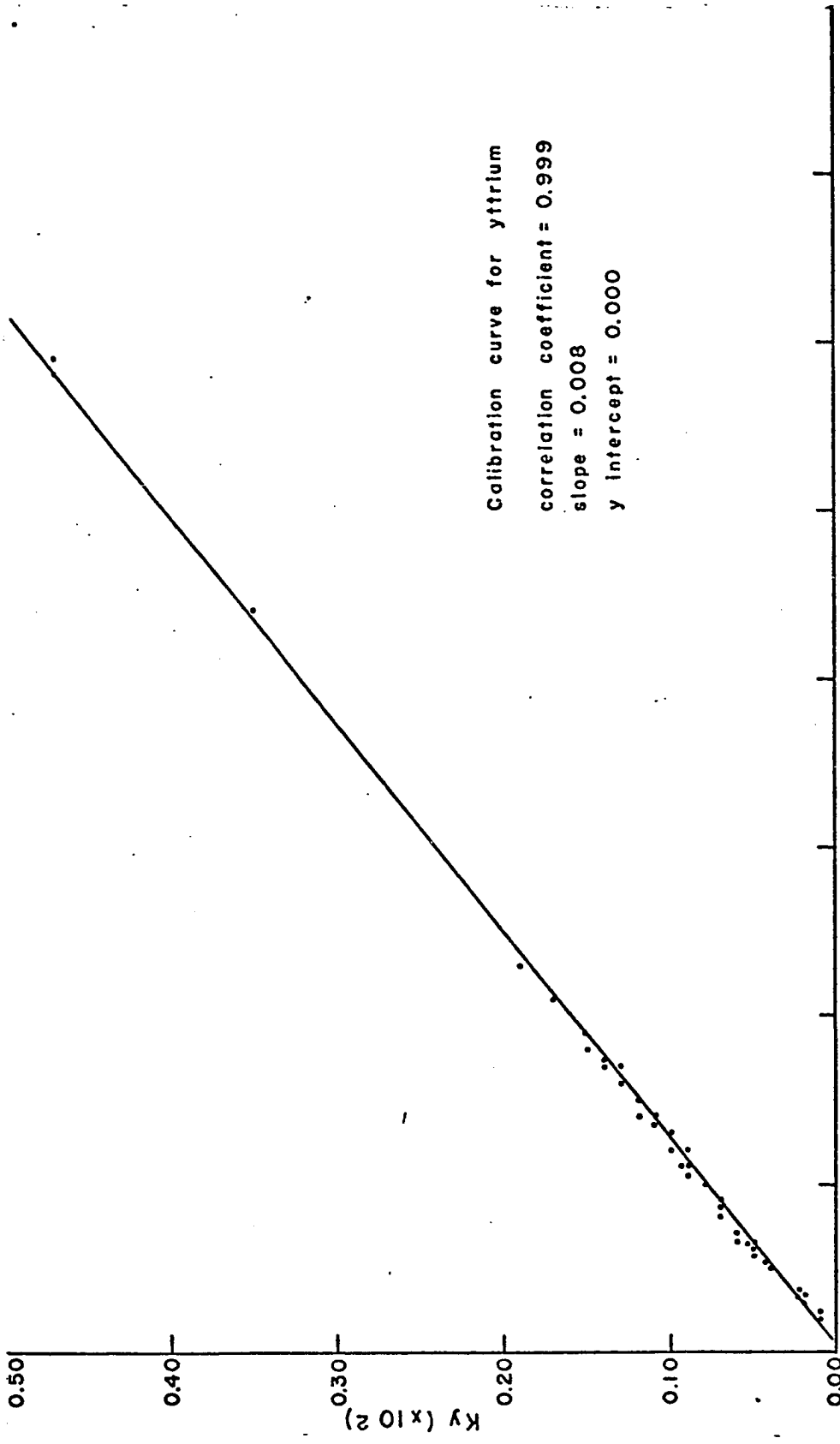

Fig. 25c

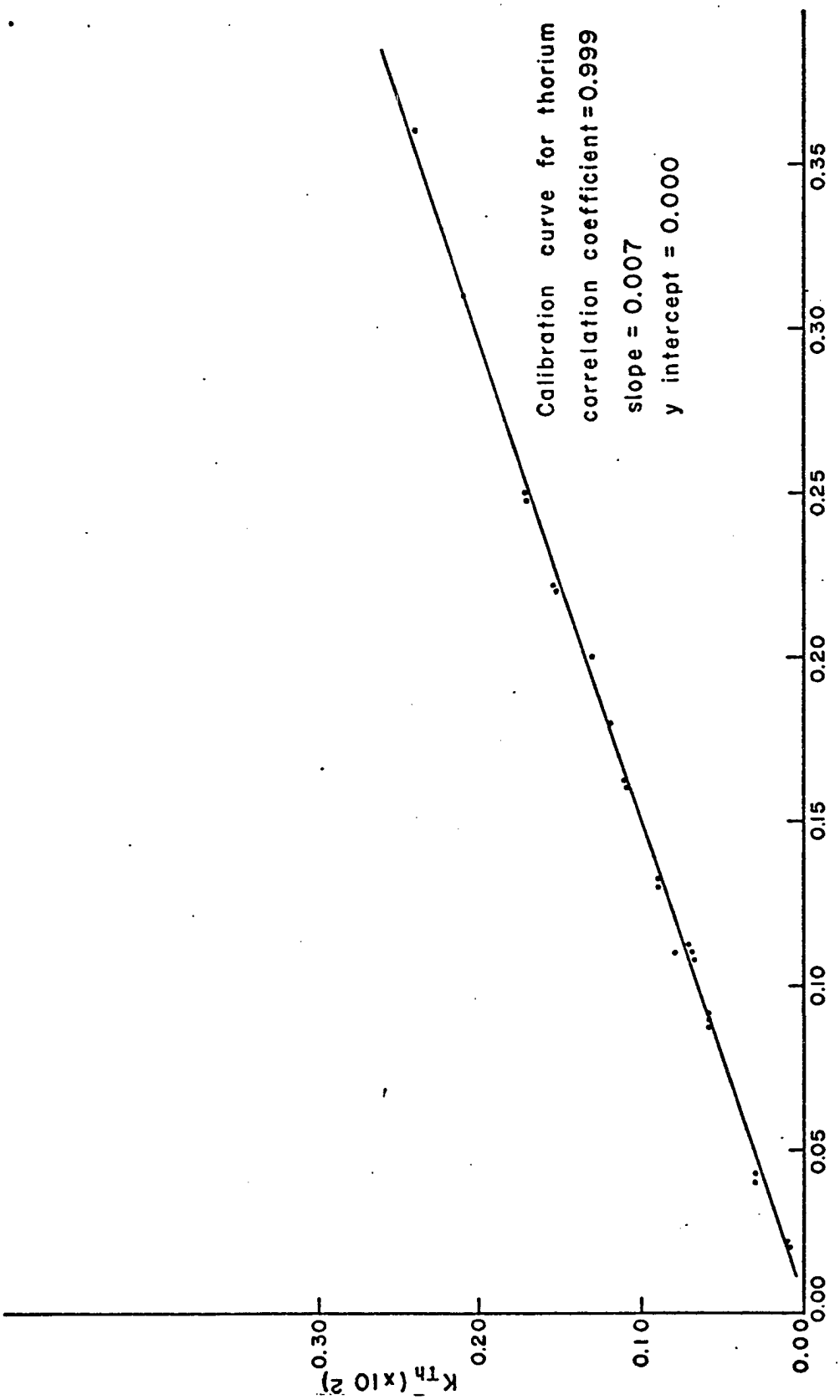

Fig. 25d.

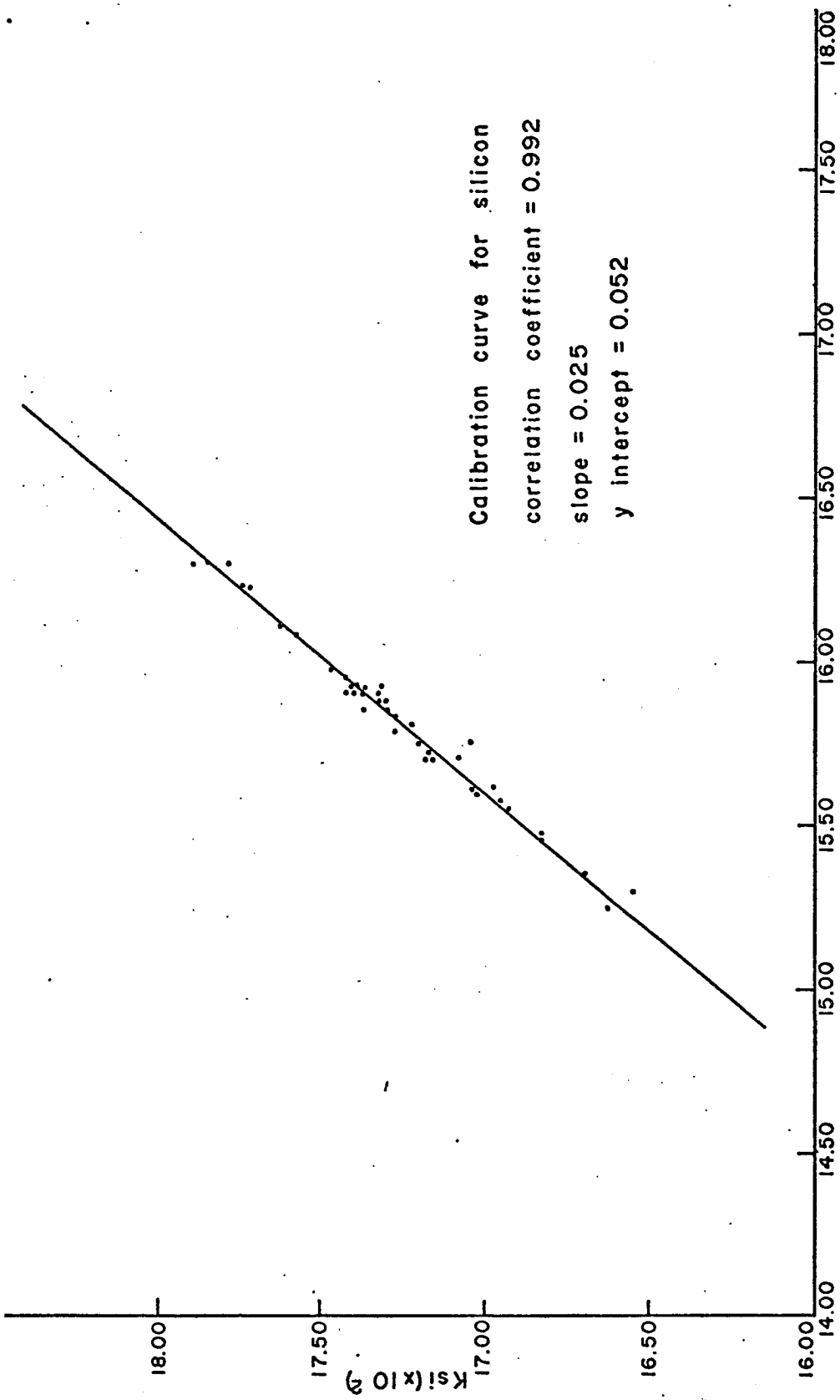

Fig. 25e

equation 1. Since the calibration curves for the elements were established, it was a simple task to define the calibration curve using the equation for a straight line: $y = mx+b$. Another Wang 500 program, which incorporated the equation for the calibration curve, was used to determine true concentration of the elements for input K values.

Since there are no primary natural or synthetic zircon standards available today, matrix corrections have to be performed on programs such as MAGIC II using single element or binary compound standards to obtain true concentrations. The accuracy of an analysis is only as good as the standard used; therefore, standards with matrices closely approximating the matrix of the unknown sample are best. The greater the correction necessary due to matrix differences between standard and sample, the less accurate the analysis. Chemical analyses of natural single zircon grains is virtually impossible by most conventional analytical techniques. A possible solution is to resort to synthetic zircons produced in the laboratory which would contain all the elements reported from zircon in the appropriate proportions.

BIBLIOGRAPHY

Alper, A. M., and Poldervaart, A., 1957, Zircons from the Animas stock and associated rocks, New Mexico: Econ. Geol., v. 52, p. 952-971.

Beaman, D. R., and Isasi, J. A., 1970, A critical examination of computer programs used in quantitative electron microprobe analysis: Anal. Chem., v. 42, pp. 1540-1568.

Becraft, G. E., 1956, Uranium deposits in the northern part of the Boulder batholith: Econ. Geol., v. 81, pp. 362-374.

Becraft, G. E., and Pinckney, D. M., 1961, Preliminary geologic map of the northwest quarter of the Boulder quadrangle, Montana: U. S. Geol. Survey Min. Invest. Field Studies, Map MF-183.

Becraft, G. E., Pickney, D. M. and Rosenblum, S., 1963, Geology and mineral deposits of the Jefferson City quadrangle, Jefferson, and Lewis and Clark Counties, Montana: U. S. Geol. Survey Prof. Paper 428, 101 p.

Buckley, H. E., 1951, Crystal growth, John Wiley and Sons, 571 p.

Buddington, A. F., 1959, Granite emplacement with special reference to North America: Geol. Soc. Am. Bull., v. 70, pp. 671-747.

Castaing, R., 1960, Electron microprobe analysis in Advances in Electronics and Electron Physics, edited by L. Martin, Academic Press, v. 13, pp. 317-386.

Colby, J. W., 1968, Quantitative microprobe analysis of thin insulating films: Advan. X-ray Anal., v. 11, pp. 287-305.

Cotton, A. F., and Wilkinson, G., 1967, Advances in Inorganic Chemistry: Interscience Publishers, 1136 p.

Dana, E. S., 1893, Descriptive mineralogy: Sixth edition, John Wiley and Sons, 1134 p.

Dana, E. S., 1932, A textbook of mineralogy: revised by W. E. Ford, fourth ed., John Wiley and Sons, 581 p.

Deer, W. A., Howie, R. A., and Zussman, J., 1962, Ortho and ring silicates: in Rock Forming Minerals, v. 1, 333 pp.

Dennen, W. H. and Shields, R., 1956, Yttria in zircon: Am. Min., v. 41, p. 655.

Doe, B. R., Tilling, R. I., Hedge, C. E., and Klepper, M. R., 1968, Lead and strontium isotope studies of the Boulder Batholith, Southwestern Montana: Econ. Geol., v. 63, pp. 884-906.

Fleischer, M., 1955, Hafnium content and hafnium-zirconium ratio in minerals and rocks: U. S. Geol. Survey Bull. 1021-A, 13 p.

Görz, H. and White, G. W., 1970, Minor and trace elements in HF-soluble zircons: Contr. Mineral. and Petr., v. 29, pp. 180-182.

Görz, H., and White, E. W., 1971, Microprobe studies of inclusions in zircons: Trans. Am. Geophy. Union, abstracts 52nd annual mtg., v. 52, pp. 370.

Gottfried, D., and Waring, C. L., 1964, Hafnium content and Hf/Zr ratio in zircons from the Southern California batholith: U. S. Geol. Survey Prof. Paper 501-B, pp. B88-B91.

Hamilton, W., and Myers, W. B., 1967, The nature of batholiths: U. S. Geol. Survey Prof. Paper 554-C, 30 p.

Heinrich, K. F. J., 1966, The electron microprobe: John Wiley and Sons, 377 p.

Holland, H. D. and Gottfried, D., 1955, The effect of nuclear radiation on the structure of zircon: Acta. Cryst., v. 81, p. 291.

Hurley, P. M., and Fairbairn, H. W., 1957, Abundance and distribution of Uranium and thorium in zircon, sphene, apatitie, epidote and monozite in granitic rocks: Trans. Am. Geophys. Union, v. 38, pp. 939-944.

Imbrie, J., 1956, Biometrical methods in the study of invertebrate fossils: Am. Mus. Nat. Hist. Bull., v. 108, pp. 211-252.

Keil, K., 1967, The electron microprobe X-ray analyzer and its application in mineralogy: Fortschr. Miner., v. 44, pp. 4-66.

Kermack, K. A. and Haldane, J. B. S., 1950, Organic correlation and allometry: Biometrika, v. 37, pp. 30-41.

Klepper, M. R., Robinson, G. D., and Smedes, H. W., 1971, On the nature of the Boulder batholith of Montana: Geol. Soc. Am. Bull., v. 82, pp. 1563-1580.

Klepper, M. R., Weeks, R. A., and Ruppel, E. T., 1957, Geology of the southern Elkhorn Mountains, Jefferson and Broadwater Counties, Montana: U. S. Geol. Survey Prof. Paper 292, 82 p.

Knopf, A., 1957, Boulder bathylith of Montana: Am. Jour. Sci., v. 255, pp. 81-103.

Knopf, A., 1963, Geology of the northern part of the Boulder bathylith and adjacent area, Lewis and Clark Counties, Montana: U. S. Geol. Survey Misc. Geol. Inv. Map I-381.

Knopf, A., 1964, Time required to emplace the Boulder bathylith, Montana - A first approximation: Am. Jour. Sci., v. 262, pp. 1207-1211.

Kosterin, A. V., Shevaleyevskii, I. D., Rybalova, E. K., and Tolok, K. P., 1963, Zr/Hf ratios in zircons from some igneous rocks in north Kazakhstan: Geochemistry, No. 10, pp. 1007-1009.

Kosterin, A. B., Zuyev, V. N., and Shevaleyevskii, I. D., 1958, Zr/Hf ratios in zircons in some igneous rocks of northern Kirgizia: Geochemistry, No. 1, pp. 116-119.

Larsen, L. H., and Poldervaart, A., 1957, Measurement and distribution of zircons in some granitic rocks of magmatic origin: Min. Mag., v. 31, pp. 544-564.

Larsen, L. H., and Poldervaart, A., 1961, Petrologic study of Bald Rock batholith, near Bidwell Bar, California: Geol. Soc. Am. Bull., v. 72, pp. 69-92.

Leonova, L. L., and Bashalov, Yu. A., 1963, Distribution of U, Th and the REE in the granitoids of the Susamyr batholith, no. 11, pp. 1047-1055.

Lipard, S. J., 1967, Eight-coordination Chemistry: in Progress in Inorganic Chemistry, v. 8, edited by F. A. Cotton, Interscience Publishers, pp. 109-195.

Lipova, I. M., and Shevaleyevskii, I. D., 1961, On the Zr/Hf ratio in zircons from pegmatites of different compositions: Geochemistry, no. 7, pp. 686-690.

Lipova, I. M., Shevaleyevskii, I. D., and Tuzova, A. M., 1957, On the ratio of zirconium and hafnium in granitoids of the Verkhissetsk intrusion: Geochemistry, no. 2, pp. 159-169.

Lyakhovich, V. V. and Barinskii, R. L., 1961, Characteristics of the rare earth assemblages in the accessory minerals of granitoids: Geo-Chemistry, no. 6, pp. 495-509.

Lyakhovich, V. V., and Shevaleyevskii, I. D., 1962, Zr/Hf ratios in accessory zircon in granitoids: Geochemistry, no. 5, pp. 508-524.

Meyer, C., Shea, E. P., Goddard, C. C. and staff, 1968, Ore deposits at Butte, Montana: Ore Deposits in the United States 1933/1967, edited by J. D. Ridge, AIME Inc., v. 2, pp. 1373-1416.

Moorehouse, W. M., 1956, The paragenesis of accessory minerals: Econ. Geol., v. 51, pp. 248-262.

Mumpton, F. A. and Roy, R., 1961, Hydrothermal stablility studies of the zircon-thorite group: Geochem. Cosmochem. Acta, v. 21, pp. 217-238.

Murthy, M. V. N., 1958, On the crystallization of accessory zircon in

granitic rocks of magmatic origin: Can. Min., v. 6, pp. 260-263.

Pavlenko, A. S., Vainshtein, E. E., and Shevaleyevskii, I. D., 1957, On the hafnium-zirconium content of igneous and metasomatic rocks: Geochemistry, no. 5, pp. 411-431.

Pinckney, D. M. and Becraft, G. E., 1961, Preliminary geologic map of the southwest quarter of the Boulder quadrangle, Montana: U. S. Geol. Survey Min. Invest. Field Studies Map MF-187.

Poldervaart, A., 1956, Zircons in rocks. 2. Igneous rocks: Am. Jour. Sci., v. 254, pp. 521-554.

Prostka, H. J., 1966, Igneous geology of the Dry Mountain Quadrangle, Jefferson County, Montana: U. S. Geol. Survey Bull. 1221-F, 21 p.

Robinson, K., Gibbs, G. V. and Ribbe, P. H., 1971, The structure of zircon: a comparison with garnet: Am. Min., v. 56, pp. 782-790.

Roedder, E., 1962, Ancient fluids in crystals: Scientific American, v. 207, no. 4, pp. 38-47.

Ruppel, E. T., 1961, Reconnaissance geologic map of the Deer Lodge quadrangle, Powell, Deer Lodge and Jefferson Counties, Montana: U. S. Geol. Survey Bull. 1151, 121 p.

Silver, L. T., and Deutsch, S., 1963, Uranium-lead isotopic variations in zircons: a case study: Jour. Geol., v. 71, pp. 721-758.

Simpson, G. G., Roe, A., Lewontin, R. C., 1960, Quantitative zoology: revised edition, Harcourt, Brace and World, 440 p.

Smedes, H. W., 1966, Geology and igneous petrology of the northern Elkhorn Mountains, Jefferson and Broadwater Counties, Montana: U. S. Geol. Survey Prof. Paper 510, 116 p.

Smedes, H. W., Klepper, M. R., Pinckney, D. M., Becraft, G. E., and Ruppel, E. T., 1962, Preliminary geologic map of the Elk Park quadrangle, Jefferson and Silver Bow Counties, Montana: U. S. Geol. Survey Min. Invest. Field Studies Map MF-246.

Smedes, H. W., Klepper, M. R., and Tilling, R. I., 1968, The Boulder Batholith: Geol. Soc. Am. Rocky Mtn. Sec., Field Trip Guide no 3, 21 p.

Smedes, H. W. and Thomas, H. H., 1965, Reassignment of the Lowland Creek Volcanics to Eocene age: Jour. Geol., v. 73, p. 508-509.

Smith, J. V., 1965, X-ray emission microanalysis of rock forming minerals. I: experimental techniques: Jour. Geol., v. 73, pp. 830-864.

Smithson, F., 1939, Statistical methods in sedimentary petrology:

Geol. Mag., v. 76, pp. 297-309, 348-361, 417-427.

Spotts, J. H., 1962, Zircon and other accessory minerals, Coast Range batholith, California: Geol. Soc. Am. Bull., v. 73, pp. 1221-1240.

Sweatman, T. R. and Long, J. V. P., 1969, Quantitative electron probe microanalysis of rock forming minerals: Jour. Pet., v. 10, pp. 332-379.

Tilling, R. I., 1964, Variation in modes and norms of a "homogeneous" pluton of the Boulder batholith, Montana: U. S. Geol. Survey Prof. Paper 501-D, p. D8-D13.

Tilling, R. I. and Gottfried, D., 1969, Distribution of thorium, uranium and potassium in igneous rocks of the Boulder batholith region, Montana, and its bearing on radiogenic heat production and heat flow: U. S. Geol. Survey Prof. Paper 614-E, 29 p.

Tilling, R. I., Klepper, M. R., and Obradovich, J. D., 1968, K-Ar Ages and time span of emplacement of the Boulder Batholith, Montana: Am. Jour. Sci., v. 266, p. 671-689.

Tomita, T., and Karakida, Y., 1958, Source identification of some granitic xenoliths in volcanic rocks: Mem. Fac. Sci., Kyushu Univ., Series D, Geology, v. 8, pp. 25-34.

Tugarinov, A. I., Vainshtein, E. E., and Shevaleyevskii, I. D., 1956, Hafnium-zirconium ratio in zircons of igneous and metasomatic rocks, 1956, Geochemistry, no. 4, pp. 361-375.

Veniale, F., Pigorini, B., and Soggetti, F., 1968, Petrological significance of the accessory zircons in the granites from Baveno, M. Orfano and Alzo (North Italy): XXIII International Geological Congress Report, v. 13, pp. 243-268.

Vlasov, K. A., 1966, Mineralogy of rare elements: in Geochemistry and Mineralogy of Rare Elements and Genetic Types of their Deposits, v. 2, 945 p.

Vlasov, K. A., 1966b, Geochemistry of rare elements: in Geochemistry and Mineralogy of Rare Earth Elements and Genetic Types of their Deposits, v. 1, 688 p.

Wager, L. R., and Mitchell, R. L., 1951, The distribution of trace elements during strong fractionation of basic magma - a further study of the Skaergaard intrusion, East Greenland: Geochem. Cosmochem. Acta, v. 1, pp. 129-208.

Wells, A. F., 1962, Structural Inorganic Chemistry: 3rd ed., Oxford Press, 1055 p.

Winchell, A. N., 1951, Part II - Description of minerals: in Elements of Optical Mineralogy, John Wiley and Sons, 551 p.

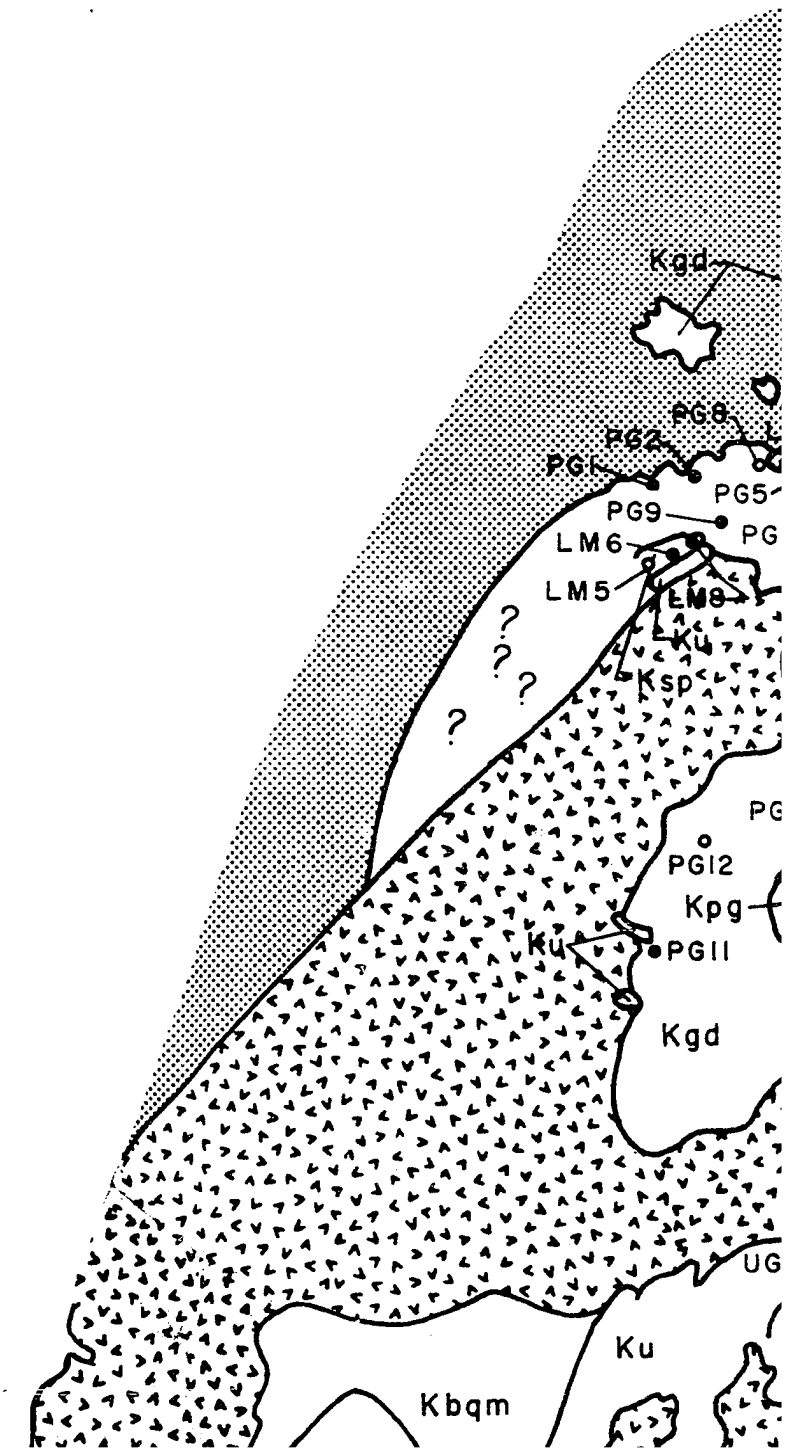

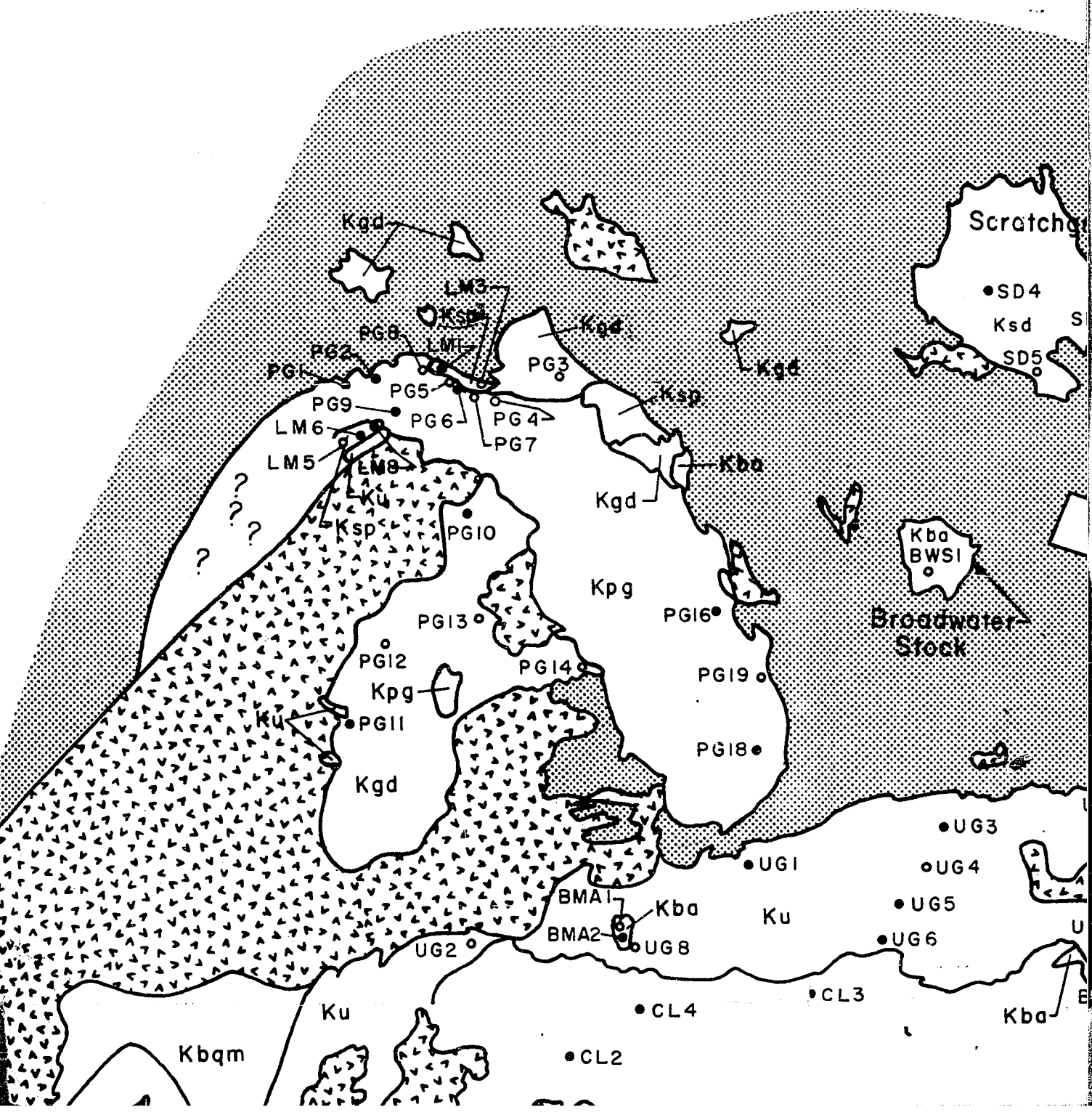

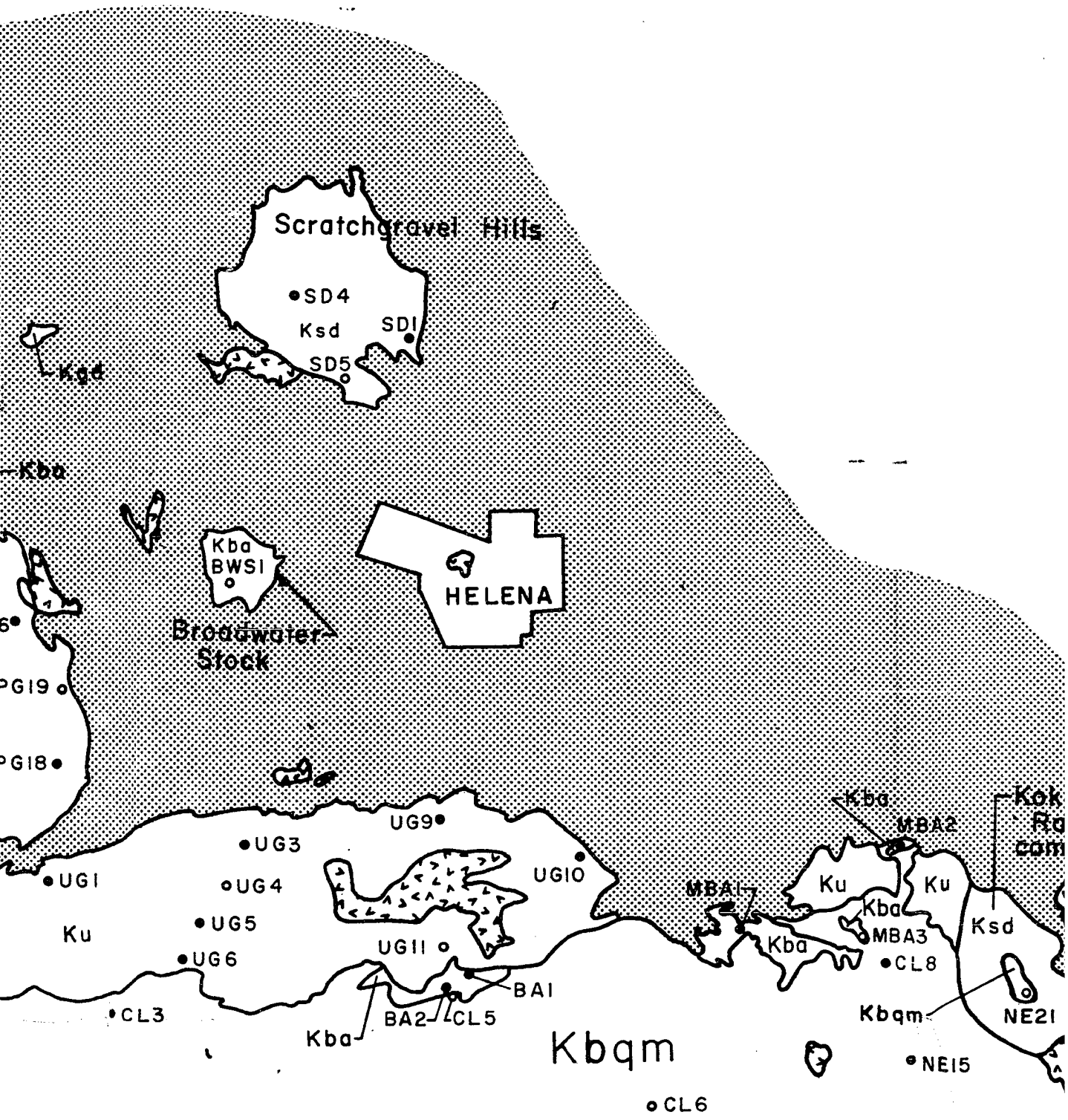

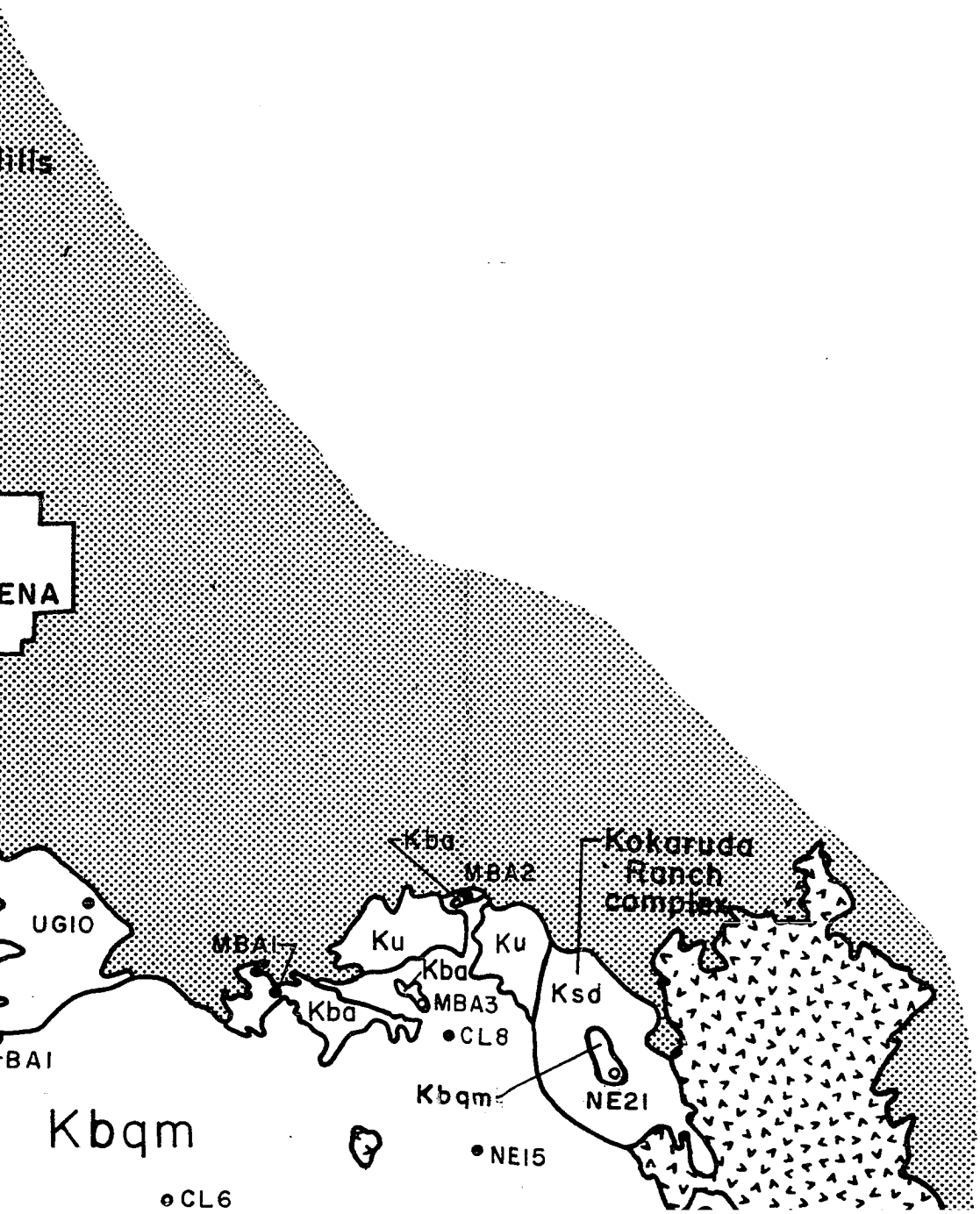

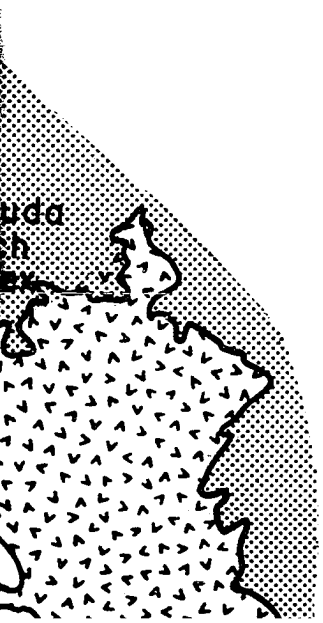

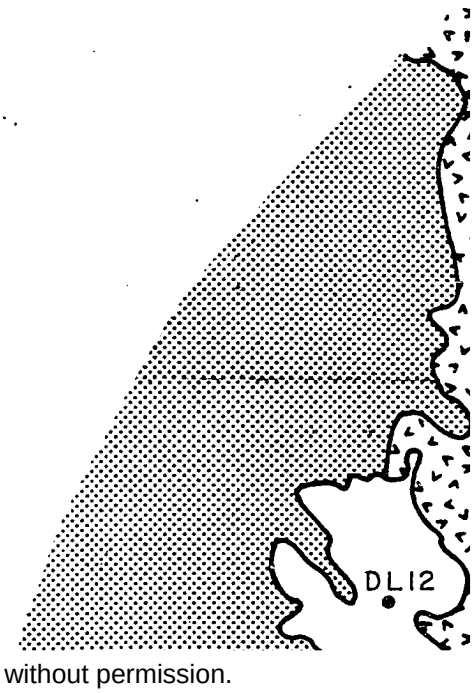

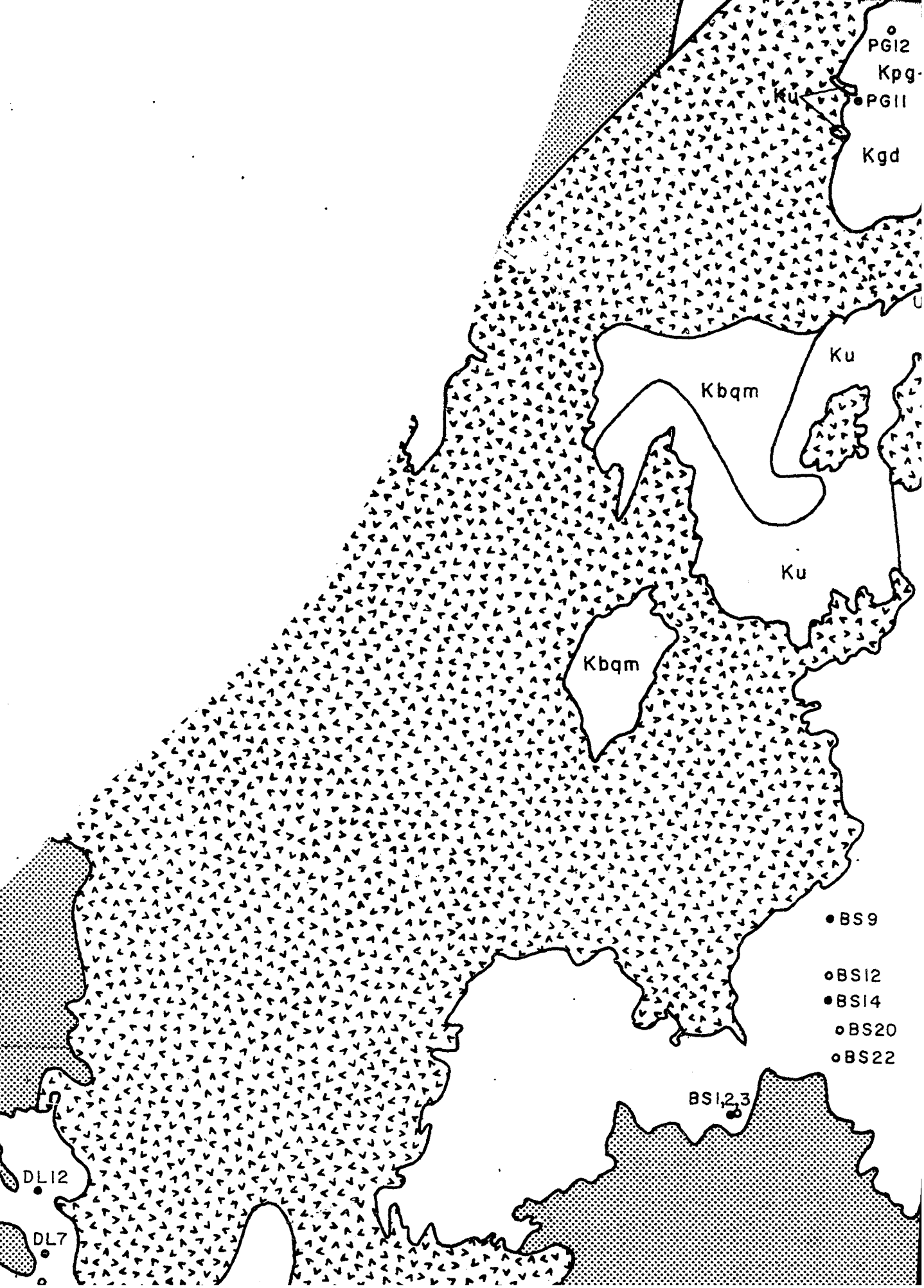

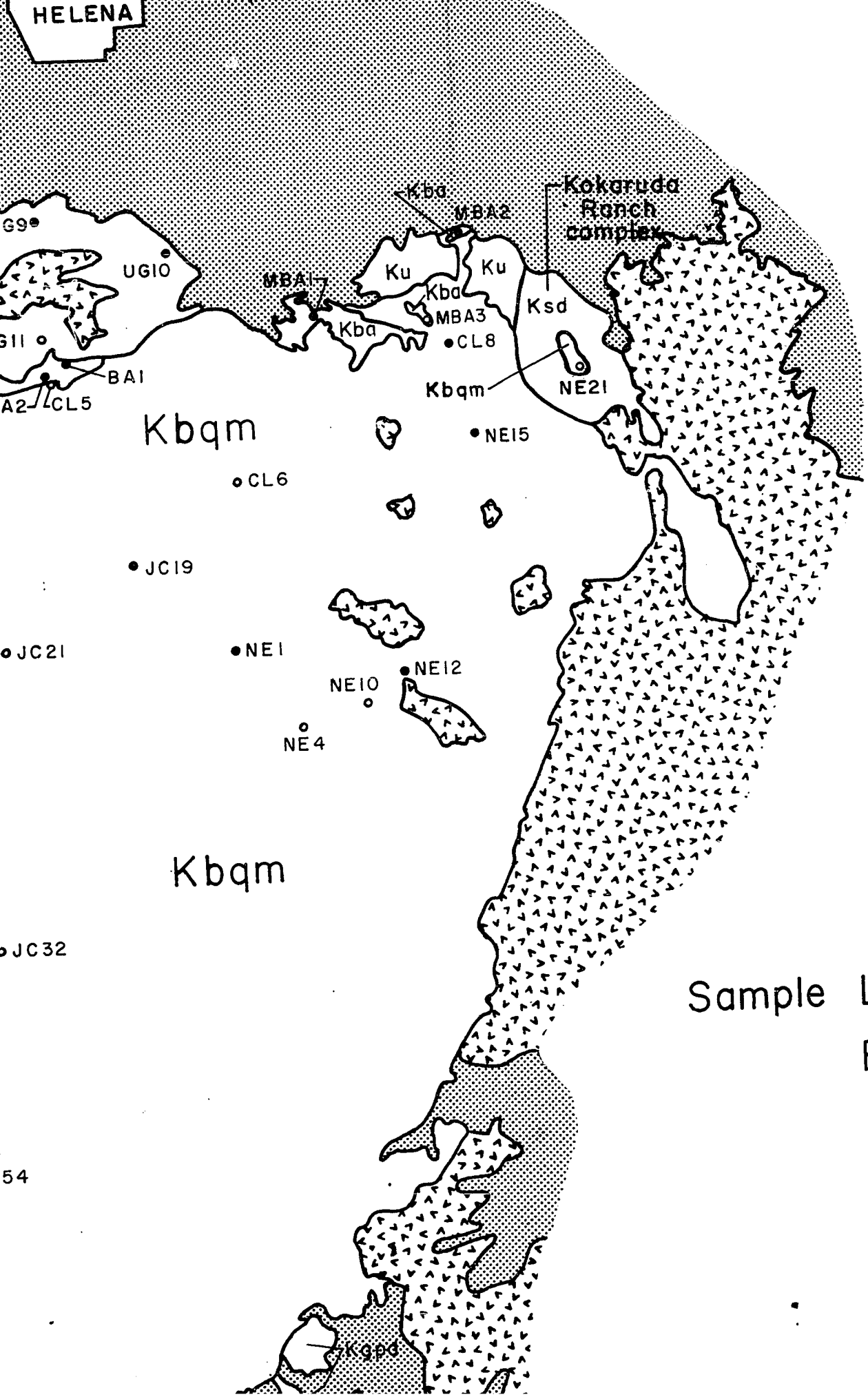

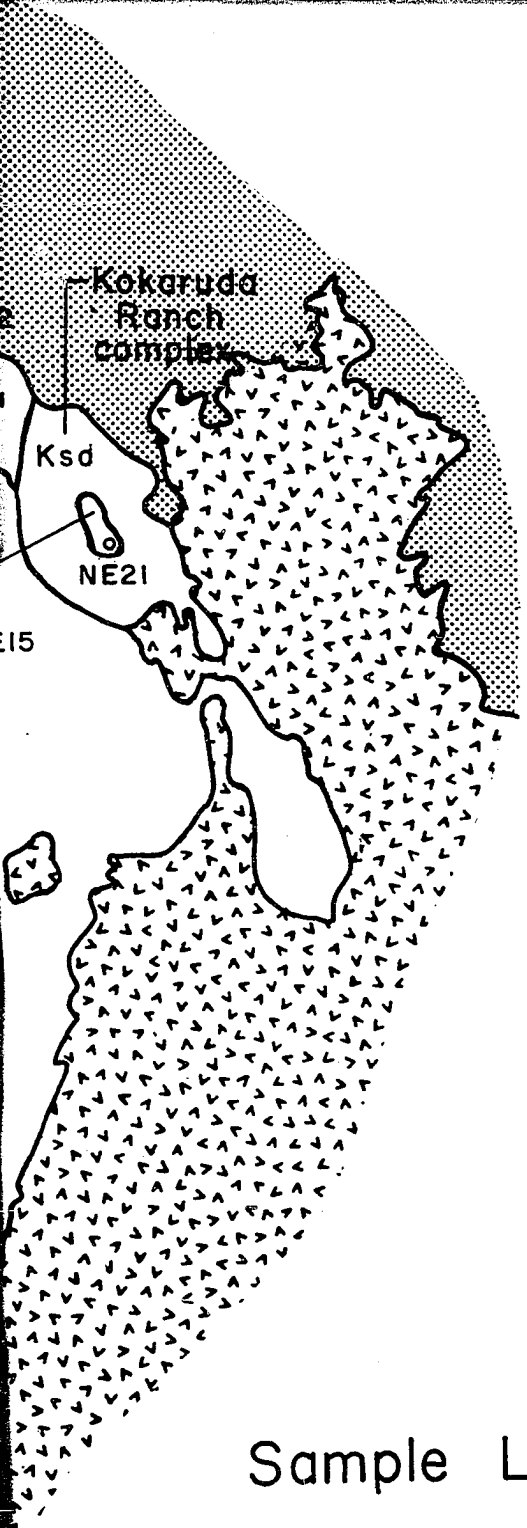

Sample Location and General Geologic
Boulder Batholith, Montana

Explanation

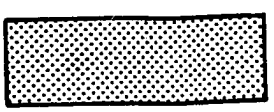

Us – Undifferentiated non-igneous rocks
Includes consolidated and unconsoli

cation and General Geologic Map

ulder Batholith, Montana

Explanation

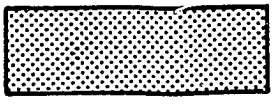

s – Undifferentiated non-igneous rocks-
Includes consolidated and unconsolidated

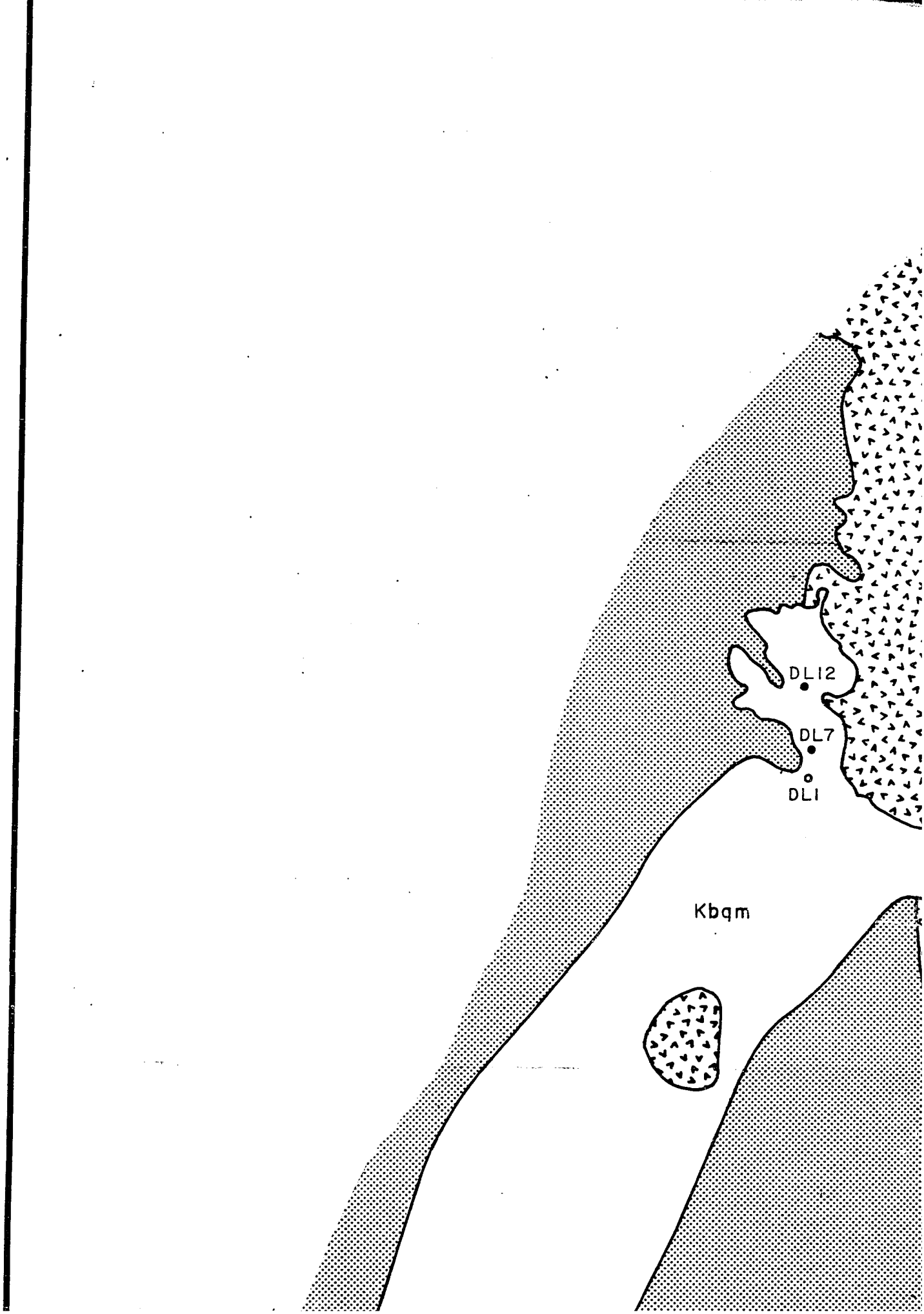

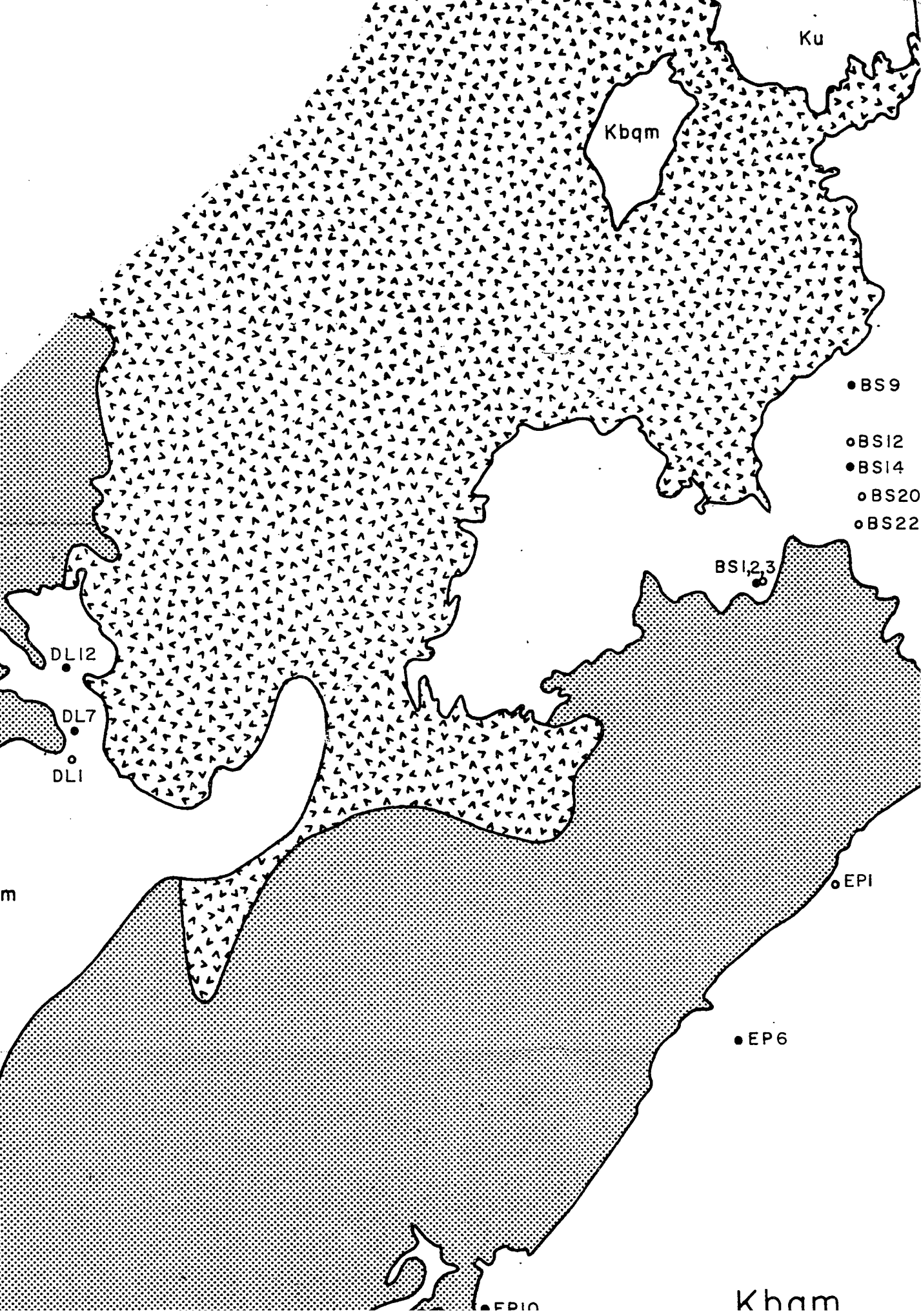

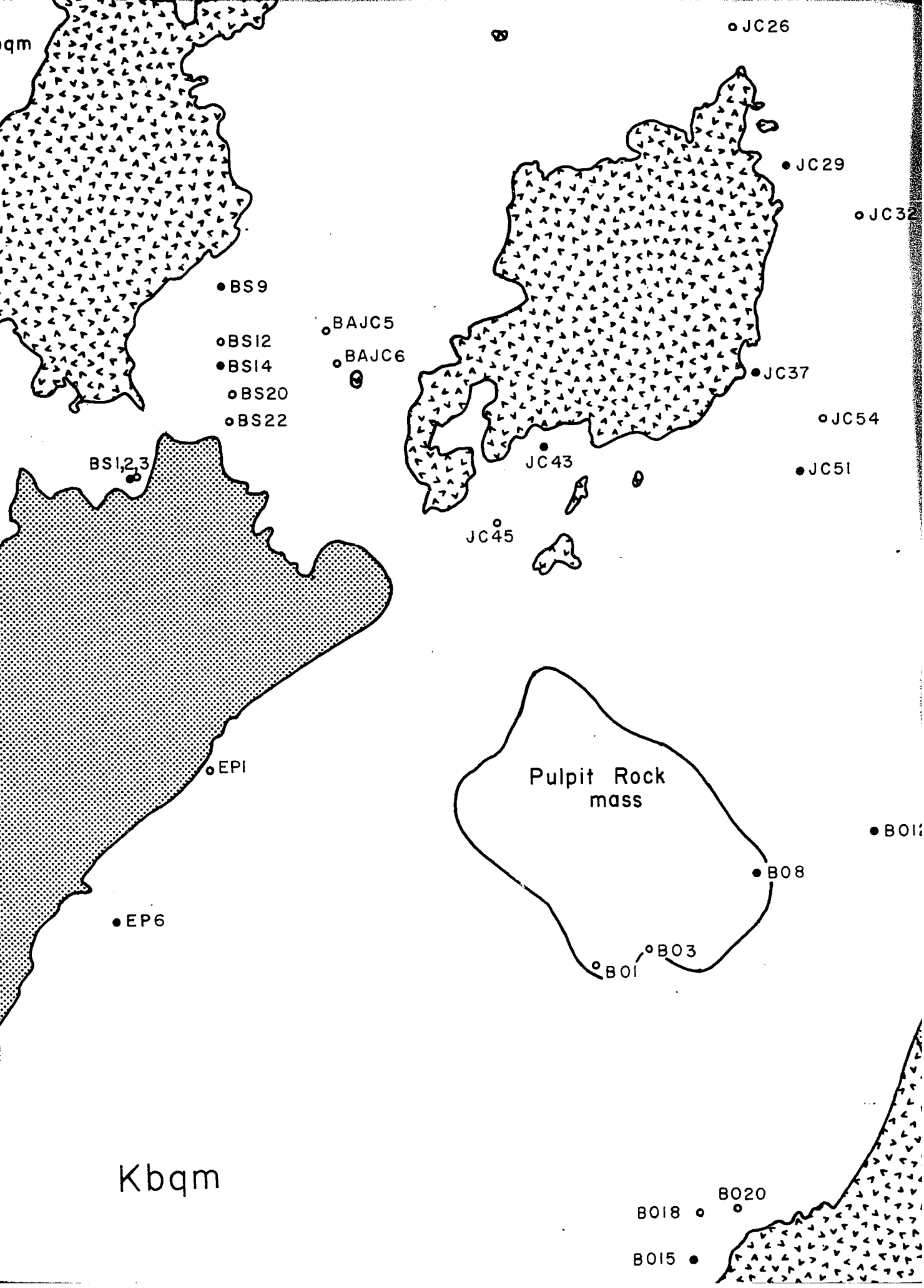

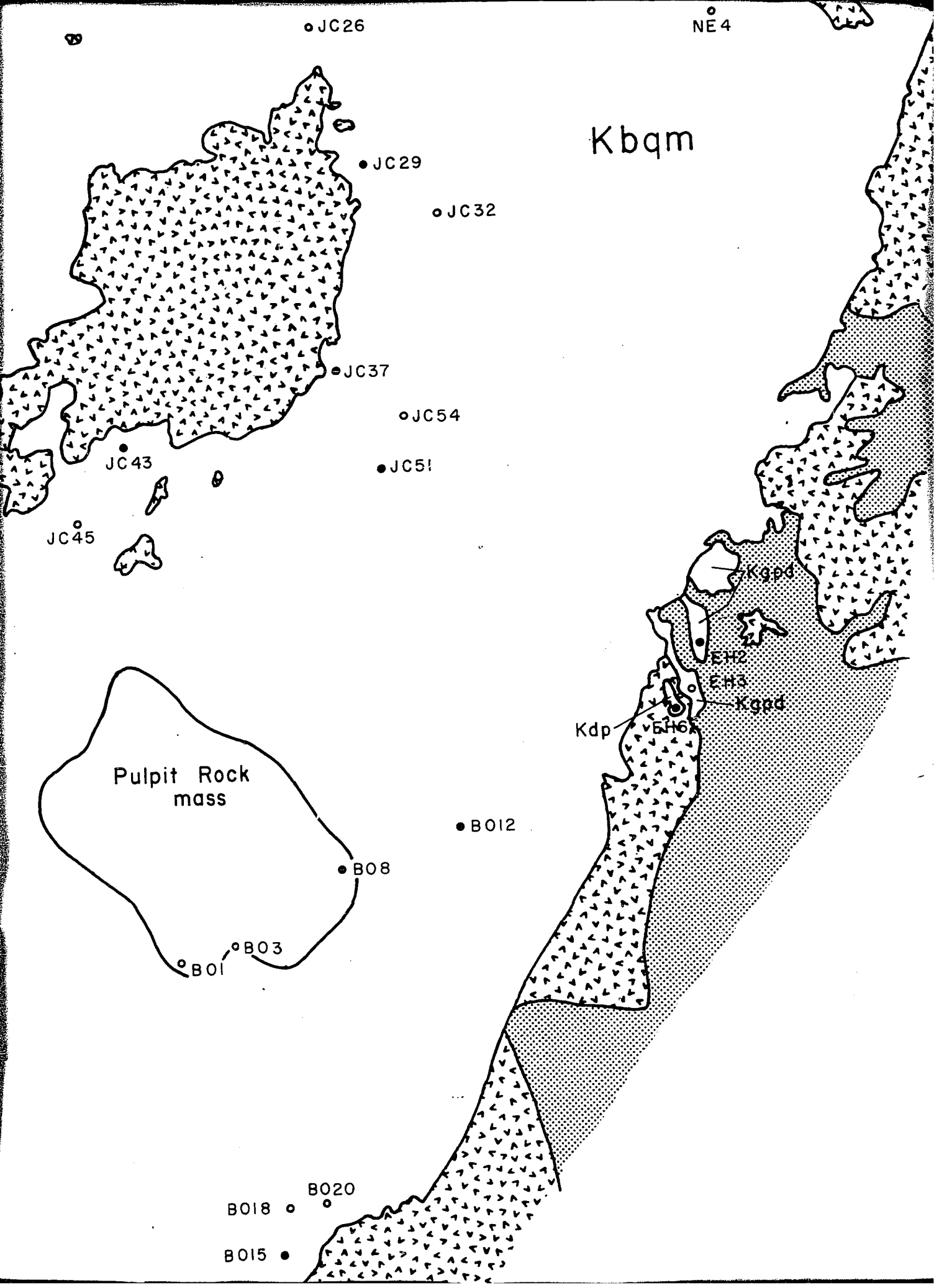

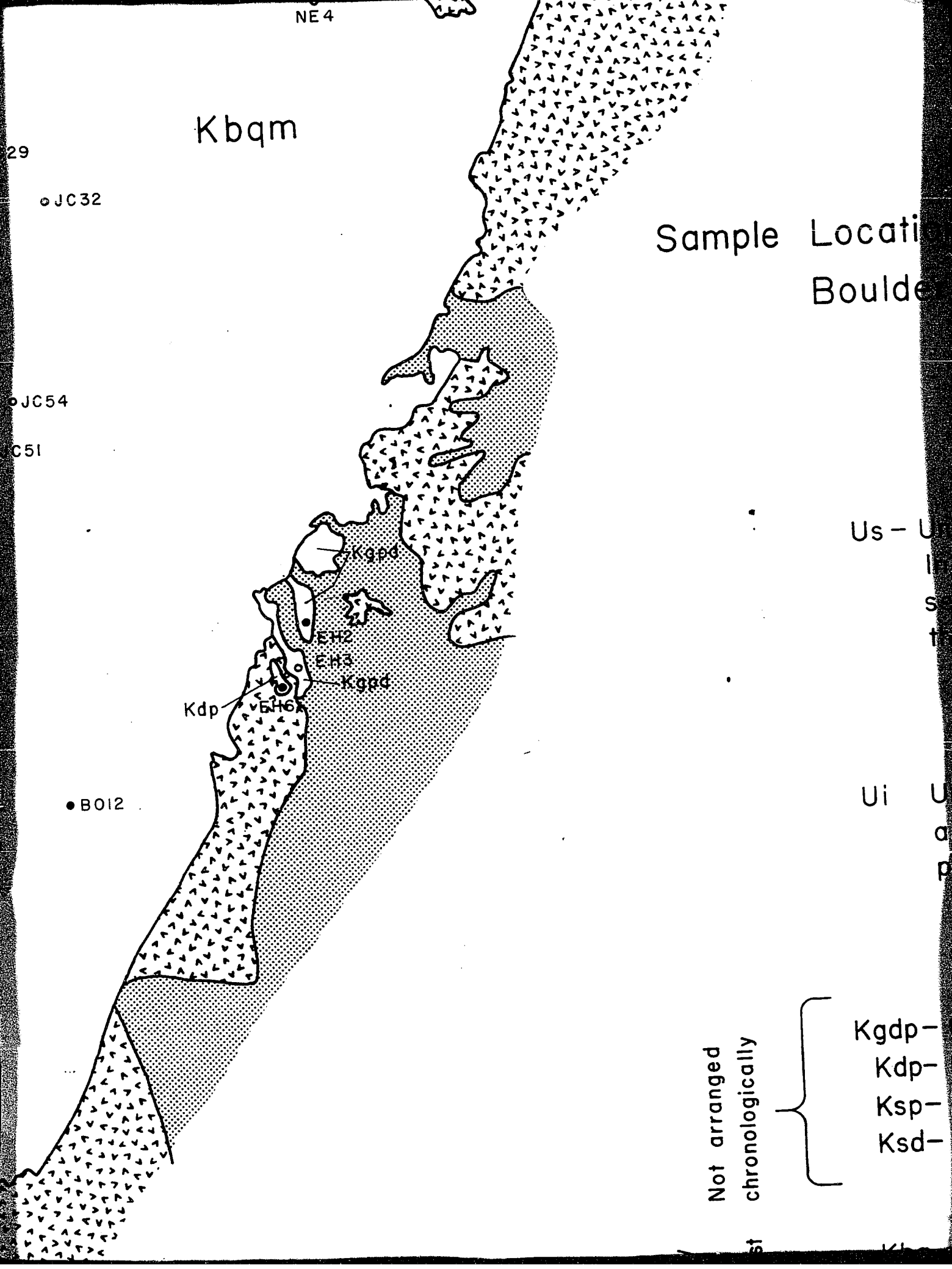

Sample Location and General Geologic
Boulder Batholith, Montana

Explanation

Us – Undifferentiated non-igneous ro
Includes consolidated and uncon
sedimentary strata of all ages
their contact metamorphosed e

Ui Undifferentiated igneous rocks.
all extrusive and most minor int
phases.

Not arranged chronologically

Kgdp – Granodiorite porphyry } Near t
Kdp – Diorite porphyry
Ksp – Priest Pass leucomonzonite.
Ksd – Syenodiorite.

ally

gest

Kbg – Muscovite biotite granite.
Kbg – Biotite adamellite.

ocation and General Geologic Map
oulder Batholith, Montana

Explanation

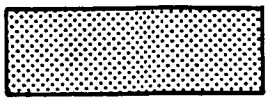

Us – Undifferentiated non-igneous rocks- Includes consolidated and unconsolidated sedimentary strata of all ages as well as their contact metamorphosed equivalents.

Ui Undifferentiated igneous rocks. Includes all extrusive and most minor intrusive phases.

Kgdp – Granodiorite porphyry
Kdp – Diorite porphyry
} Near town of Elkhorn

Ksp – Priest Pass leucomonzonite.

Ksd – Syenodiorite.

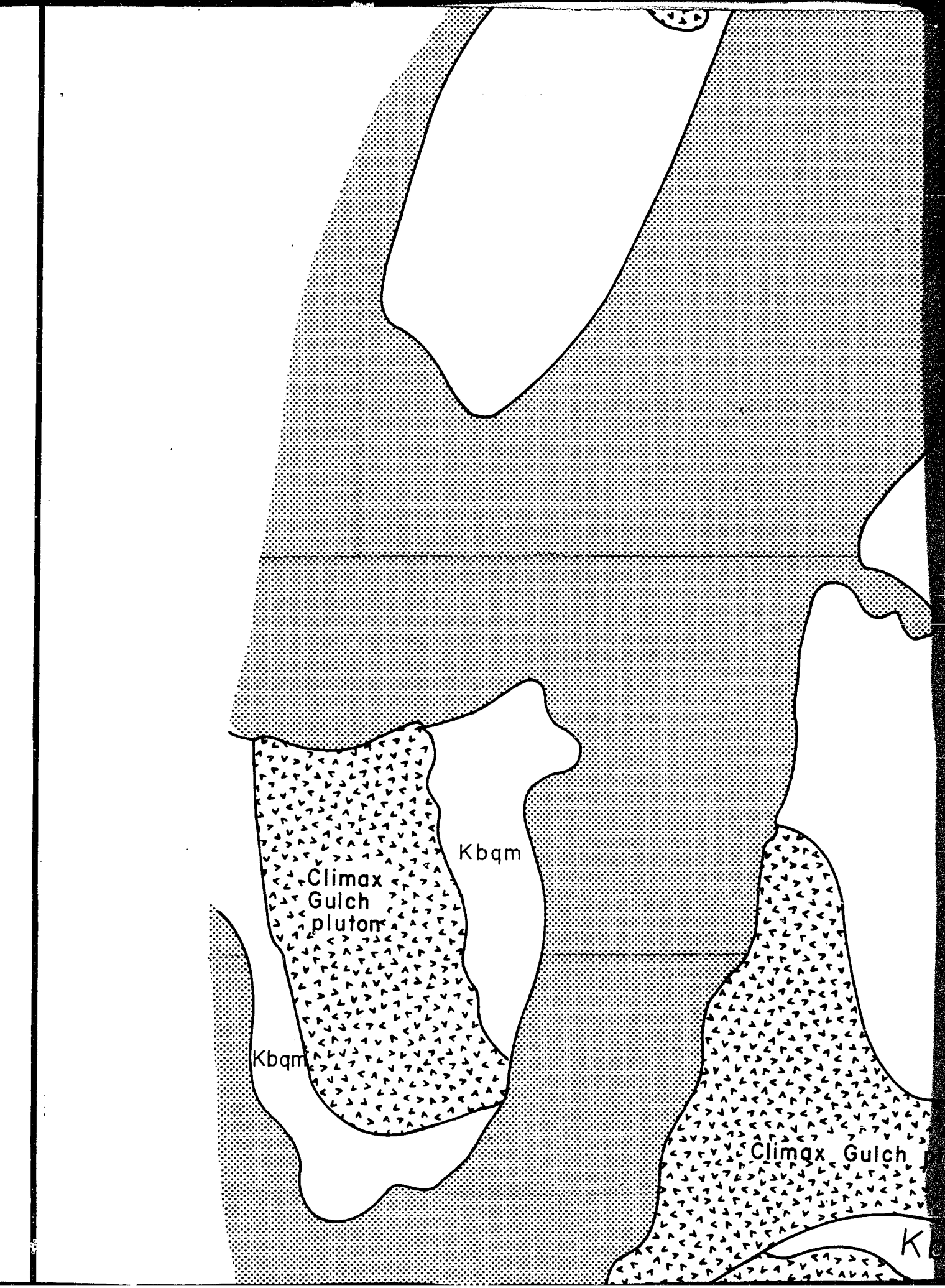

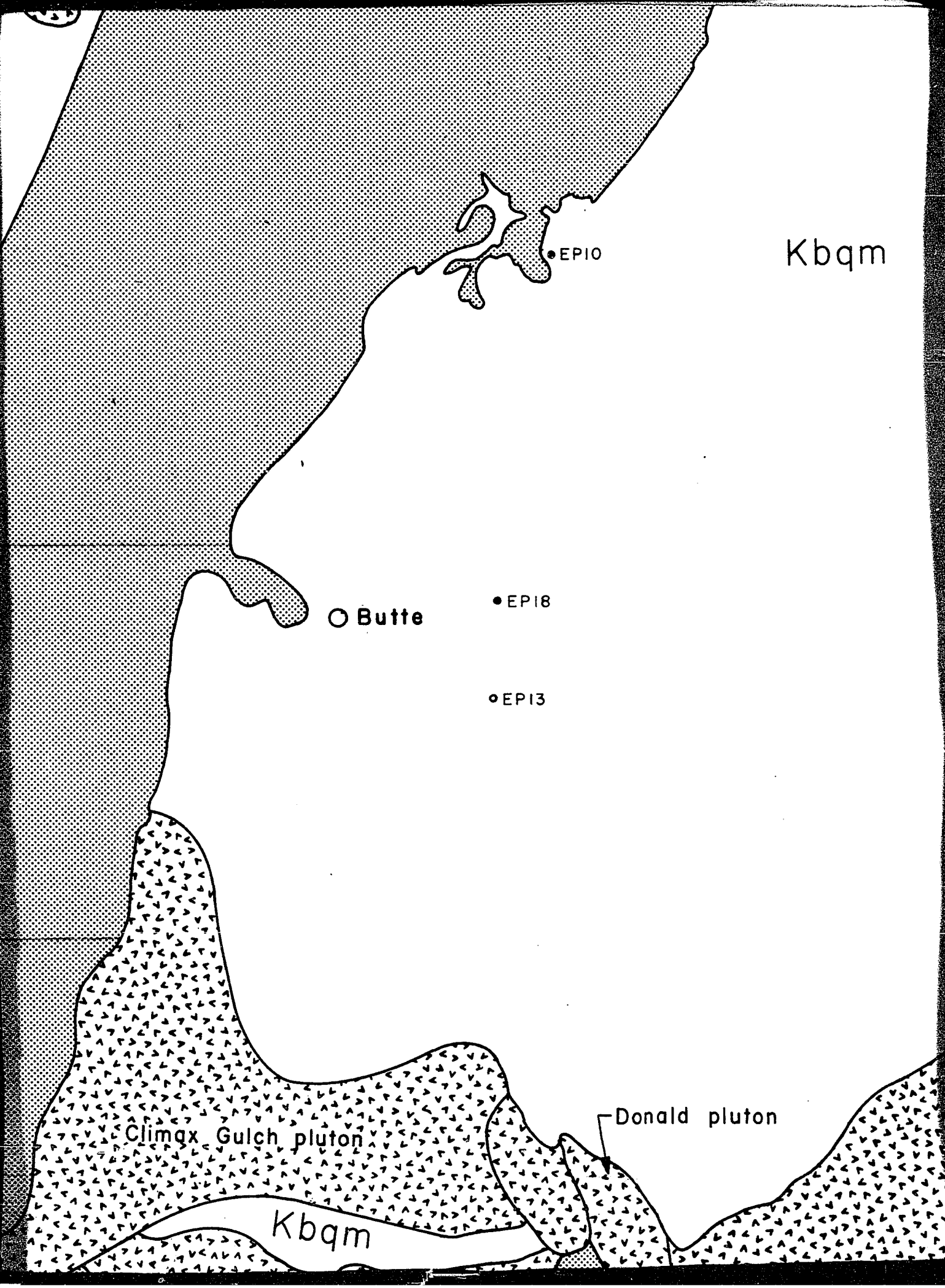

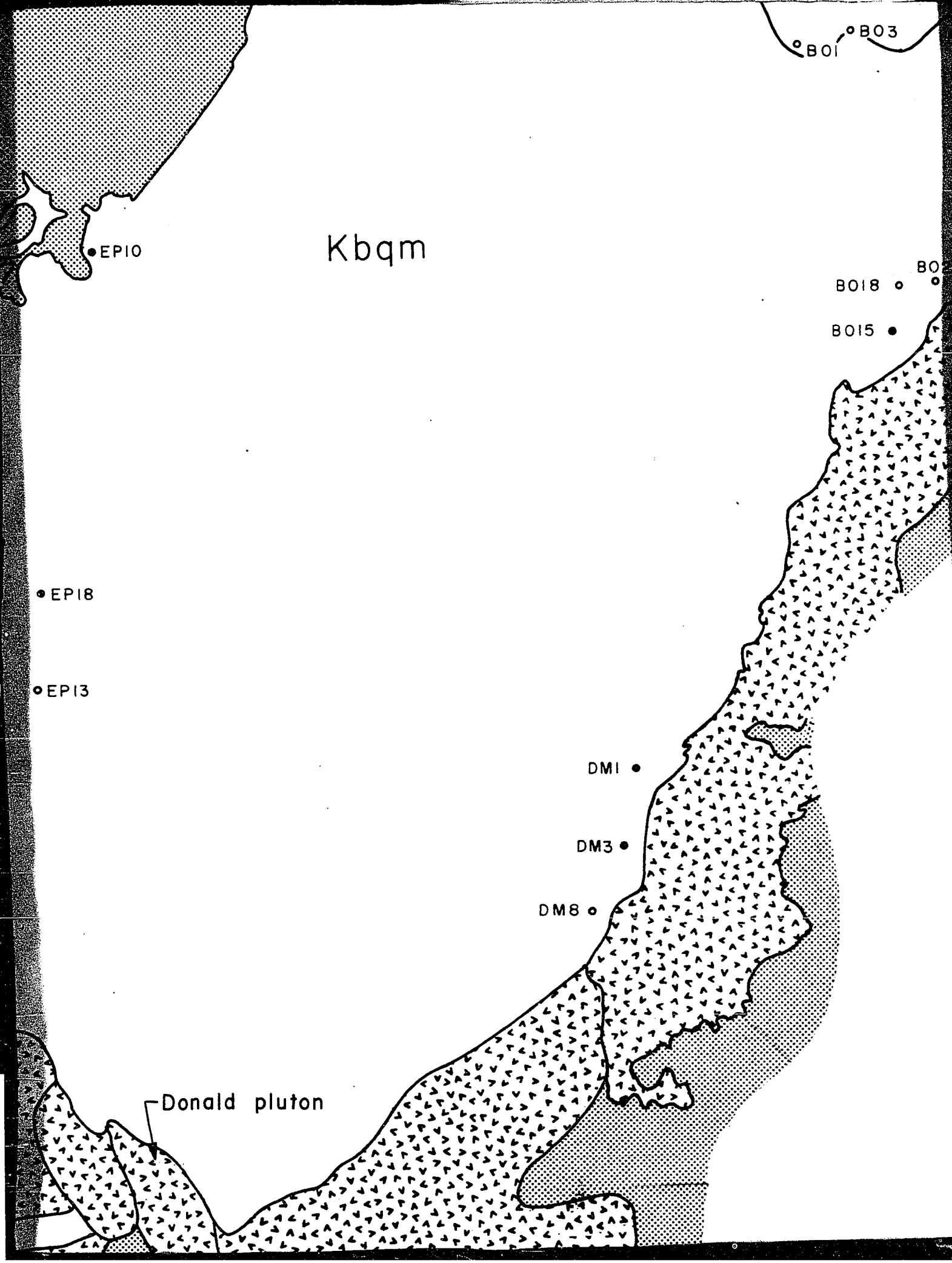

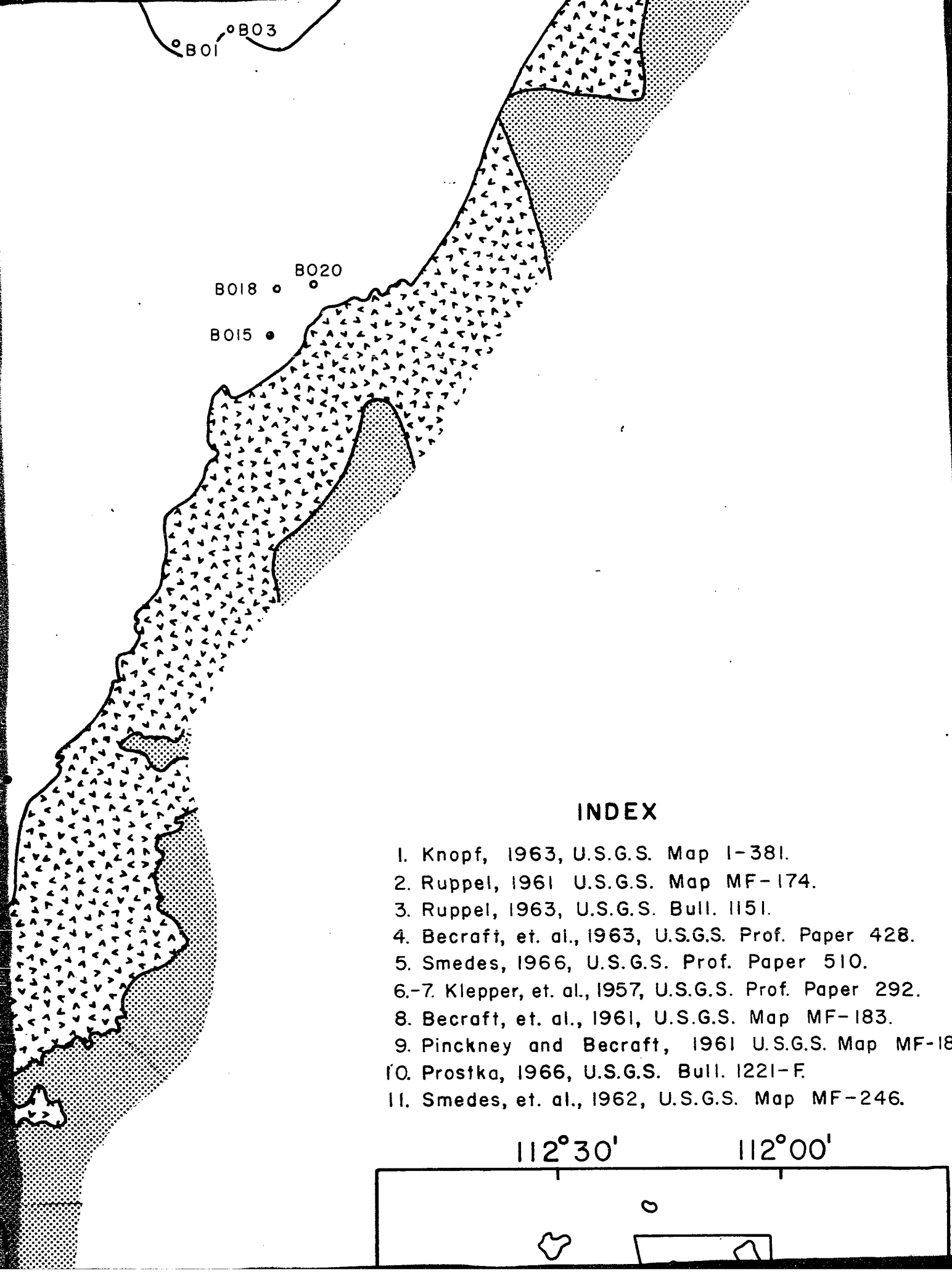

INDEX

1. Knopf, 1963, U.S.G.S. Map I-381.
2. Ruppel, 1961 U.S.G.S. Map MF-174.
3. Ruppel, 1963, U.S.G.S. Bull. 1151.
4. Becraft, et. al., 1963, U.S.G.S. Prof. Paper 428.
5. Smedes, 1966, U.S.G.S. Prof. Paper 510.
6.-7. Klepper, et. al., 1957, U.S.G.S. Prof. Paper 292.
8. Becraft, et. al., 1961, U.S.G.S. Map MF-183.
9. Pinckney and Becraft, 1961 U.S.G.S. Map MF-18
10. Prostka, 1966, U.S.G.S. Bull. 1221-F.
11. Smedes, et. al., 1962, U.S.G.S. Map MF-246.

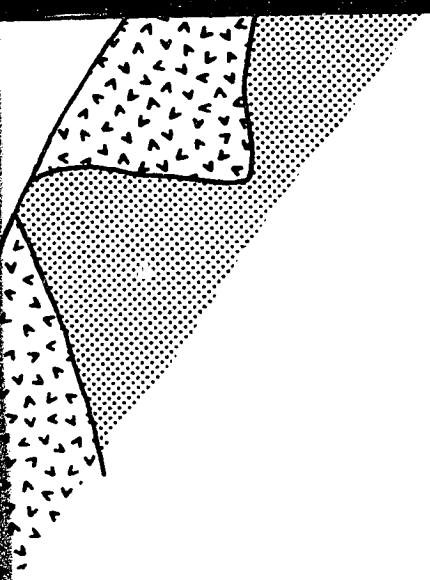

phases

Not arranged chronologically

Kgdp– Granod
Kdp– Diorite
Ksp– Priest
Ksd– Syenod

Arranged chronologically (Knopf, 1963) oldest ——— youngest

Kbg– Muscov
Kba– Biotite
Kpg– Porphy
Kgd– Non po
Kbqm– Butte
Knopfs
Ku— Unionvi

○ Zircon
variati

● Zircon
and c

INDEX

1963, U.S.G.S. Map I-381.
, 1961 U.S.G.S. Map MF-174.
, 1963, U.S.G.S. Bull. 1151.
t, et. al., 1963, U.S.G.S. Prof. Paper 428.
s, 1966, U.S.G.S. Prof. Paper 510.
per, et. al., 1957, U.S.G.S. Prof. Paper 292.
t, et. al., 1961, U.S.G.S. Map MF-183.
ey and Becraft, 1961 U.S.G.S. Map MF-187.
a, 1966, U.S.G.S. Bull. 1221-F.
es, et. al., 1962, U.S.G.S. Map MF-246.

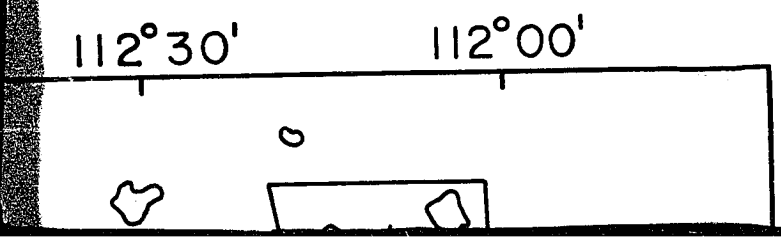

phases.

Not arranged chronologically

- Kgdp– Granodiorite porphyry } Near town
- Kdp– Diorite porphyry } Near town
- Ksp– Priest Pass leucomonzonite.
- Ksd– Syenodiorite.

Arranged chronologically (Knopf, 1963) oldest — youngest

- Kbg– Muscovite biotite granite.
- Kba– Biotite adamellite.
- Kpg– Porphyrytic granodiorite.
- Kgd– Non porphyrytic equivalent of Kpg.
- Kbqm– Butte quartz monzonite. Equivalent Knopf's (1963) Clancy granodiorite.
- Ku— Unionville granodiorite.

○ Zircon samples studied for morpho variation.

● Zircon samples studied for morpho and chemical variation.

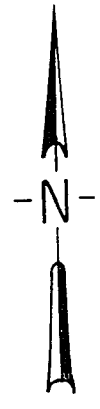

2.

F-187.

phases.

gdp– Granodiorite porphyry } Near town of Elkhorn
Kdp– Diorite porphyry }

Ksp– Priest Pass leucomonzonite.

Ksd– Syenodiorite.

Kbg– Muscovite biotite granite.

Kba– Biotite adamellite.

Kpg– Porphyrytic granodiorite.

Kgd– Non porphyrytic equivalent of Kpg.

qm– Butte quartz monzonite. Equivalent of Knopf's (1963) Clancy granodiorite.

Ku— Unionville granodiorite.

○ Zircon samples studied for morphological variation.

● Zircon samples studied for morphological and chemical variation.

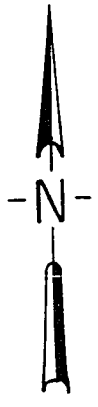

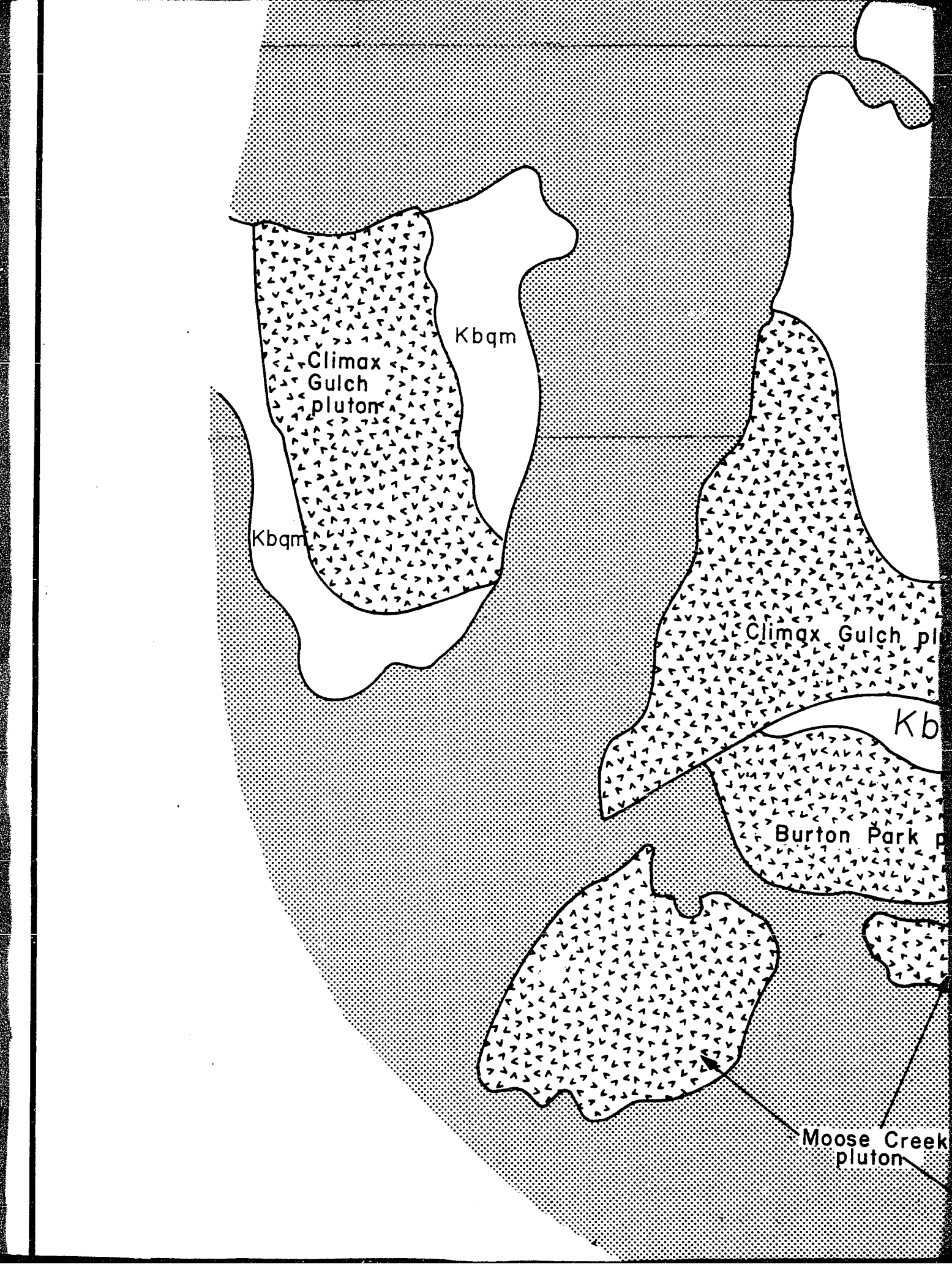

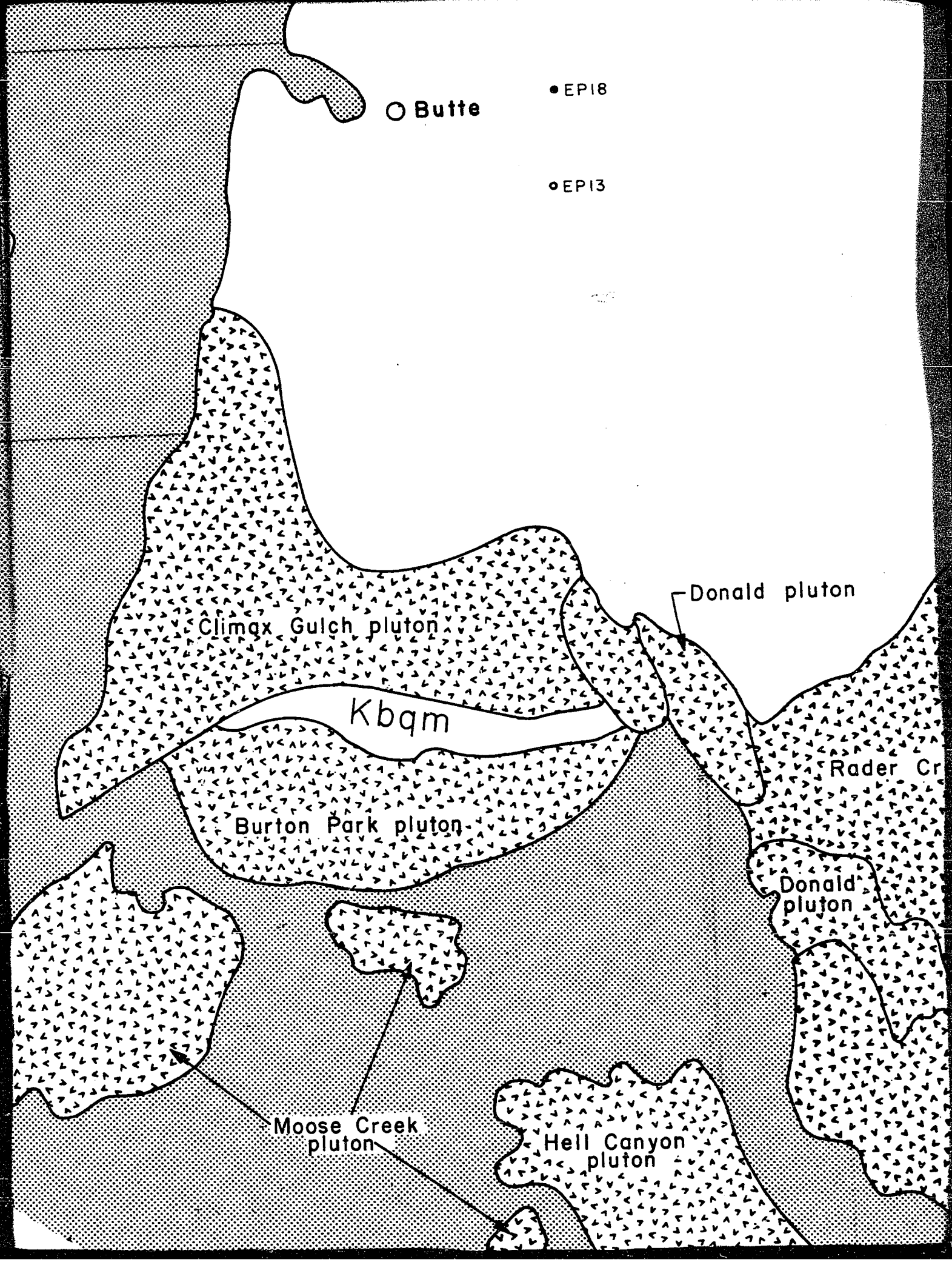

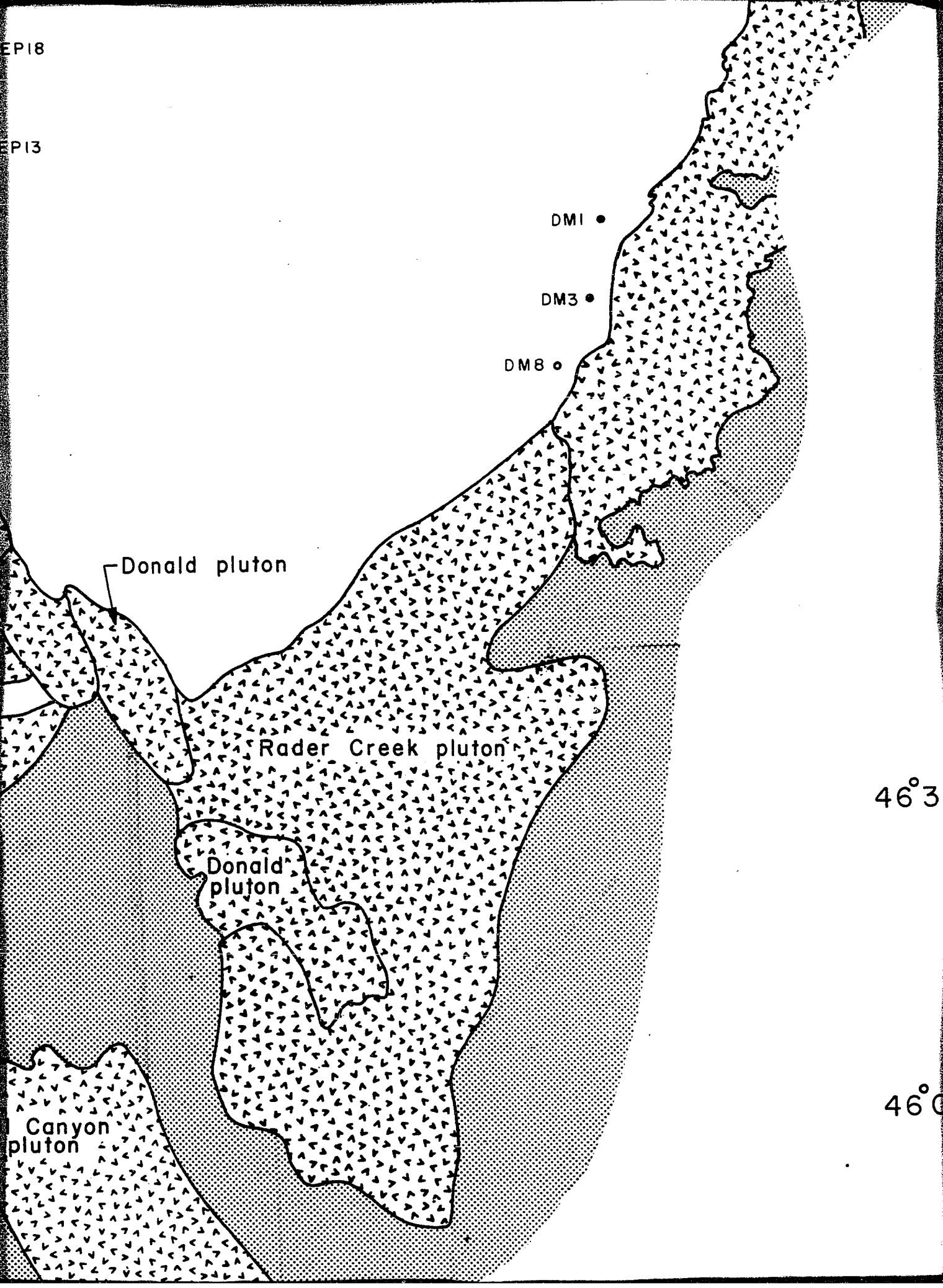

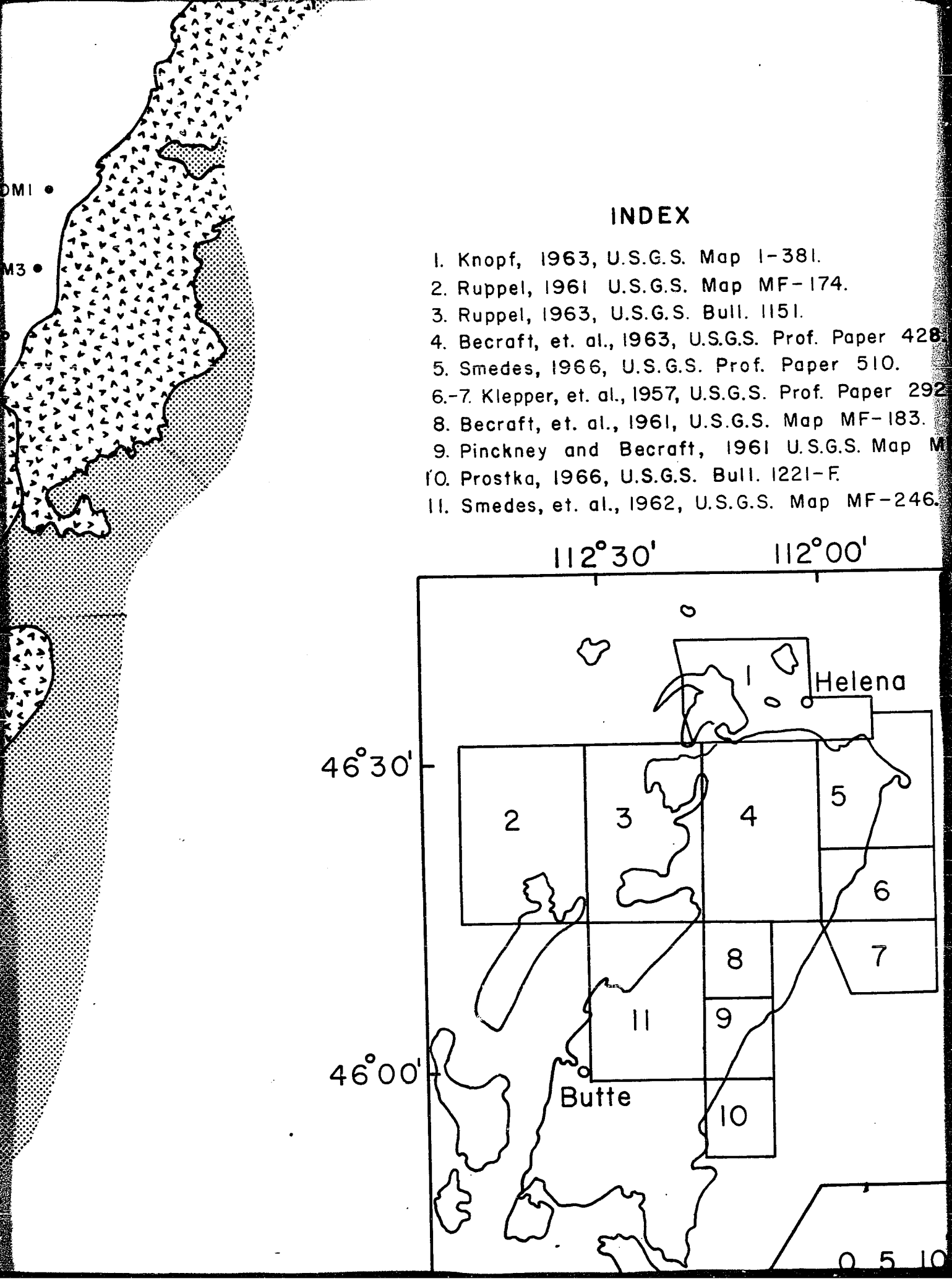

INDEX

63, U.S.G.S. Map I-381.
961 U.S.G.S. Map MF-174.
63, U.S.G.S. Bull. 1151.
. al., 1963, U.S.G.S. Prof. Paper 428.
966, U.S.G.S. Prof. Paper 510.
et. al., 1957, U.S.G.S. Prof. Paper 292.
t. al., 1961, U.S.G.S. Map MF-183.
and Becraft, 1961 U.S.G.S. Map MF-187.
966, U.S.G.S. Bull. 1221-F.
t. al., 1962, U.S.G.S. Map MF-246.

o Zircon so
variation

● Zircon s
and cher

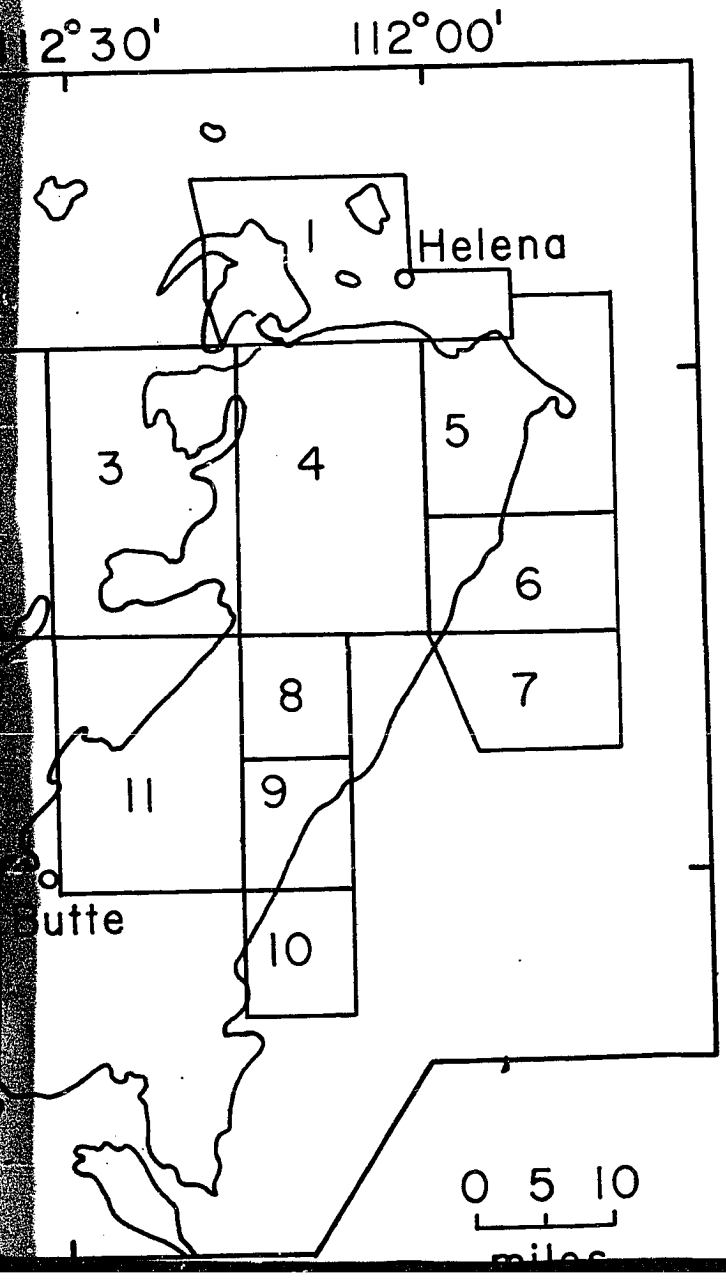

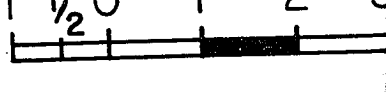

○ Zircon samples studied for morpholo variation.

● Zircon samples studied for morpholo and chemical variation.

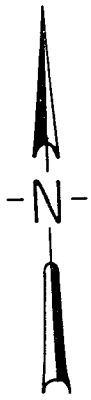

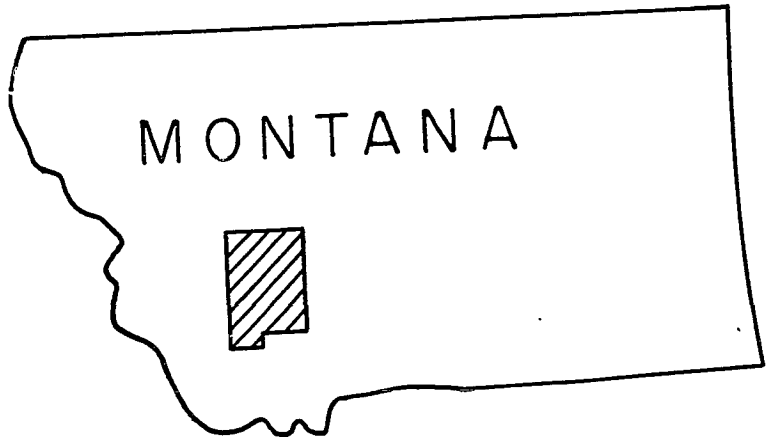

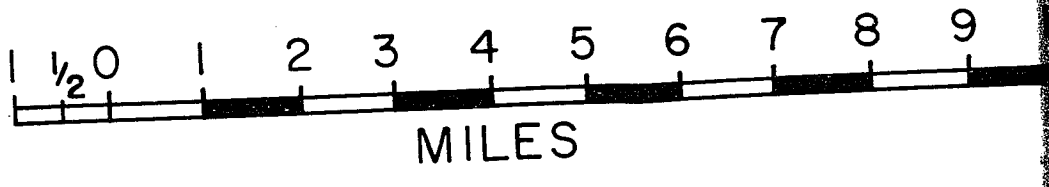

o Zircon samples studied for morphological variation.

● Zircon samples studied for morphological and chemical variation.

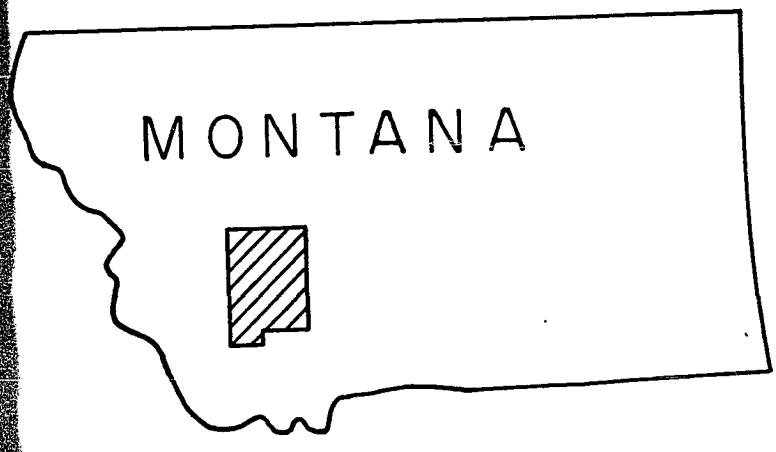

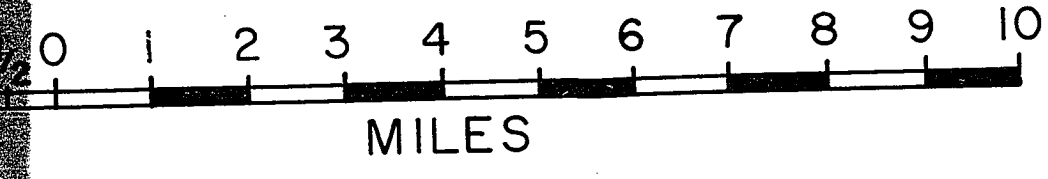

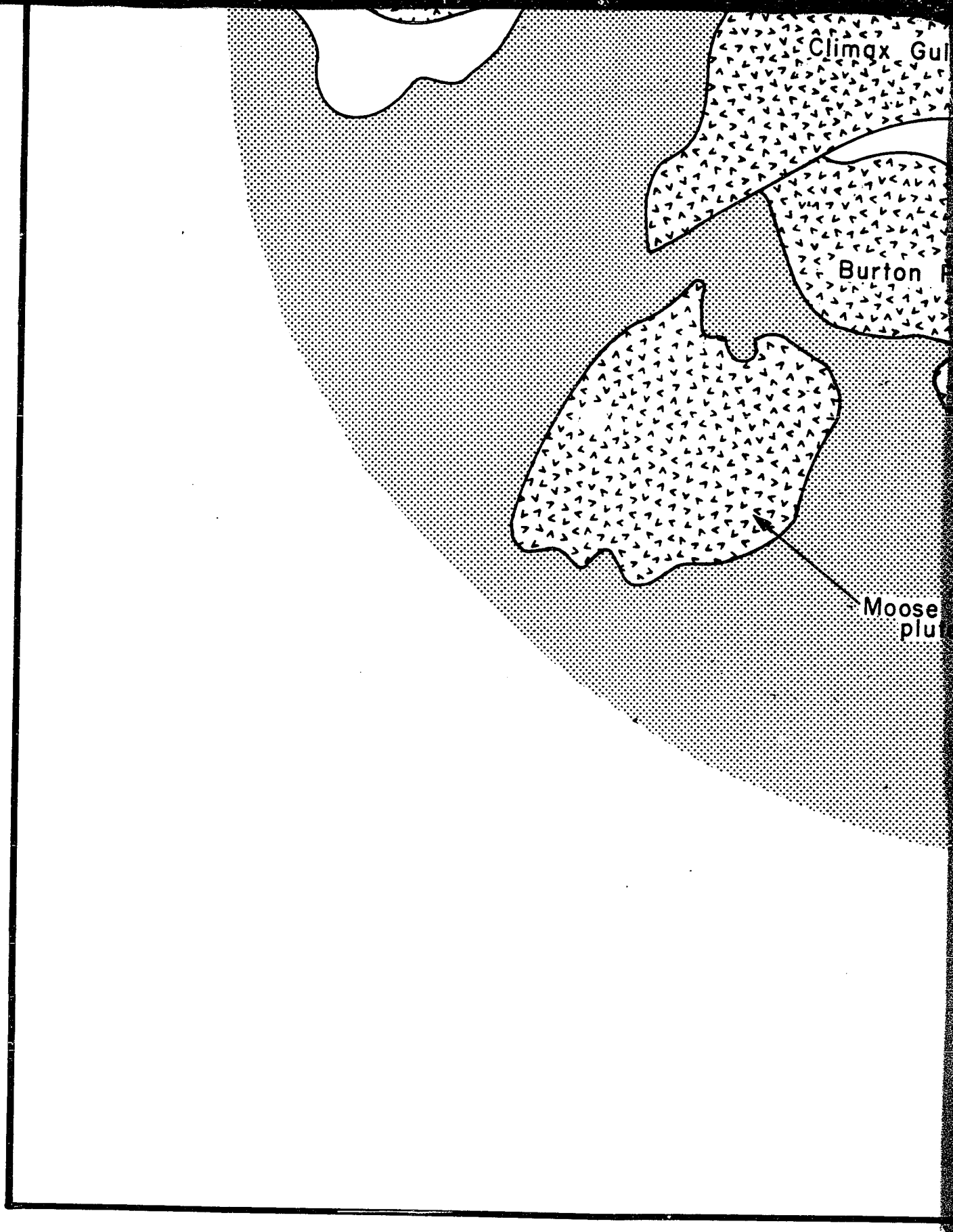

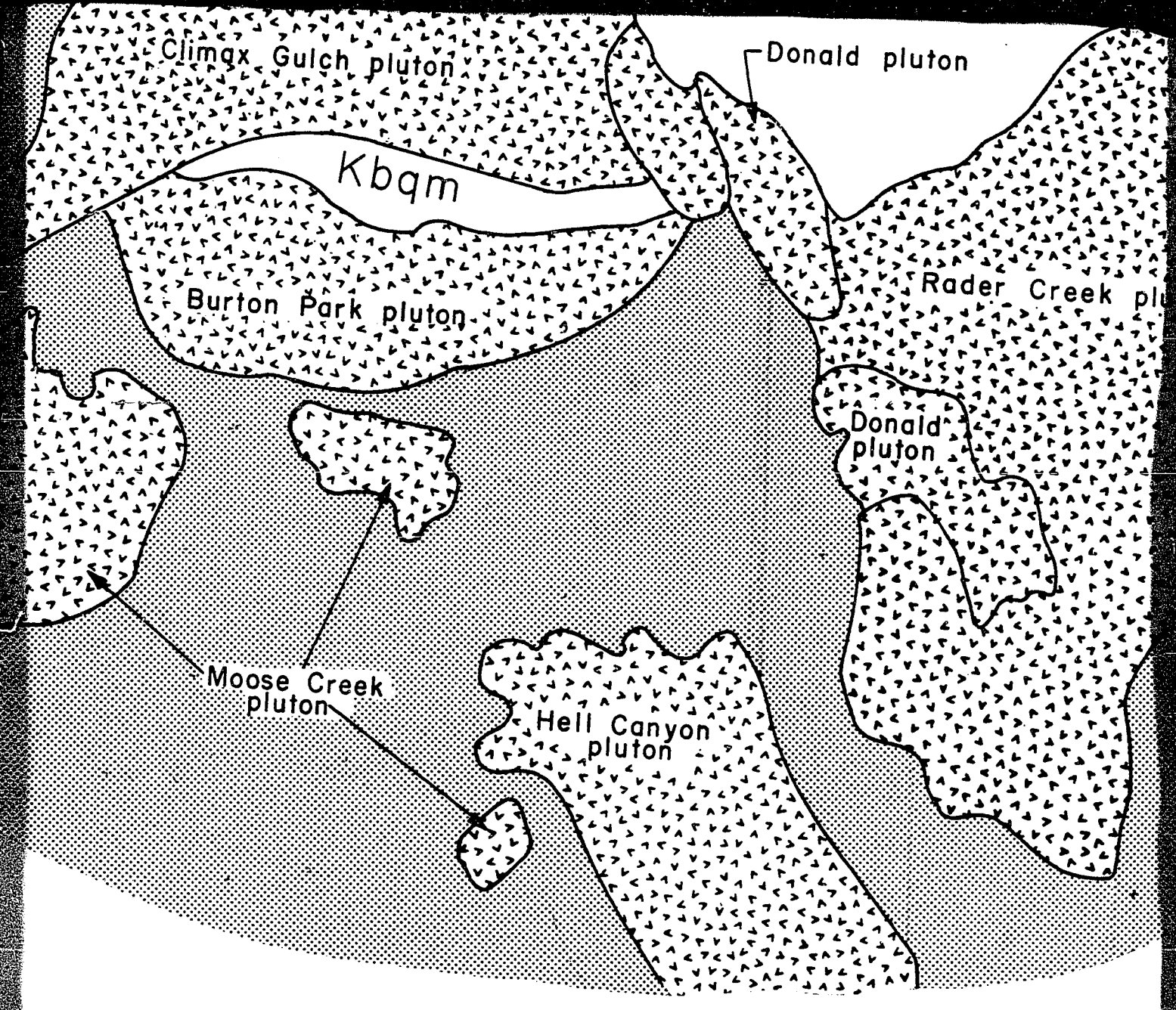

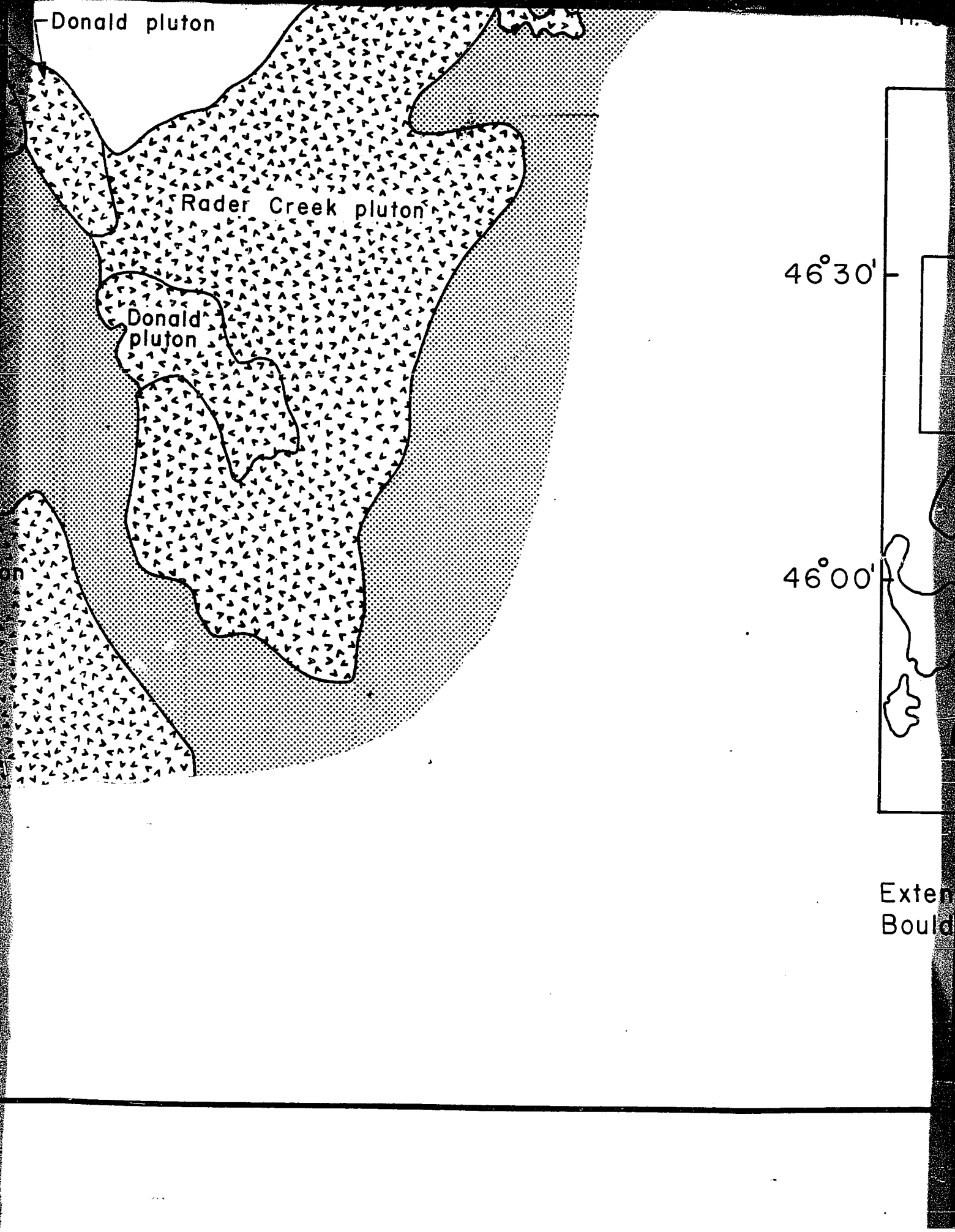

H. Smedes, et. al., 1962, U.S.G.S. Map MF-246.

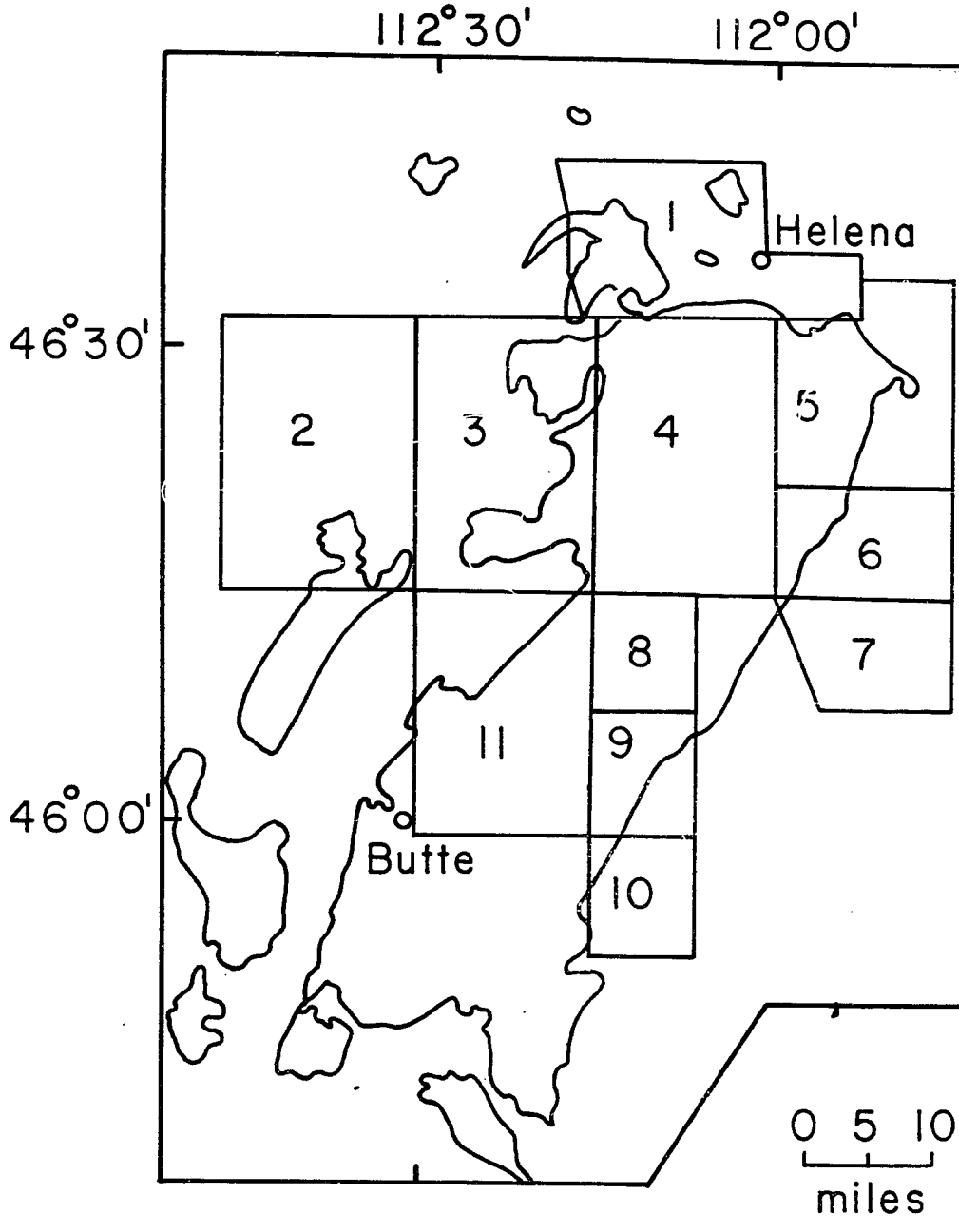

Extent of maps published for the Boulder Batholith (1971).

des, et. al., 1962, U.S.G.S. Map MF-246.

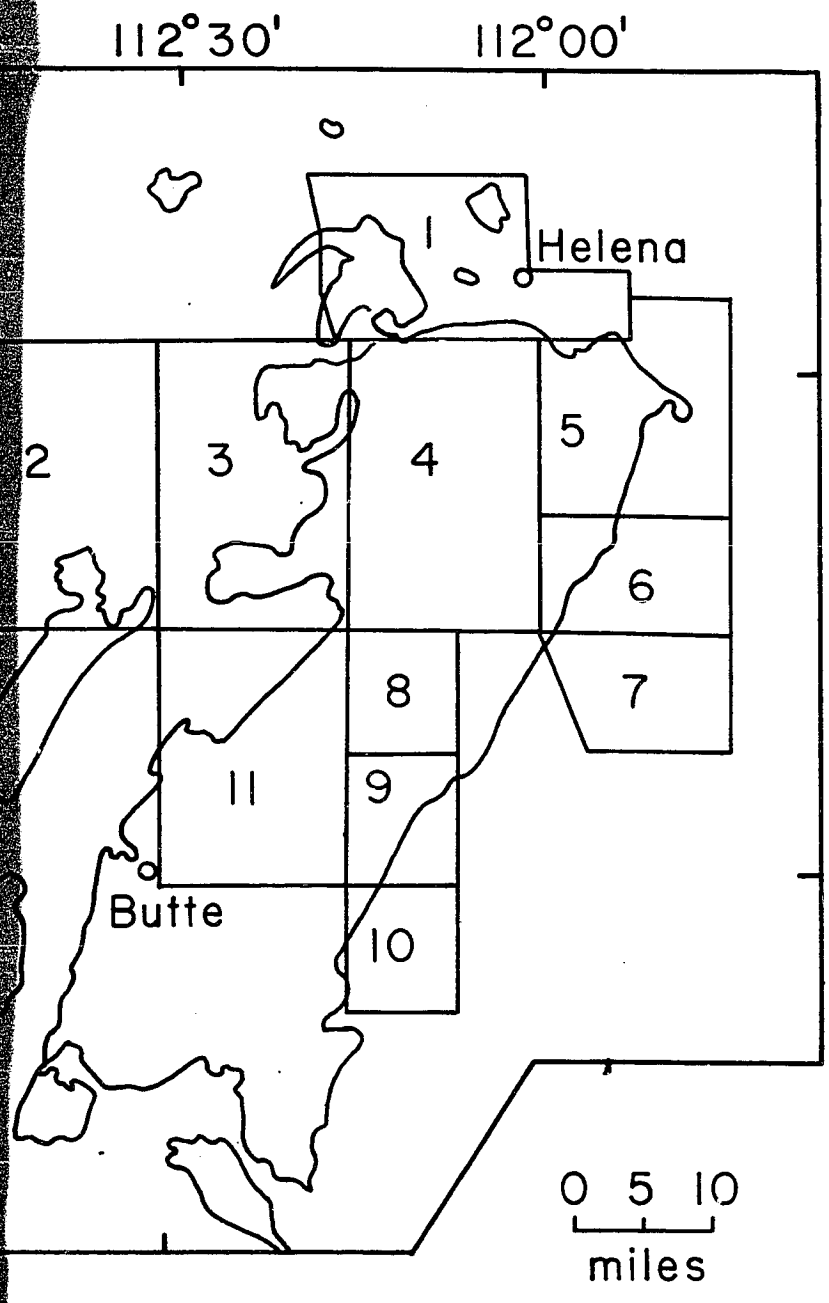

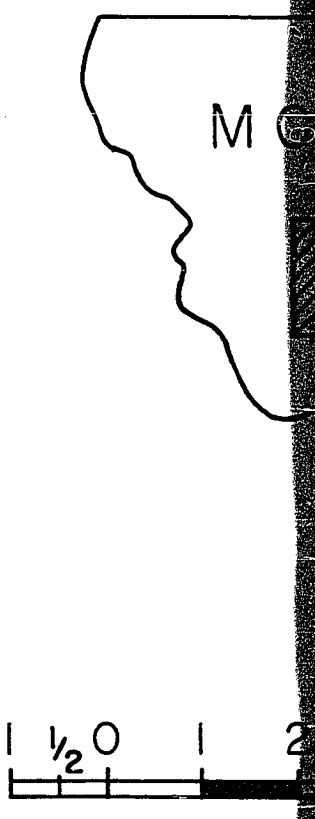

nt of maps published for the
der Batholith (1971).

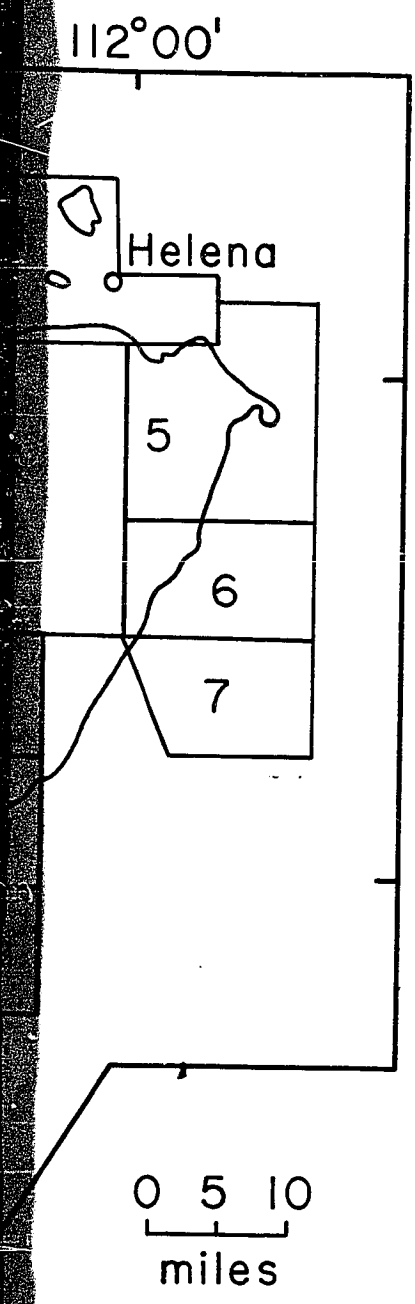

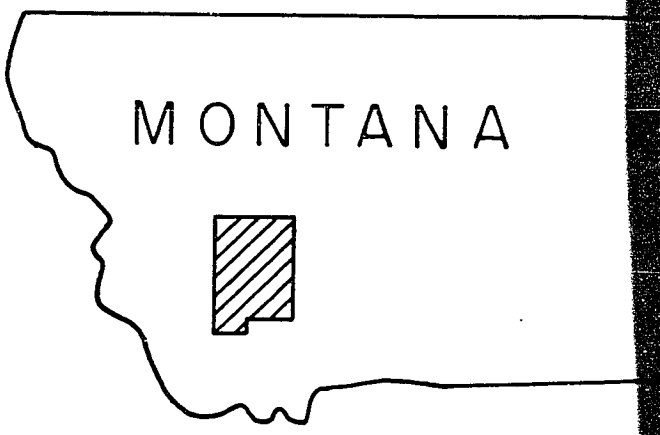

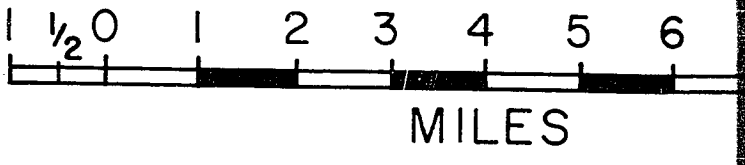

hed for the
).